RESEARCH ARTICLE SUMMARY

PALEONTOLOGY

Early giant reveals faster evolution of large body size in ichthyosaurs than in cetaceans

P. Martin Sander*, Eva Maria Griebeler*, Nicole Klein, Jorge Velez Juarbe, Tanja Wintrich, Liam J. Revell, Lars Schmitz*

INTRODUCTION: The iterative evolution of secondarily marine tetrapods since the Paleozoic offers the promise of better understanding how the anatomy and ecology of animals change when returning to the sea. Recurring patterns of convergence in the geological past may suggest predictability of evolution when transitioning from full-time life on land to full-time life in the ocean. Ichthyosaurs (fish-shaped marine reptiles of the Mesozoic) and today's cetaceans (whales, dolphins, and porpoises) are two of the most informative lineages to exemplify secondary returns to the sea. The notable resemblance in body shape and lifestyle of ichthyosaurs and cetaceans contrasts with their separation in time by nearly 200 million years, providing an often-cited example of convergent evolution. Ichthyosaurs arose 249 million years ago and populated the oceans for the next 150 million years. Cetaceans did not evolve until about 56 million years ago. As tail-propelled swimmers, ichthyosaurs and cetaceans evolved not only convergent body shapes but also large body sizes.

RATIONALE: The integration of fossil and extant data can improve understanding of aquatic adaptation and gigantism as patterns of convergent evolution, particularly when interpreted in an ecological context. Our paleontological fieldwork in the Fossil Hill Member (Middle Triassic, Nevada, USA) provided the basis for the marine reptile data and resulted in finds of giant ichthyosaurs as part of the pelagic Fossil Hill Fauna. We compiled data for both fossil and living whales from the extensive literature. Together, these data provide the basis for computational analyses of maximum body size and its evolution over time. Modeling of energy flux in the Fossil Hill Fauna helps in understanding how the Fossil Hill ecosystem could have supported several large to giant tetrapod ocean consumers so early in ichthyosaur evolutionary history.

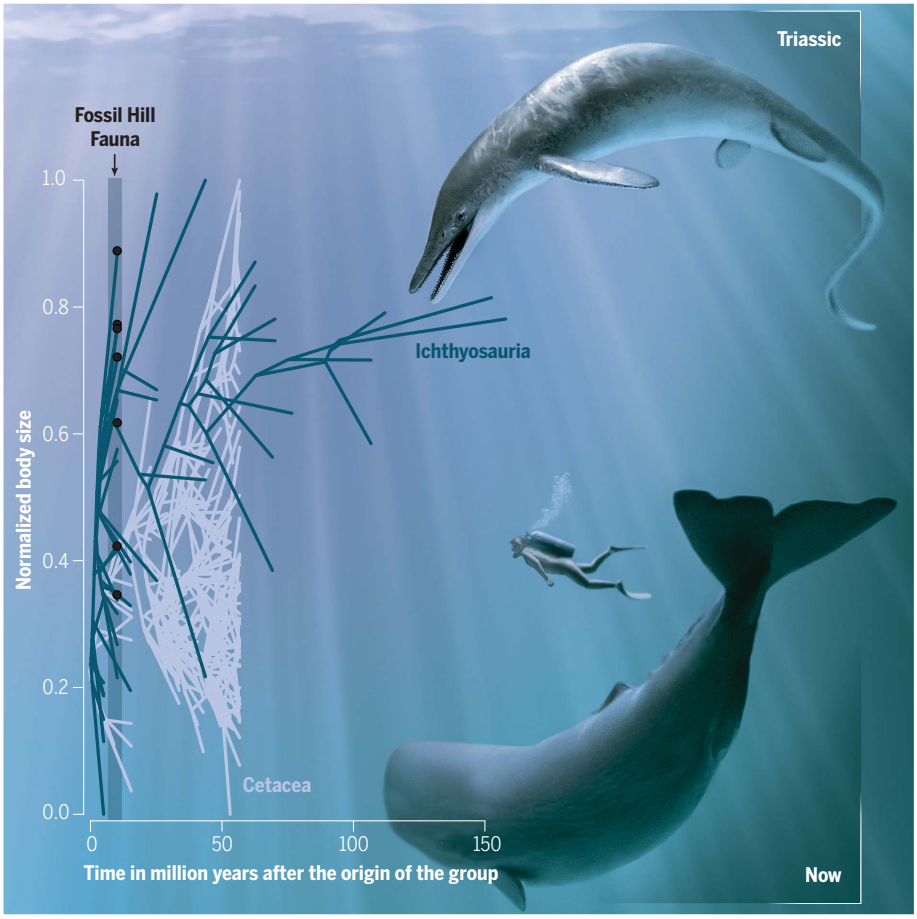

Ichthyosaurs evolved large body sizes earlier in their history than cetaceans. The Fossil Hill Fauna of the Middle Triassic of Nevada, USA, is critical for recognizing this pattern. It features the first ocean giant among tetrapods, only 3 million years after ichthyosaurs first appeared. Whales took comparatively longer to attain similarly large body sizes.

RESULTS: We describe an ichthyosaur with a 2-m-long skull from the Fossil Hill Fauna as a new species of *Cymbospondylus*. At present, this is the largest known tetrapod of its time, on land or in the sea, and is the first in a series of ocean giants. The Fossil Hill Fauna includes several other large-bodied ichthyosaurs in the *Cymbospondylus* radiation. The body-size range in this Triassic fauna rivals the range seen in modern whale faunas, from a total length of about 2 m in *Phalarodon* to more than 17 m in the new species. As preserved in the fossil record, the Fossil Hill Fauna represents a stable trophic network and could even have supported another large ichthyosaur if it bulk fed on small, but abundant, prey such as ammonoids. In absolute time, the new ocean giant lived 246 million years ago, only about 3 million years after the appearance of the first ichthyosaurs. Our research suggests that ichthyosaurs evolved large body size very early on in the clade's history, comparatively earlier than whales.

CONCLUSION: Ichthyosaurs and cetaceans both evolved very large body sizes, yet their respective evolutionary pathways toward gigantism were different. Ichthyosaurs seem to have benefited from the abundance of pelagic conodonts and ammonoids after the recovery from the end-Permian mass extinction, even in the absence of modern primary producers. Cetaceans took different routes, but all appear to be related to trophic specialization, including the loss of teeth in baleen whales (Mysticeti) and the evolution of raptorial feeding and deep diving in toothed whales (Odontoceti). ■

The list of author affiliations is available in the full article online.
*Corresponding author. Email: martin.sander@uni-bonn.de (P.M.S.); em.griebeler@uni-mainz.de (E.M.G.); lschmitz@kecksci.claremont.edu (L.S.)
Cite this article as P. M. Sander *et al.*, *Science* **374**, eabf5787 (2021). DOI: 10.1126/science.abf5787

READ THE FULL ARTICLE AT
https://doi.org/10.1126/science.abf5787

Downloaded from https://www.science.org at Claremont Colleges Library on December 24, 2021

CREDIT: STEPHANIE ABRAMOWICZ

RESEARCH ARTICLE

PALEONTOLOGY

Early giant reveals faster evolution of large body size in ichthyosaurs than in cetaceans

P. Martin Sander[1,2]*, Eva Maria Griebeler[3]*, Nicole Klein[1], Jorge Velez Juarbe[4], Tanja Wintrich[1,5], Liam J. Revell[6,7], Lars Schmitz[2,8]*

Body sizes of marine amniotes span six orders of magnitude, yet the factors that governed the evolution of this diversity are largely unknown. High primary production of modern oceans is considered a prerequisite for the emergence of cetacean giants, but that condition cannot explain gigantism in Triassic ichthyosaurs. We describe the new giant ichthyosaur *Cymbospondylus youngorum* sp. nov. with a 2-meter-long skull from the Middle Triassic Fossil Hill Fauna of Nevada, USA, underscoring rapid size evolution despite the absence of many modern primary producers. Surprisingly, the Fossil Hill Fauna rivaled the composition of modern marine mammal faunas in terms of size range, and energy-flux models suggest that Middle Triassic marine food webs were able to support several large-bodied ichthyosaurs at high trophic levels, shortly after ichthyosaur origins.

Body size is a fundamental attribute of any organism, and extreme body sizes are of special interest to evolutionary biologists. Gigantism is found in different guises in the terrestrial and marine realms (*1*). Several lineages of mammals and reptiles secondarily adapted to marine habitats and diversified to become species-rich clades (*2*), best exemplified by marine mammals since the Paleogene and by marine reptiles of the Mesozoic. Today, multiple species of cetaceans (toothed whales, or odontocetes, and baleen whales, or mysticetes) and pinnipeds (seals and sea lions) inhabit the pelagic ecosystem and differ in body size, feeding strategy, and trophic level (*3*), ranging from macropredatory raptorial feeding (top of the food chain, e.g., killer whales or orcas, *Orcinus orca*) to filter feeding (low in the food chain, e.g., baleen whales). Large marine mammals, especially cetaceans, have been pivotal components of pelagic food webs since at least the late Paleogene, superseding the ichthyosaurs, plesiosaurs, and mosasaurs of the Mesozoic in this role. Body size appears to be a major axis of the phylogenetic and ecological diversification of secondarily marine amniotes.

[1]Abteilung Paläontologie, Institut für Geowissenschaften, Universität Bonn, 53115 Bonn, Germany. [2]The Dinosaur Institute, Natural History Museum of Los Angeles County, Los Angeles, CA 90007, USA. [3]Institut für Organismische und Molekulare Evolutionsbiologie, Evolutionäre Ökologie, Johannes Gutenberg–Universität Mainz, 55099 Mainz, Germany. [4]Department of Mammalogy, Natural History Museum of Los Angeles County, Los Angeles, CA 90007, USA. [5]Anatomisches Institut, Universität Bonn, 53115 Bonn, Germany. [6]Department of Biology, University of Massachusetts Boston, Boston, MA 02125, USA. [7]Universidad Católica de la Santísima Concepción, Concepción, Chile. [8]W.M. Keck Science Department of Claremont McKenna, Scripps, and Pitzer Colleges, Claremont, CA 91711, USA.
*Corresponding author. Email: martin.sander@uni-bonn.de (P.M.S.); em.griebeler@uni-mainz.de (E.M.G.); lschmitz@kecksci.claremont.edu (L.S.)

Analyses of the evolution of body size in independent lineages of pelagic amniotes offer the promise to improve the understanding of the patterns and processes of adaptation to life in marine environments. Repeated transitions from fully terrestrial to obligate marine habitats document how the anatomy and ecology of each lineage evolved in response to the shift from terrestrial to aquatic habitats. Recurring evolutionary patterns may suggest predictability of ecology as well as physiological constraints to maximum and minimum sizes (*4*, *5*). Ichthyosaurs and cetaceans are among the most prominent lineages to exemplify secondary aquatic adaptations. Both clades offer a well-suited model system to understand size evolution in secondary aquatic adaptation and in the sea in general (*2*).

As tail-propelled pelagic tetrapods, ichthyosaurs and cetaceans not only evolved convergent body shapes, lifestyles, physiologies, and feeding strategies as an adaptation to their habitat, but both lineages also evolved after the near-complete collapse of marine ecosystems. However, emerging evidence suggests different trajectories of body-size evolution in the two groups. Mysticetes shifted from gradual evolution of body size to rapid evolution of exceptionally large body sizes late in the history of the clade, concomitant with the extinction of small species. This pattern is presumed to have been facilitated by abundant resources and coastal upwelling (*6*). By contrast, the morphological disparity, the estimated evolutionary rates of discrete characters, and the evolution of skull size of ichthyosaurs all reached an early peak in the Triassic (*7*). The fast increases in disparity measures in early ichthyosaurs reflect rapid lineage diversification and dietary specialization (*8*), including the first aquatic raptorial tetrapod, *Thalattoarchon*, from the early Middle Triassic Fossil Hill Fauna of Nevada, USA (*8*). The presence of an orca-like predator suggested the emergence of food webs that are more similar to modern webs when compared with preceding Paleozoic webs.

However, the giant body sizes of filter-feeding mysticetes and suction-feeding sperm whales (*Physeter macrocephalus*) seemed out of reach for Early and Middle Triassic ichthyosaurs, especially given the absence of environmental indicators of high productivity such as diatoms, autotrophic dinoflagellates, and coccolithophores (*9*). By increasing the amount of energy available for the higher trophic levels of marine ecosystems, the evolution of these relatively large-bodied, planktonic, primary producers is considered to have been a critical precondition for the emergence of modern giants (*3*, *9*). By contrast, small-bodied plankton probably made up the bulk of the primary producers in Triassic oceans, thus limiting the amount of energy available to large-bodied species at higher trophic levels (*3*). By this logic, one would hypothesize that Triassic marine ecosystems should have fewer large species at high trophic levels than modern faunas.

In this contribution, we combine traditional paleontology with computational trait evolution and food web modeling to compare the patterns of body size evolution of ichthyosaurs and cetaceans in an ecological context (Fig. 1). We describe a new ichthyosaur from the early Middle Triassic Fossil Hill Fauna of Nevada, USA (*10*) as *Cymbospondylus youngorum* sp. nov. (Fig. 2) of giant body size (tables S1 and S2) from well-preserved material. The new ichthyosaur lived close to the beginning of Mesozoic marine reptile evolution as part of the recovery from the end-Permian mass extinction (Fig. 3) 252 million years (Ma) ago. The discovery reinforces the emerging pattern of rapid evolution of body size in ichthyosaurs, which, in contrast to cetaceans, must have experienced their most active phase of size evolution in their early evolutionary history, despite the absence of modern primary producers. We infer that the pelagic ecosystems of the early Middle Triassic (244 Ma ago) could, surprisingly, support several large tetrapod ocean consumers.

Systematic Paleontology

Reptilia Linnaeus, 1758 (*11*)
Diapsida Osborn, 1903 (*12*)
Ichthyosauria Blainville, 1835 (*13*)
Cymbospondylus Leidy, 1868 (*14*)

Type species

Cymbospondylus piscosus Leidy, 1868 (*14*)

Referred species

Cymbospondylus petrinus Leidy, 1868 (*14*); *Cymbospondylus buchseri* (*15*); *Cymbospondylus nichollsi* (*16*); *Cymbospondylus duelferi* (*17*); *Cymbospondylus youngorum* sp. nov.

Downloaded from https://www.science.org at Claremont Colleges Library on December 24, 2021

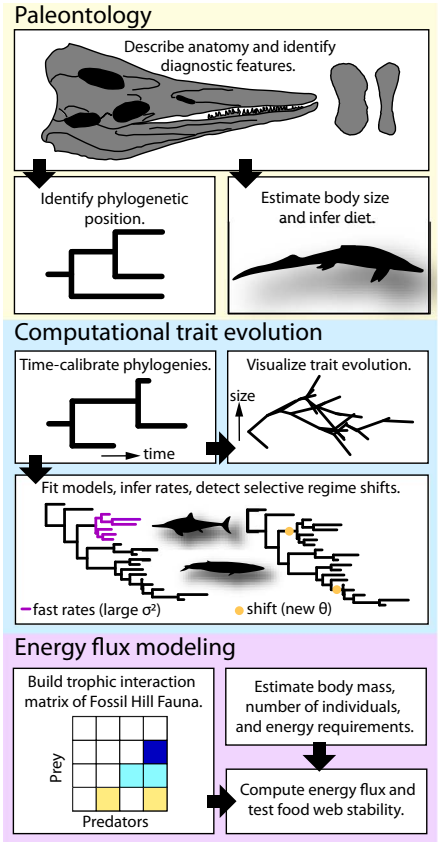

Fig. 1. Conceptual approach of our integrated study. We combine traditional paleontology with computational trait evolution and energy-flux modeling to study macroevolutionary patterns of body size evolution in marine amniotes.

Genus diagnosis

For a recent detailed diagnosis of the genus, see (*17*). In addition, the results of the phylogenetic analysis in this study offer an apomorphy-based diagnosis.

Cymbospondylus youngorum sp. nov. (Fig. 2 and figs. S1 to S5)

Etymology

The species is named in honor of Tom and Bonda Young.

Holotype and only specimen

LACM DI 157871 is the holotype and, as of now, the only recognized individual. LACM DI 157871 is largely articulated and complete from the anterior of the trunk region to the skull, preserved ventral side up. The cervical column back to the middle dorsal vertebrae is present with ribs in articulation. The shoulder girdle is articulated, and the two humeri are situated close to their respective glenoid. At present, the skull (Fig. 2, A to F; figs. S1 and S2; and table S1), the right humerus (Fig. 2, G to K), parts of the shoulder girdle (fig. S3), and some vertebrae are prepared (fig. S3)

Horizon and locality

LACM DI 157871 comes from the Anisian age Fossil Hill Member of the Favret Formation at Favret Canyon, Augusta Mountains, Pershing County, Nevada, USA. The type locality, LACM 8025, is on the northern slope of the rear of Favret Canyon at an elevation of 1676 m. Exact coordinates are on file at the repository. LACM DI 157871 originates from the same general level as the holotype of the macropredatory ichthyosaur *Thalattoarchon saurophagis* (*8*) and the pistosaur *Augustasaurus hagdorni* (*10*) in the lower third of the Fossil Hill member and pertains to the middle Anisian *Taylori* Zone (*18*).

Diagnosis

C. youngorum sp. nov. is diagnosed by a unique combination of the following eight characters (see data S1 for character descriptions and data S3 for a list of synapomorphies): squamosal, participates in supratemporal fenestra (character 72, state 0; Fig. 2); dentary, labial shelf present (character 117, state 1; fig. S2C); angular, extent of anterior lateral exposure is extensive, at least as high and anteriorly as the surangular's exposure (character 120, state 1; Fig. 2); angular, extent of posterior lateral exposure is extensive, with surangular exposure reduced to a thin strip on the lateral surface of the retroarticular process (character 121, state 1; Fig. 2); lower jaw glenoid, deeply excavated and present (character 126, state 1; Fig. 2); dentition, definition of the base of the enamel layer is well defined and precise (character 147, state 1; fig. S2, E and F); humerus, anterior flange is absent (character 200, state 0; Fig. 2 and fig. S6); and humerus, relative anteroposterior width in dorsal view, excluding dorsal and ventral processes, is approximately equal or the proximal end is wider than the distal end (character 206, state 1; Fig. 2 and fig. S6).

The new taxon is characterized by the following autapomorphies: a thick base of bone of attachment of the teeth (Fig. 2 and fig. S2, C and E), the distinctive shape of the scapula with a very large and wide dorsal blade and a narrow ventral part (figs. S3 and S6), the distinctive humerus morphology with a wider proximal than distal end, and a triangular proximal head and triangular shaft cross section (Fig. 2 and fig. S6). Note that these autapomorphies were not added as characters to our character matrix. A differential diagnosis and detailed anatomical descriptions (figs. S2 and S3) and comparisons (figs. S4 to S6 and tables S2 and S3) are provided in the supplementary materials (*10*).

Phylogenetic position

Phylogenetic analyses (*10*) (table S4) indicate that *C. youngorum* sp. nov. is nested within a clade of closely related *Cymbospondylus* species that account for much of the lineage diversity and morphological disparity of large-bodied Early and Middle Triassic ichthyosaurs (Fig. 3 and fig. S7). The close relationship of these species points to an adaptive radiation (as much as one can be recognized in the fossil record of Mesozoic reptiles). Further evidence for such a radiation is that there are no other four seemingly sympatric species of any ichthyosaur genus in the ichthyosaur record and that other finds of *Cymbospondylus* from the late Early and early Middle Triassic are widely distributed across the Northern Hemisphere (*16*).

Our analysis with TNT (a software for phylogenetic analysis) and its "new technology" search algorithm resulted in a tree length of 1225 steps. The four most parsimonious trees were retained (table S4), and the nearly fully resolved strict consensus of the four trees is shown in Fig. 3 and fig. S7. The consistency index of this tree is 0.259, coupled with a retention index of 0.627. The absolute Bremer support of the nodes varies from 1 to 5 (fig. S7). Additional analyses (table S4) confirmed the placement of LACM DI 157871 in a clade with other cymbospondylids, yet the position of the *Cymbospondylus* clade varies with the selection of taxa that were included in the analyses (*10*). We note that the interrelationships of ichthyosaurs remain difficult to resolve, both in the Triassic and the Jurassic part of the tree. This uncertainty reflects the difficulty in resolving ichthyosaur interrelationships in general (*19*) and the need for a concerted effort of redefining and rescoring characters.

Inferred diet and estimated body size

The conical, bluntly pointed tooth crowns of *C. youngorum* sp. nov., in conjunction with the elongate snout, suggest a generalist diet of fish and squid (*20*), as inferred for most ichthyosaurs from teeth and stomach contents (*21*). Considering its size, *C. youngorum* sp. nov. could also have preyed on smaller and juvenile marine reptiles (*10*). The right lower jaw of *C. youngorum* sp. nov. measures 1970 mm from the tip of the dentary to the end of the retroarticular process (table S1). At a total length of 1890 mm (table S1), the skull of LACM DI 15787 is one of the largest complete ichthyosaur skulls known. Although post-Triassic ichthyosaurs never reached the size of Triassic ones again (*7*), there are skulls of *Temnodontosaurus* from the Lower Jurassic of England and Germany (*22*) that are the same length as that of LACM DI 15787 within the limits of preservation. However, these large ichthyosaurs probably were less than 9 m long, having proportionally larger skulls (*22*). Larger skulls than those of LACM DI 15787 and these largest *Temnodontosaurus* specimens are only known from Late Triassic ichthyosaurs, specifically *Shonisaurus popularis* and *Shastasaurus sikanniensis*, with estimated skull lengths of 2750 and 3000 mm, respectively (*7*).

Humerus length is another commonly used proxy for ichthyosaurian body size [(*16*, *17*, *23*);

Downloaded from https://www.science.org at Claremont Colleges Library on December 24, 2021

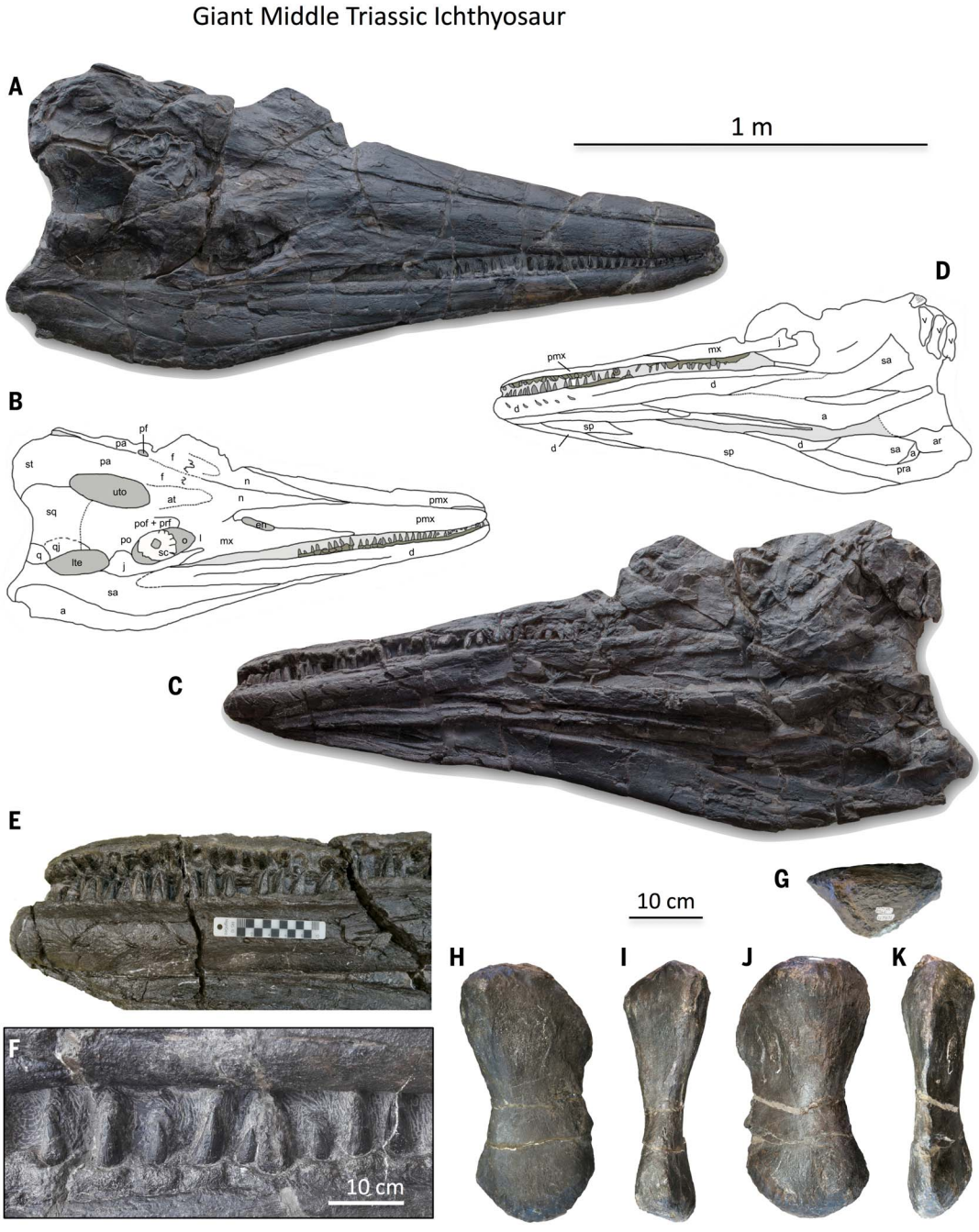

Fig. 2. Skull of the holotype of *C. youngorum* sp. nov. LACM DI 157871. (**A**) Skull in right dorsolateral view. (**B**) Skull sutures. (**C**) Skull in left ventrolateral view. (**D**) Skull sutures. (**E**) Snout in left ventrolateral view. (**F**) Middle part of dentary tooth row in right dorsolateral view. Note the bone of attachment. (**G** to **K**) Right humerus in proximal (G), dorsal (H), posterior (I), ventral (J), and anterior view (K). a, angular; ar, articular; at, anterior terrace; d, dentary; en, external nares; f, frontal; j, jugal; l, lacrimal; lte, lower temporal embayment; mx, maxilla; n, nasal; o, orbita; pa, parietal; pf, parietal foramen; pmx, premaxilla; po, postorbital; pra, prearticular; prf, prefrontal; q, quadrate; qj, quadratojugal; sa, surangular; sc, scleral ring; sq, squamosal; st, supratemporal; uto, upper temporal opening; v, cervical vertebra.

fig. S8A], even though it is available for fewer ichthyosaur taxa than skull length. At 453 mm, the humerus of the holotype of *C. youngorum* sp. nov. is the second largest ichthyosaurian humerus known, translating into a total length of 17.65 m (*10*). The lower 95% prediction interval of its length is 12.48 m; the upper 95% prediction interval is 24.96 m (*10*) (fig. S8A). We also estimated body mass based on a recent dataset for ichthyosaurs (*10*, *24*) (table S5). The regression function (fig. S8B) yielded a body mass estimate of 44,699 kg for the 17.65-m-sized LACM DI 15787 specimen (table S5). The lower mass based on the 95% prediction interval of both regressions is 14,712 kg (lower limit of the 95% prediction interval of body mass against length evaluated for 12.48 m); the upper mass is 135,809 kg (upper limit of the 95% prediction interval of body mass against length evaluated for 24.96 m). These body size metrics of *C. youngorum* sp. nov. result in one of the highest length and mass estimates for any ichthyosaur and the largest taxon of the Middle Triassic: Based on length and scaled-up mass data in Gutarra *et al.* (*24*), *S. popularis* from the late Carnian (about 230 Ma ago) was 13.5 m long and had a mass of 21,651 kg, whereas the middle Norian (about 212 Ma ago) *S. sikanniensis* was 21 m long and had an estimated body mass of 81,497 kg. Taken together, these length and mass estimates place ichthyosaurs in the range of body sizes of living cetaceans, but it appears that ichthyosaurs reached their largest sizes much earlier in clade history than whales.

The fossil record of body-size evolution

Despite the recent interest in ocean gigantism (*4*, *6*, *23*, *24*), detailed comparison of the evolutionary paths to giant body size in cetaceans and ichthyosaurs is lacking so far, as is a phylogenetically comprehensive analysis of

Downloaded from https://www.science.org at Claremont Colleges Library on December 24, 2021

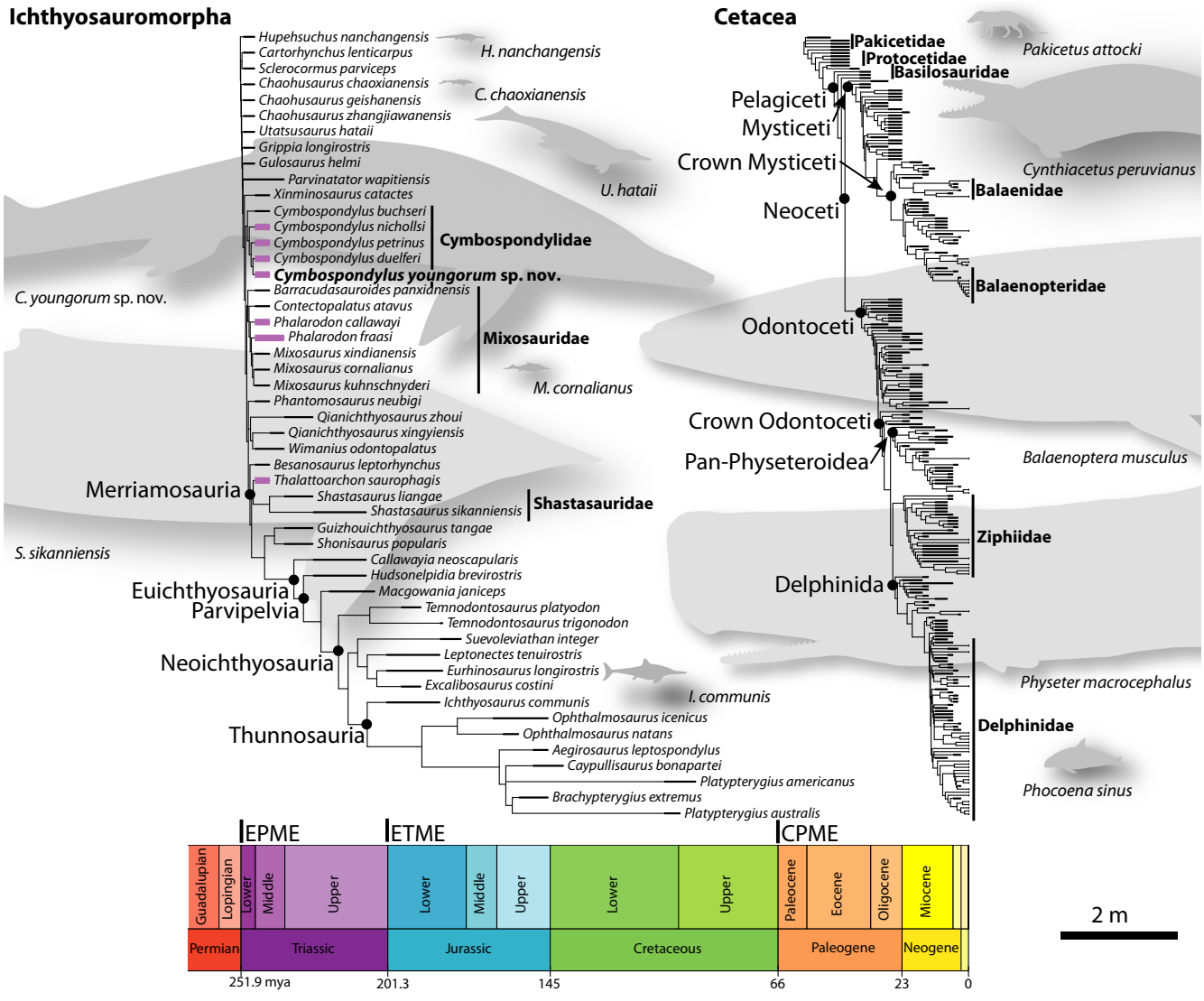

Fig. 3. Time-calibrated phylogenies and body-size illustrations of Ichthyosauria and Cetacea and the relationships of the new giant ichthyosaur *C. youngorum* sp. nov. Ichthyosaurs originated in the late Early Triassic shortly after the end-Permian mass extinction (EPME), survived the end-Triassic mass extinction (ETME), and went extinct in the early Late Cretaceous. Lilac stratigraphic ranges denote taxa from the Fossil Hill Fauna. Cetaceans originated in the late Paleocene after the Cretaceous-Paleogene mass extinction (CPME). See (*10*) for sources of phylogenies and table S6 for image credits. mya, million years ago.

body-size evolution in all Cetacea, including stem taxa (fig. S9). Both ichthyosaurs and cetaceans evolved after mass extinction events (Ichthyosauria after the end-Permian mass extinction event and Cetacea after the Cretaceous-Paleogene mass extinction; Fig. 3), with their respective terrestrial ancestors invading marine ecosystems that differed radically from those that existed before each mass extinction.

The early-branching members of both ichthyosaurs and cetaceans are small compared to later taxa, and both show aquatic adaptations, but to various degrees. The ichthyosaur *Cartorhynchus lenticarpus* from the Early Triassic had a skull length of 55 mm (*7*, *25*), whereas the skull of the cetacean *Pakicetus attocki* from the Eocene reached a width of 127 mm (*10*, *26*). The limbs of *C. lenticarpus* have been interpreted to allow limited terrestrial locomotion, where the cartilage-rich forelimb may have functioned analogously to seal flippers (*25*). The short trunk and snout may have been beneficial for terrestrial locomotion, whereas pachyostotic ribs added to the weight of the animals and perhaps helped with navigating surging water near shores (*25*). *Pakicetus* is interpreted to have inhabited freshwater systems, wading and swimming in shallow water similar to extant hippos, despite its terrestrially adapted limbs (*27*). Upward facing eyes are reminiscent of a crocodilian-like lifestyle at the water surface, enabling vision through air while being submerged in water [analogous to *Tiktaalik* (*28*)]. Increased bone mass through osteosclerosis, stable isotopes, and preferred diet inferred from tooth microwear (*27*, *29*, *30*) further corroborate an aquatic lifestyle.

A literal reading of the geologic time scale implies that body size evolved considerably faster in ichthyosaurs than in cetaceans. Fossils document a rapid size increase in ichthyosaurs from *Cartorhynchus* (55-mm skull length) in the Olenekian at 248.5 Ma ago (*25*) to *C. youngorum* sp. nov. (1890-mm skull length) a mere 2.5 Ma later. Fossils record slower evolution of body size in cetaceans, for example, from *P. attocki* (127-mm skull width) in the late Ypresian (*10*, *26*) to *Basilosaurus isis* (600-mm skull width) in the Priabonian [(*10*) and data S5] 10 to 14 Ma later, and in odontocetes, from *Simocetus rayi* (238-mm skull width) in the Rupelian [(*10*) and data S5] to *Livyathan melvillei* (1970-mm skull width) in the Tortonian [(*10*)

Downloaded from https://www.science.org at Claremont Colleges Library on December 24, 2021

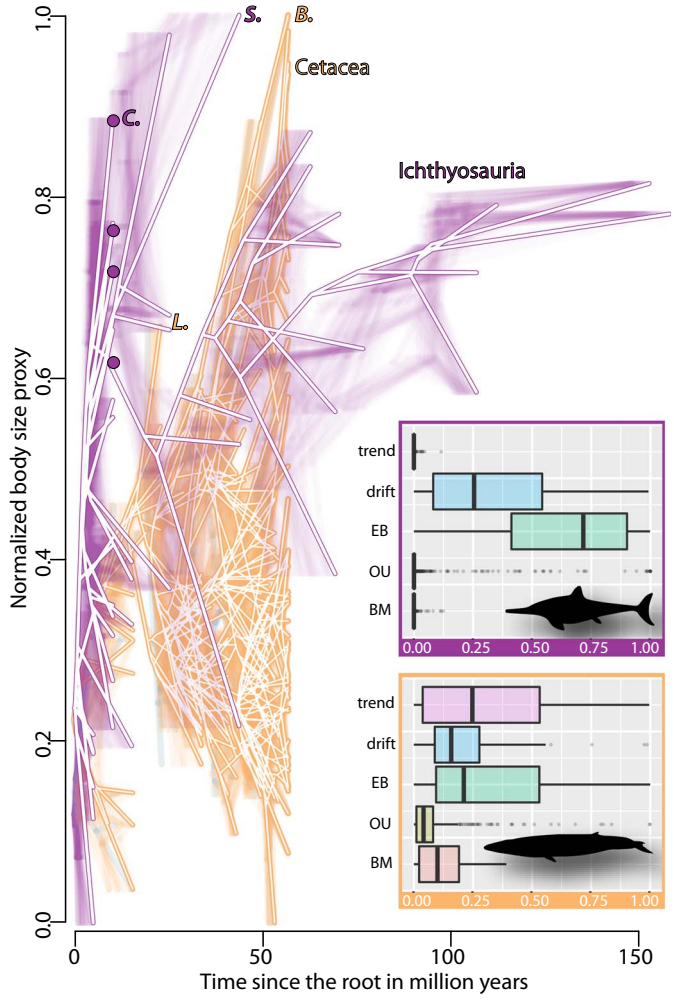

Fig. 4. Body-size evolution in ichthyosaurs and cetaceans compared. Traitgram of body size, normalized such that 0 corresponds to the smallest body size in each group and 1 to the largest for ichthyosaurs (lilac; based on an early-burst model) and cetaceans (ochre; based on a Brownian motion model) (see Methods). Lilac dots indicate *Cymbospondylus* species from the Fossil Hill Fauna. B., *Balaenoptera musculus*, blue whale; C., *C. youngorum* sp. nov.; L., *Llanocetus denticrenatus*, early giant baleen whale; S., *S. sikanniensis*, the largest named ichthyosaur. The inset shows model-fitting results expressed as Akaike weights for five different evolutionary models from 1000 iterations. Boxes represent the interquartile ranges (IQRs), with whiskers extending 1.5 times the IQR outside the boxes. Vertical lines inside the boxes show the median. BM, Brownian motion; EB, early burst; OU, Ornstein-Uhlenbeck.

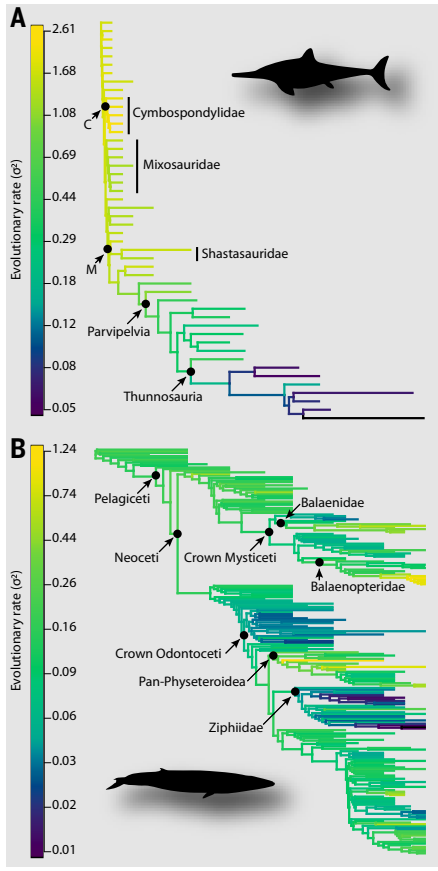

Fig. 5. Exploration of the rate heterogeneity of body-size evolution. (**A** and **B**) Ichthyosaurs (A) feature the fastest rates of body evolution early in their history, whereas cetaceans (B) show a more complex pattern, with fastest rates occurring in later stages of their history. C, Cymbospondylidae; M, Merriamosauria.

and data S5] more than 25 Ma later. These examples illustrate the short time spans of size increases in ichthyosaurs compared with those of cetaceans, but does this pattern hold when analyzed in the context of time-calibrated phylogenies?

Computational modeling of body-size evolution

We first compared the evolutionary patterns of body-size evolution through traitgrams that account for the uncertainty tied to the time calibration of the phylogenies (*10*). These evolutionary traitgrams of ichthyosaur and cetacean body sizes, normalized to maximum body size to enable a better comparison of the pattern, reinforce the notion of fast body-size evolution in ichthyosaurs (Fig. 4). The maximum body size of ichthyosaurs increased dramatically early in their history, whereas cetacean maximum body size increased up to the present day. In our clade-wide model-fitting approaches, the early-burst and trend models are strongly preferred over all other evolutionary models for ichthyosaurs [Fig. 4 and fig. S10; see (*10*)]. By contrast, no strong preference is indicated for any particular model in cetaceans (Fig. 4). Resampling of the cetacean dataset to adjust for differences in sample size, trophic specialization, and the mixture of fossil and extant data did not reveal strong support for an early-burst model (see fig. S11). When restricting the cetacean dataset to the Pelagiceti to account for the differing degrees of aquatic adaptation in the early-branching lineages, an early-burst model is slightly preferred over the others tested (see fig. S11), but the pattern is not nearly as strong as for ichthyosaurs.

To explore the evolutionary patterns at smaller phylogenetic scales and therefore avoid problems related to the impact of taxon selection, we assessed the heterogeneity of the rate of body-size evolution across both the ichthyosaur and cetacean trees (Figs. 5 and 6 and fig. S12). Models that allow for rate heterogeneity can identify specific regions of the tree that signify evolutionary changes and thus circumvent the problem of a clade-wide approach that would ignore the various degrees of aquatic adaptations in the early ichthyosaurs and cetaceans.

Results from a variable-rate model based on Brownian motion, which uses penalized likelihood to estimate the evolutionary rates along all branches in the tree (*31*), support fast evolution of body size in early ichthyosaurs (Fig. 5A). In congruence with observations from the fossil record and clade-wide model fitting, the highest evolutionary rates are found in the

Downloaded from https://www.science.org at Claremont Colleges Library on December 24, 2021

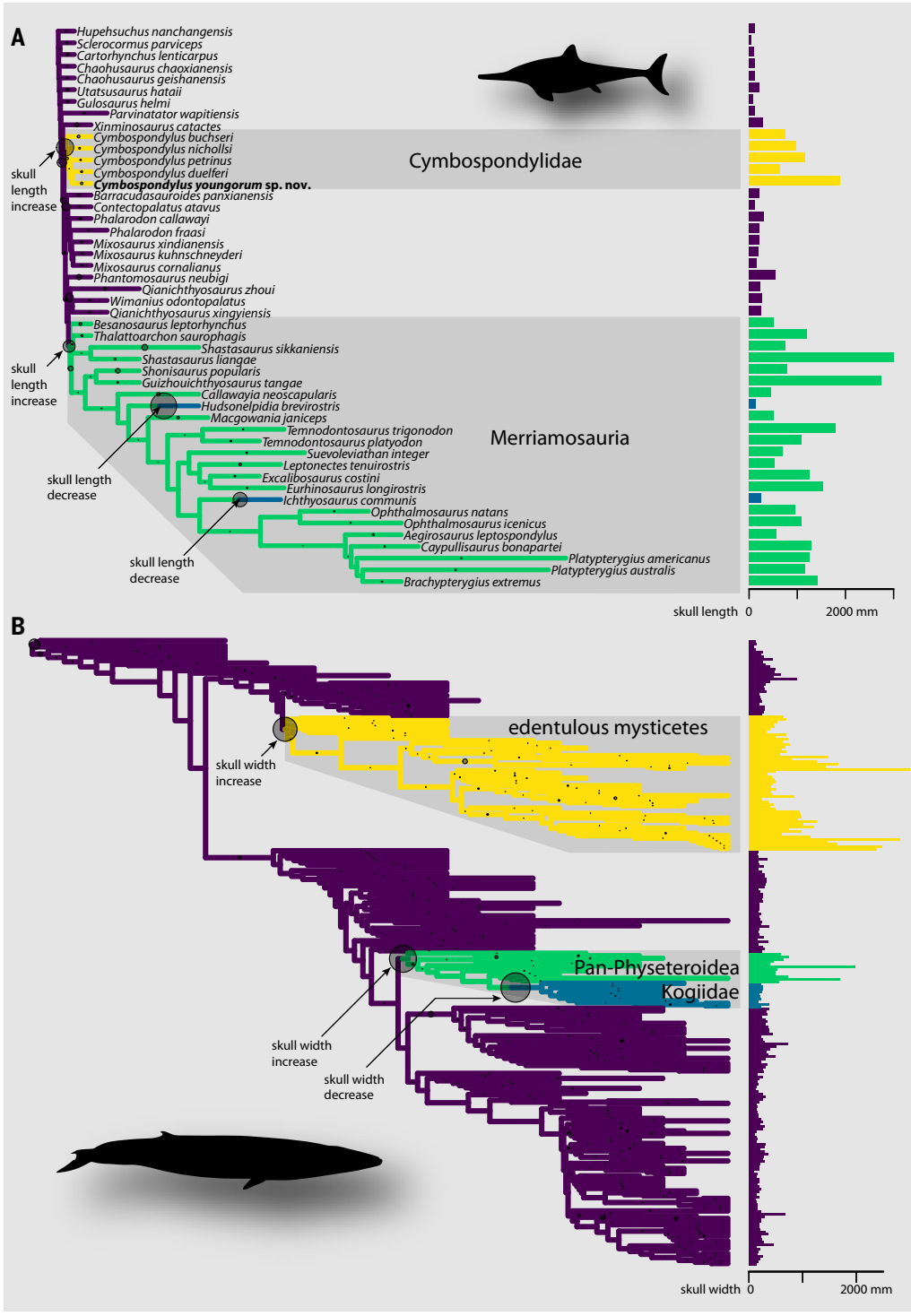

Fig. 6. The adaptive landscape of body-size evolution. (**A** and **B**) Ichthyosaurs (A) feature two early adaptive shifts toward larger skull length, whereas cetaceans (B) entered selective regimes that promoted larger skull width much later in their evolution.

deep regions of the ichthyosaur tree, with some indication that fastest size evolution may have occurred in cymbospondylids and the early phase of merriamosaurs (Fig. 5A). After the initial burst, the estimated evolutionary rates slowed over time.

The distribution of evolutionary rates in the cetacean tree forms a stark contrast to the ichthyosaur pattern (Fig. 5B). The deep parts of the cetacean tree feature average rates. Surprisingly, the body size of both early crown mysticetes and odontocetes evolved slowly, before accelerating in two clades of mysticetes with living representatives, the Balaenidae (right and bowhead whales) and Balaenopteridae (rorquals), as found in a previous study (*6*). Among odontocetes, the fossil lineages of the Pan-Physeteroidea, in particular, a clade that contains living sperm whales, are characterized by fast rates, whereas Ziphiidae (beaked whales) have comparatively slow rates of size evolution (Fig. 5B).

Whereas rate heterogeneity models can identify phases of fast and slow morphological evolution, the determination of the direction of evolution, that is, evolution toward larger and smaller body sizes in specific lineages,

Downloaded from https://www.science.org at Claremont Colleges Library on December 24, 2021

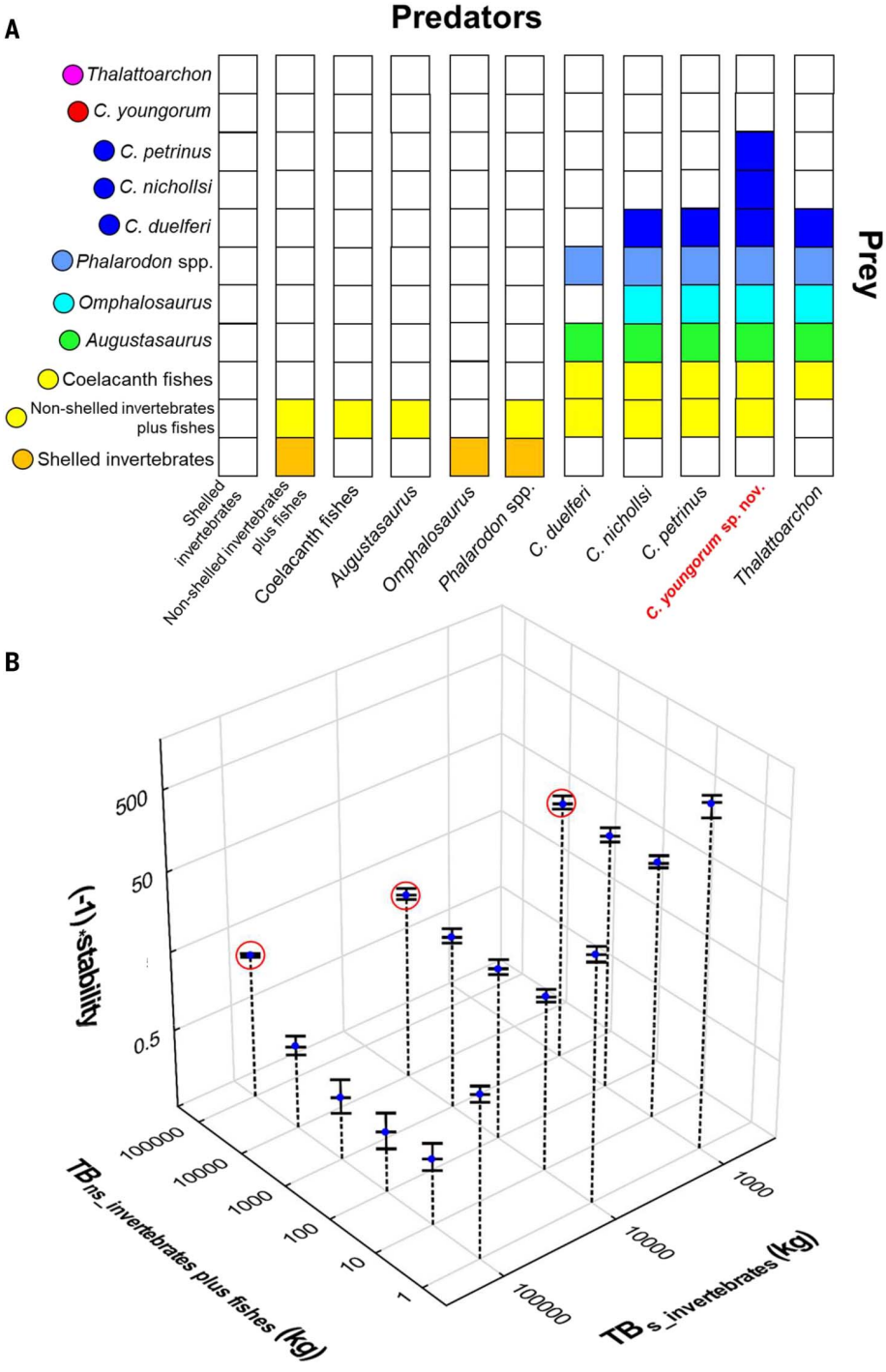

Fig. 7. Energy-flux model and food web stability. We tested whether the food web as preserved is functional and stable over ecological time. All shelled invertebrates (specifically ammonoids), fish, and amniote taxa discovered in the Fossil Hill Fauna are modeled as members of a food web. The member "shelled invertebrates" is basal to the food web and comprises primarily ammonoids but also halobiid bivalves and crustaceans. The member "nonshelled invertebrates plus fishes" ("fish") pools coleoid cephalopods such as squid and small- to medium-sized fish. See Methods and table S11 for food web members and their body masses, total biomasses, and energetic demands. (**A**) Trophic interaction matrix used for modeling energy-flux across members. Stacked bars represent the diet of predatory taxa. Filled squares within bars indicate that a taxon is taken by the predator, whereas white indicates that it is not. (**B**) Stability values calculated by the model for different combinations of total biomass of the two food web members "shelled invertebrates" and "fish." More negative stability values indicate a more stable food web. Error bars for blue dots represent model results assuming maximum and minimum body mass estimates for ichthyosaur taxa (table S11). Greater body masses result in less-stable food webs than smaller body masses. Stability values of extant food webs range between −10 and 0 (*41*). Note that we multiplied stability values by −1 for plotting. TB, total biomass (kg); red circles, the total biomass of "shelled invertebrates" equals that of "fish."

requires complementary approaches. We chose a Bayesian implementation of the Ornstein-Uhlenbeck model of trait evolution (*10*, *32*) to infer whether and when adaptive shifts of body size occurred through evolutionary time and whether smaller or larger body sizes were selected for in the new regime (Fig. 6 and fig. S12). Analyses of the selective regime also enable an evolutionary definition of giants and dwarfs. Adaptive shifts toward larger body size define clades comprising giants, with evidence for selection of larger body sizes, whereas shifts toward smaller body sizes identify dwarfs.

Analyses of the selective regime provide support for two independent shifts toward larger body sizes early in the evolution of ichthyosaurs, defining two clades of giants. One shift toward larger size is reconstructed for the branch leading to the Cymbospondylidae with *C. youngorum* sp. nov., and another shift is placed on the branch leading to the Merriamosauria (Fig. 6A). Both selective regime shifts thus occurred around the boundary between the Early and Middle Triassic. Shifts toward regimes selecting smaller body sizes were inferred for the *Hudsonelpidia brevirostris* and *Ichthyosaurus communis* tip branches (Fig. 6A).

In cetaceans, the geologically oldest shift toward a regime selecting larger body sizes occurred in the late Eocene (Fig. 6B), coinciding with the loss of functional teeth in some lineages of mysticetes (*33*). The Pliocene accelerations of body-size evolution in crown mysticetes are not detected as distinct adaptive

Downloaded from https://www.science.org at Claremont Colleges Library on December 24, 2021

shifts. However, a second shift toward the evolution of large body sizes occurred in the Oligocene, fitted to the branch leading to the Pan-Physeteroidea, which evolved a raptorial feeding mode by the middle Miocene (i.e., *Brygmophyseter shigensis*). An evolutionary reduction of body sizes is inferred for the Kogiidae, a clade nested within the Pan-Physteroidea, with two living species, *Kogia breviceps* and *Kogia sima*, the pygmy and dwarf sperm whales, respectively. Another shift toward smaller body-size evolution may have occurred early in the history of cetacean evolution, in the pakicetids, yet the support for this regime shift is not nearly as strong as the other three identified shifts (Fig. 6B).

Estimates of the phylogenetic half-life [see Methods and (*10*)] suggest that ichthyosaur body size evolved an order of magnitude faster than cetacean body size when entering a new selective regime. Ichthyosaurs thus evolved large body sizes very quickly and very early on in their evolution (Fig. 4 and fig. S10), in oceans thought to be less favorable for large-bodied ecosystem members at higher trophic levels (*9*). Intriguingly, many Cymbospondylidae, which constitute one of the two shifts toward large body sizes, were present in the same assemblage, the Fossil Hill Fauna from the Fossil Hill Member of the Favret and Prida formations of northern Nevada, USA, including *C. youngorum* sp. nov.

The composition of the Fossil Hill Fauna of Nevada

The Favret Formation of the Augusta Mountains (fig. S13), Nevada, USA, spans the middle to late Anisian (Middle Triassic), a period covering more than 2 Ma (*34*). The Fossil Hill Member itself (fig. S13) is a black shale unit of variable thickness deposited in anoxic bottom waters below the storm wave base (*35*). Surface waters were well aerated and must have supported marine reptiles and abundant ammonoids and other invertebrates (*18*, *35*), but there was no benthic life, with the possible exception of halobiid bivalves. The fossils found in the unit thus represent a pelagic ecosystem and food web.

Fish fossils are only rarely preserved (*8*, *10*), but a diverse chondrichthyan fauna (*36*) from just below the Fossil Hill Member suggests that their rarity is due to preservational bias. Comprising eight taxa, the most common marine reptile fossils of the Fossil Hill Fauna are ichthyosaurs (table S10), making it the most speciose ichthyosaur fauna known. Sauropterygia are only represented by a single taxon, the pistosauroid *A. hagdorni* (*8*), in stark contrast to the rich record of sauropterygian fossils from the Tethys Middle Triassic (*37*). Among the ichthyosaurs, *C. youngorum* sp. nov. stands out because of body size, *T. saurophagis* as the oldest apex predator among secondarily aquatic amniotes (*8*), and the holotype of *C. duelferi* (*17*) as the geologically second-oldest gravid ichthyosaur. There are two more large *Cymbospondylus* species (table S3), *C. petrinus* (*38*) and *C. nichollsi* (*16*). Two species of small ichthyosaurs (*Phalarodon fraasi* and *P. callawayi*) differ in the extent of their crushing dentition (*39*). The enigmatic medium-sized *Omphalosaurus* (*40*) is interpreted as a specialized ammonoid feeder (*10*). Notably, filter feeders appear to be absent from the Fossil Hill Fauna.

The enormous size range of marine amniotes in the Fossil Hill Fauna (table S11) rivals the size range seen in modern marine mammal faunas. This range is perplexing given that Middle Triassic oceans lacked the high productivity that is thought to sustain such ecosystems today (*9*). We therefore turned to a new approach in paleontology, energy-flux modeling, to explore whether the Fossil Hill Fauna, as preserved in the fossil record, was a stable food web.

Energy-flux modeling

To test for the stability of the trophic network in the Fossil Hill Fauna, we modeled energy flux with a new tool implemented in R and derived from quantitative ecosystem ecology, "fluxweb" (*41*), which is based on allometric trophic network theory (*42*) and estimates energy fluxes in a top-down approach. In our new implementation for the fossil ecosystem, the model input is preserved taxa and census data and their estimated body masses, energy demands (table S11), and potential prey (Fig. 7A and fig. S14A) (*10*). This tool assesses the food web's stability as the smallest equilibrium total biomass of all modeled food web members by applying a predator-prey multispecies model. Small-shelled invertebrates, including ammonoids, represent the trophically basal member of the food web in the model. The small-shelled invertebrates provide energy directly or indirectly to all trophically higher food web members.

We found that the Fossil Hill food web, with its high phylogenetic diversity and morphological disparity of large to giant endothermic (*10*) ichthyosaurs, was indeed stable (Fig. 7B and fig. S16A). The preserved ammonoids alone provided sufficient energy to the food web as recorded by the fossils (fig. S16C and table S12). Sensitivity analyses demonstrate that the results of the energy-flux model are robust with respect to errors in body mass estimates for ichthyosaurs (figs. S16 and S17) and basal shelled invertebrates (fig. S15) and do not hinge on the assumption of ichthyosaurian endothermy (figs. S15 and S18). Thus, the primary production in the middle to late Anisian was sufficient to support the Fossil Hill food web, including the giant ichthyosaur *C. youngorum* sp. nov. The stability of the Fossil Hill Fauna is also consistent with the lack of pre-Triassic ichthyosaur fossils and the notion that gigantism in ichthyosaurs evolved rapidly in the first few million years of their known history because no hidden Permian history of the clade needs to be invoked (*43*).

The results from our energy-flux model challenge the hypothesis of energetic limitation of maximum body size in Mesozoic food webs (*9*) and provide insights into the functioning of a trophic network without modern primary producers. An important functional characteristic of food webs is the production rate, which is the energy that an individual stores in its body plus the energy that it allocates to reproduction, normally about one-quarter of its basal metabolic rate (*44*). Thus, the sum of the production rates of all individuals in a given trophic level defines the energy that can be transferred to the next level. Our estimates for the production rate of the preserved ammonoid population is congruent with the average production rate of multiple invertebrate species and several modern marine ecosystems (tables S12 and S13). Given that the primary producers of Mesozoic food webs were less productive than their modern equivalents (*9*) and that the trophic level of the largest ichthyosaurs equaled that of the largest living marine carnivores (*8*) and assuming that the energy losses between trophic levels had been the same as those in modern marine ecosystems, the Fossil Hill food web must have had shorter food chains than modern marine food webs.

Although the inferred production rate of all vertebrates in the Fossil Hill Fauna is similar to modern marine ecosystems (table S13), the contributions to this rate by nonamniotes and amniotes differ substantially. The production rates of modern marine amniotes (cetaceans, pinnipeds, birds) are about two magnitudes smaller than the inferred rates for the Fossil Hill Fauna (marine reptiles; table S13), whereas the rates of modern nonamniotes are up to two magnitudes larger than the modeled rates of nonamniotes from the Fossil Hill Fauna (table S13). In comparison to modern marine food webs, the trophic network of the Fossil Hill Fauna was thus dominated by marine amniotes, unlike modern marine food webs that are dominated by nonamniotes. Thus, ichthyosaurs likely occupied niches that are held by fish and whales in modern ecosystems. However, compared with their energetic demands, modeled production rates of the largest ichthyosaur species are small (table S14) and suggest that their densities were lower than suggested by the Fossil Hill Member census.

Comparison of the production rate of preserved ammonites with that modeled for the member "invertebrates" reveals an untapped

Downloaded from https://www.science.org at Claremont Colleges Library on December 24, 2021

energy surplus (fig. S16C and table S12). This surplus may indicate that the food web of the Fossil Hill Fauna as now known is incomplete, perhaps lacking a bulk feeder or other taxa yet to be discovered. Alternatively, the energy surplus actually was untapped in the rather young Fossil Hill food web, being only a few million years old, and consumers of the surplus might have been added in the course of evolution later. Our energy-flux modeling indeed shows that the food web could have supported another giant marine amniote, if it fed in bulk low in the food chain (fig. S19), for example, by filter feeding (*4*). This mode of life possibly arose later in ichthyosaurs, as suggested by the existence of some Late Triassic giant toothless ichthyosaurs (*45*). Filter feeding is important in modern marine vertebrates, for example, baleen whales, the whale shark *Rhincodon typus*, and the basking shark *Cetorhinus maximus* (*46*). Even with a giant bulk feeder, the estimated energy flux from the trophic group comprising the shelled invertebrates passed on to higher trophic levels is still smaller than the estimated amount of energy provided by the preserved ammonoids (figs. S20 and S21 and table S13). Whereas there is no fossil evidence for a filter-feeding ichthyosaur in the Fossil Hill Fauna yet, the results of the energy-flux model demonstrate that this fauna was not only stable but, with its abundant ammonoids and short, amniote-dominated food chains, also set the environmental stage that led to the evolution of large body sizes early on in the evolution of ichthyosaurs.

Implications for body-size evolution of marine amniotes

The appearance of marine amniotes in the Triassic followed on the heels of amelioration of environmental conditions in the first 2 Ma of the Triassic together with a general recovery of marine ecosystems (*47*, *48*). At an estimated body mass of more than 40 tonnes and a geologic age of 246 Ma, *C. youngorum* sp. nov. was a giant marine amniote, attaining a body size comparable to that of today's ocean giants. This new giant may even have approached the size of today's largest cetacean *Balaenoptera musculus* (total length: mode of 25 m) [dataset in (*46*)], given that the Fossil Hill energy-flux model remained stable when we performed the analysis with the upper limit of the body-mass estimate of *C. youngorum* sp. nov. (24.96 m, 135,809 kg). On land, equivalent body masses did not evolve until >40 Ma later, among sauropod dinosaurs of the Jurassic. Apparently, the pelagic environment may be more conducive to the evolution of giant tetrapods. Alternatively, ecosystem recovery from the end-Permian extinction was much slower on land than in the sea. In the sea, only other ichthyosaurs in the Late Triassic and cetaceans since the late Paleogene (38 Ma ago) reached this body size again. The discovery of a giant ichthyosaur so early in the phylogenetic history of the clade underscores the existence of major selective advantages of large body size (*49*).

The Fossil Hill Fauna records a surprisingly diverse and morphologically disparate fauna of large-bodied to giant ichthyosaurs shortly after the end-Permian mass extinction. Unlike the contemporaneous faunas from the western Tethys and China, which are representative of shallow seas on continental shelves, shallow basins, and lagoons (*50*), the Fossil Hill Fauna provides a glimpse into the pelagic habitats of the Middle Triassic. We propose that ichthyosaurs initially benefited from the rapid recovery of conodonts (*51*) and pelagic ammonoid cephalopods (*47*), permitting giant body size soon after oceanic geochemical conditions had stabilized in the Middle Triassic (*48*). Ichthyosaurs may have been able to increase the total amount of resources available to them by virtue of their large eyes (*52*). Large eyes improve the range from which prey can be detected in the clear water of the pelagic realm, both in well-illuminated water near the surface and at greater depth (*53*). Proportionately large eyes seem to have evolved very early in the evolutionary history of the group (*52*), possibly enabling ichthyosaurs to better exploit their food resources. Their energetically costly endothermy could have increased their foraging capacity (speed and success) and energy intake in cold-water habitats, as found in colder geographic regions or in deeper waters (*54*). Mesothermy, which enabled body temperatures intermediate to those of ecto- and endotherms, was important in the evolution of elasmobranch gigantism (*55*).

We have identified two major evolutionary pathways to large body size in cetaceans. Size evolution in odontocetes may be linked to the evolution of raptorial feeding mode in some taxa and deep diving in others (*4*, *56*). Raptorial feeding is one of the drivers for the independent evolution of large body sizes in different clades. This is further evidenced by the earliest inferred raptorial feeder, *Ankylorhiza tiedemani*, which is considered to be the largest Oligocene odontocete with an estimated body length of 4.8 m (*57*), and in the extant delphinid *O. orca*. The evolution of echolocation, which allowed odontocetes to forage at greater depths in search of cephalopods unavailable to early cetaceans lacking a biosonar, is not directly coupled with evolution of size. Biosonar evolved more than 14 Ma before our reconstructed shift toward larger body sizes in the pan-physesteroids (*58*). In mysticetes, the initial shift toward large body sizes coincides with a loss of functional teeth in some lineages of mysticetes and presumably a switch of diet preference. In addition to evolving bulk-feeding adaptations, gigantism in mysticetes appears to be driven by global oceanic changes, particularly over the past few million years, which affected prey distribution and density (*6*, *59*). *C. youngorum* sp. nov. thus demonstrates that the lack of carbon sinks and modern primary producers is not a prerequisite for gigantism [contra (*9*)], challenging the notion that changes in ocean productivity and ecological escalation are necessary preconditions for the evolution of giant body size. Although both cetaceans and ichthyosaurs evolved very large body sizes, their respective evolutionary trajectories toward gigantism were different.

Methods

Phylogenetic analysis of ichthyosaurs

We scored the holotype specimen of *C. youngorum* sp. nov. (LACM DI 157871) into the character matrix of (*17*). This matrix (*17*) had been modified from other recent work (*7*, *60*) and appeals because the character descriptions are drawn from many different sources. We could score 40% of the 287 characters in the matrix with confidence for the new taxon (data S1) but note that many characters in this list were initially defined for post-Triassic ichthyosaurs. We edited the character-taxon matrix with Mesquite v. 3.02 (*61*). Our primary analysis (analysis I; Fig. 3 and fig. S7) included the taxon set of (*17*) with *C. youngorum* sp. nov. added (totaling 60 taxa) and was performed with TNT (*62*) using both "new technology" (search parameters: xmu=hit 20 drift 10) and "traditional" searches. See table S4 for statistics of this and the following analyses. To test for the influence of taxon sampling on the phylogenetic relationships, we used a reduced taxon set with a focus on Triassic ichthyosaurs (analysis II). This reduced taxon set is equivalent to the list of taxa used in (*63*) with the addition of *C. duelferi* and *C. youngorum* sp. nov. Note that we did not use the taxon-character matrix of (*63*), only the same taxa (data S2). A further modification was that we included three representative parvipelvians (*H. brevirostris*, *I. communis*, and *Stenopterygius quadriscissus*), instead of a clade Parvipelvia as in (*63*), to represent this derived clade (analysis III). Finally, we analyzed this matrix with PAUP* 4.1b (*64*) on a Mac computer (analysis IV). Using the heuristic search algorithm and 1000 replicates, 308 most parsimonious trees (MPTs) of 843 steps in length were retained (table S4). The strict consensus was poorly resolved, but the 50% majority rule consensus of these 308 trees shows the same topology as that found by TNT using the same matrix.

The major difference between the four analyses is in the placement of the *Cymbospondylus* clade. The analyses of the modified Klein *et al.* (*17*) taxon set (analyses I and II) recover the clade as earlier branching than, or in a trichotomy with, mixosaurids. The TNT analyses of the

Downloaded from https://www.science.org at Claremont Colleges Library on December 24, 2021

modified Huang *et al.* (*63*) taxon set (analysis III) finds *Cymbospondylus* as later branching than mixosaurids and the Carnian *Toretocnemus*, *Qianichthyosaurus*, and *Californosaurus*. The PAUP analysis (analysis IV) finds the genus as later branching than the Carnian *Toretocnemus* and in an unresolved trichotomy with the Carnian *Qianichthyosaurus* and *Californosaurus*. Because the first analysis (analysis I) is the most conservative in showing the greatest similarity with recently published analyses of Triassic ichthyosaurs (*17*, *63*) and has a fully resolved strict consensus and a low number of MPTs (table S4), we consider analysis I to be our preferred hypothesis (data S3).

Total length estimate for LACM DI 157871

Of the commonly used body-size proxies—total length, skull length, humerus length, and body mass—only two, skull length and humerus length, can be directly measured in LACM DI 157871 and the other two must be estimated. We estimated the total body length of LACM DI 15787 from its humerus length after having conducted a revised regression analysis on a published dataset for Triassic ichthyosaurs (*23*) (fig. S8A and table S5). Contrary to Scheyer *et al.* (*23*), we log10-transformed total body length and humerus length before linear regression analysis, related body length to humerus length, and calculated 95% prediction intervals around the regression line (fig. S8A). This regression analysis was conducted in the software R, version 3.5.2 (*65*).

Body-mass estimates for the Fossil Hill Fauna ichthyosaurs

To estimate body mass of *C. youngorum* sp. nov. (as represented by LACM DI 15787) and the other ichthyosaur species in the Fossil Hill Fauna from total length, we generated a new dataset of body masses for Triassic ichthyosaurs (table S5) for a regression analysis of body mass on total body length (fig. S8B). This new dataset is based on a published compilation of the total body lengths of selected ichthyosaur fossil specimens (*24*). This publication further provides species-specific reference body masses for 1-m-long digital models of these fossils. To estimate body mass for each of the ichthyosaurs in the dataset (table S5), we used the respective reference mass (*24*) for each and up- or down-scaled its body mass to total body length. Note that we excluded the Jurassic ichthyosaurs from consideration because of their different body shape. After having log10-transformed total body length and body mass data from table S4, we carried out a linear regression analysis (fig. S8B) that again includes 95% prediction intervals. This regression analysis was conducted in the software R, version 3.5.2 (*65*).

Phylogenetic hypothesis for cetaceans

To look into body-size evolution in cetaceans, we compiled a comprehensive phylogeny with a special focus on early whales. This phylogeny (fig. S9) includes 250 taxa from the earliest cetaceans to representative extant species. Most large morphological or combined phylogenetic analyses of cetaceans derive from the character state matrix first published by Geisler and Sanders (*66*), with modifications made in subsequent works (*10*). However, taxon sampling in those large data matrices tends to fall short for specific groups (e.g., Ziphiidae, Pan-Physeteroidea). To have a more complete taxon sampling represented in our tree, we used the results of morphological analyses using character state matrices with less taxa, but with a more thorough sampling for specific groups, for example, for Pan-Physeteroidea (*10*). Our phylogeny is thus a combination of the results of several analyses using a variety of different morphological matrices. Although taxon sampling sometimes varies among these works, the relationships between different cetacean groups are generally stable and consistent.

The topology of our composite phylogeny agrees well with a new, comprehensive phylogenetic hypothesis presented in a recent study (*67*) regarding the position and relationships of major clades, only differing in a few minor regards. The first is that our taxon sampling is smaller, in large part because we prioritized the inclusion of species for which proxy data for body size (i.e., bizygomatic width or orbital and postorbital width) were available. Because of this requirement, we did not include *Himalayacetus subathuensis*, which is considered as the earliest cetacean, because the specimen consists of an incomplete mandible (*68*) and instead chose *P. attocki* as our earliest cetacean, which is known from more complete cranial material (*26*). The topology of Lloyd and Slater (*67*) differs from ours by having a polytomy amongst some of the more basal mysticetes (i.e., *Llanocetus denticrenatus*, *Mystacodon selenensis*). Our topology differs in the more inclusive definition of Aetiocetidae that includes *Borealodon osedax* and *Aetiocetus* (*Niparajacetus*) palmadentis, following (*69*). Concerning the odontocete section of the phylogeny, we are using a more inclusive Platanistoidea and Kentriodontidae (*70*, *71*). These differences largely derive from the analyses we used to construct our phylogeny but do not affect our results.

Time calibration of phylogenies

We used stratigraphic ranges at the stage level to time-calibrate the phylogenies (*10*). First and last appearance dates of taxa were defined as the beginning and end of each geologic stage in which the tip taxon is found (data S4 and S5). The geologic age in million years for each stage was taken from Walker *et al.* (*34*). The time calibration of the trees was performed using the R package "paleotree" (*10*) (data S6). Given that the stratigraphic occurrence of many ichthyosaurs and fossil cetaceans is not well defined, we used the most simplistic a posteriori dating approach, implemented in the "timePaleoPhy" function of "paleotree." The initial root ages were set to 251.9 and 56 Ma ago for ichthyosaurs and cetaceans, respectively. We generated sets of time-calibrated trees with the "equal" method (*10*) combined with the "minMax" option. Polytomies were resolved randomly, and for each random resolution, an internal branch length of 1 Ma was added to the tree. This is an arbitrary but, we think, reasonable estimate given the overall tree height of the clades we were working with. For plotting (Fig. 4) and applying methods that allow heterogeneity of parameters across the tree, we also generated trees with the "firstLast" setting, with terminal edges added. The "firstLast" option treats the stratigraphic bins as hard constraints. Trees shown in Fig. 4 were time calibrated with the "DatePhylo" function of the R package "strap" (*10*), also using the "equal" method, and then plotted against the geologic time scale with the "geoscalePhylo" function. The resulting time-calibrated trees for ichthyosaurs agree well with previously published phylogenies for the group, and our cetacean tree generally agrees with those of McGowen *et al.* (*72*) and Lloyd and Slater (*67*). Our divergence estimates for major clades are sometimes a few million years older (e.g., Balaenidae), younger (e.g., Balaenopteridae), or nearly identical (e.g., Pan-Physeteroidea). Such discrepancies likely reflect differences in taxon sampling and time-binning methods (*10*).

Computational analysis of body-size evolution summary

We chose skull-related metrics because skull width (bizygomatic width) is an established size proxy in cetaceans [e.g., (*73*)], as is skull length in ichthyosaurs (*7*). We used the latter dataset for ichthyosaurs, including some additional data from the recent literature and this study (data S4). Specifically, we added the skull length of two more species of *Chaohusaurus*, *C. chaoxianensis* and *C. zhangjiawanensis*, among Early Triassic taxa. Note that the specimen of *C. chaoxianensis* that provides the skull length has recently been assigned to a new species, *C. brevifemoralis*, sister taxon to *C. chaoxianensis* (data S4). Among Middle Triassic taxa, we added the specimen described in this study and the recently described *C. duelferi* from the same beds (*17*) to the dataset. The dataset of cetacean bizygomatic width relies on many sources and includes a number of new data points (data S5).

We first evaluated the fit of trait evolution models to the data for the given phylogenies

Downloaded from https://www.science.org at Claremont Colleges Library on December 24, 2021

(fig. S10) with a maximum likelihood approach, using the "fitContinuous" function of the R package "geiger" (*10*) (data S6). We fit five different models with macroevolutionary relevance [(*10*) and table S7]. We ran the primary analyses over 1000 trees with slightly differing time calibration and the subsequent resampling analyses to explore the data in more depth over 100 different trees. For each iteration, we normalized branch lengths to avoid computational problems. We evaluated model fit by means of the sample-size corrected Akaike information criterion (AICc) and their corresponding Akaike weights over the entire tree sets. Akaike weights are useful because they represent the conditional probability for each of the tested models (*10*). To account for any artifactual or other nonbiological differences between our ichthyosaur and cetacean datasets, we not only performed model fitting for the entire dataset but also carried out several resampling approaches of the cetacean data. Altogether, we completed nine different model-fitting approaches (see fig. S11).

To illustrate the patterns of body-size evolution in ichthyosaurs and cetaceans, we selected a new modification of the well-established evolutionary traitgram approach (*10*). In evolutionary traitgrams, the phylogeny is combined with ancestral state reconstructions for the nodes through a projection of the tree into a space defined by the trait value on the y axis and time on the x axis (or sometimes vice versa). We intended to achieve a direct comparison of ichthyosaur and cetacean body-size evolution in the same diagram. To realize this type of visualization, we had to overcome several hurdles. First, we used different size proxies for ichthyosaurs (skull length) and cetaceans (skull width), and thus the trait values are not directly comparable in visual terms. To solve this issue, we normalized the trait values so that the smallest and largest trait values for both ichthyosaurs and cetaceans ranged from 0 to 1, respectively (Fig. 4). Second, ichthyosaurs and cetaceans originated at different times in geologic history. To facilitate their direct comparison, we started each traitgram at the root of the tree (Fig. 4), irrespective of absolute geologic time. Third, the mode of body-size evolution differs between ichthyosaurs and cetaceans, with early burst–like processes dominating ichthyosaurs and no clear pattern for the full cetacean dataset. We therefore reconstructed the traitgrams for cetaceans with the simplest evolutionary model (Brownian motion) and for ichthyosaurs using an early-burst model (fig. S10). Finally, to illustrate uncertainty stemming from the difficulties of proper time calibration, we devised and applied a new approach for traitgram plotting. The stratigraphic ranges of many extinct taxa are not well defined, and as such, the branch lengths of our trees are uncertain. To take this uncertainty into account, we plotted a range of different possible evolutionary traitgrams into the same diagram, using semitransparent colors (Fig. 4 and fig. S10). Dense, more opaque areas in the traitgram space therefore indicate evolutionary time and trait combinations with a high probability of containing the true evolutionary path of body size, whereas empty areas are less probable (Fig. 4 and fig. S10). For both ichthyosaurs and cetaceans, we also added the traitgrams that one would expect if the last appearance date were taken at face value, that is, if all taxa existed to the very end of the stage they have been documented for. These traitgrams are in white color. The evolutionary traitgram approach was implemented using the R package "phytools" (*31*) (data S6).

To identify regions of the tree with accelerated phases of evolution, we explored heterogeneity in the rate of trait evolution across the phylogeny using the function "multirateBM" of the R package "phytools" (*10*, *31*). This method is based on a penalized likelihood in which we fit a multirate Brownian motion trait evolution model in which the rate (σ^2) evolves by a correlated random-walk process. Every edge of the tree is consequently allowed to have a slightly different value of σ^2. The penalty term, which is based on the probability density of the evolutionary rates σ^2 along all branches in the tree multiplied by a user-specified coefficient denominated λ, is necessary to identify both the evolutionary rates along all the edges of the tree, as well as the rate of Brownian evolution of the rate itself. Low values for the penalty coefficient λ (e.g., 0.01) will tend to accord very little penalty to rate variation among edges, whereas higher values (e.g., λ = 100) permit the rate to differ little. Intermediate λ values (e.g., 1) balance the probability of the data under the model and the probability of the rate variation among edges, given a Brownian evolution process for rate variation. We set λ = 0.1 for both ichthyosaur and cetacean datasets and verified that the overall pattern remains consistent for $0.01 \leq \lambda \leq 1$. Given that we did not perform a full cross-validation of λ, we consider the results exploratory.

The second approach to assess body-size evolution along the edges of the phylogeny is founded on a Bayesian implementation of the Ornstein-Uhlenbeck method [R package "bayOU" (*32*)]. The Ornstein-Uhlenbeck model of trait evolution is an extension of the Brownian motion model and describes a random walk coupled with the tendency of trait values to stay in proximity of a stationary peak (θ). The tendency of the trait to remain close to the peak is measured by the parameter α, which is interpreted as the strength of selection. BayOU analyses thus characterize the selective regime of a trait.

BayOU agnostically infers whether adaptive shifts of the peak θ occurred through evolutionary time and, if so, along which edge in the phylogeny these changes likely happened. Bayesian approaches to such inferences are also less prone to error for small phylogenetic comparative datasets (N < 100) than other methods (*74*), which is useful for the ichthyosaur data. Probabilistic prior settings are summarized in table S8.

The reversible jump Markov chain Monte Carlo simulations were run for 3 million generations for the ichthyosaur data and 6 million generations for the cetacean data, of which the first 30% was discarded as burn-in. We ensured that independent chains had converged on similar regions in the parameter space by Gelman's R for log likelihood, σ^2, and α (fig. S12 and table S9). We also checked for convergence by plotting the posterior probabilities for shifts along branches against each other. If convergence was achieved, the posterior probabilities should fall along a line with a slope of 1 (fig. S12). We considered an adaptive shift well-supported if its respective posterior probability was far outside the main distribution of posterior probabilities for all branches.

Among ichthyosaurs, four branches with mean posterior probabilities of 0.41 to 0.86 [39 to 81 times greater than their prior probability (0.01)] were chosen (see table S8). The mean estimate of α is 0.4, indicating a phylogenetic half-life [$\ln(2)/\alpha$] of 1.73 Ma. Applied to cymbospondylids, the ichthyosaurs in this clade evolved halfway from their previous adaptive peak of 135 mm to their new peak (1443 mm) in 1.73 Ma, which is congruent with the fossil record. The phylogenetic half-life of cetacean skull width is 17.3 Ma. Among cetaceans, three branches with mean posterior probabilities of 0.84 to 0.95 [413 to 472 times greater than their prior probability (0.002)] were chosen (see table S8). Another branch received a posterior probability of 0.36, far less than the other three shifts and not as clearly separated from the distribution of posterior probabilities. If supported, this adaptive shift would suggest that the Pakicetidae shifted toward smaller body size, with a new peak 62-mm skull width as opposed to the ancestral state estimate of 121 mm. Other interesting patterns are apparent in cetacean size evolution, such as the missing middle size classes in the Oligocene and repeated increases of body-size ranges in different clades, but fully exploring them is beyond the scope of this study.

Energy-flux modeling summary

To test whether the composition of the pelagic Fossil Hill Fauna as found in the fossil record (fig. S13 and table S10) represents a functional and stable food web (hypothesis 1, standard scenario), we modeled energy flux using a

Downloaded from https://www.science.org at Claremont Colleges Library on December 24, 2021

new tool from quantitative ecosystem ecology implemented in R, "fluxweb" (*41*), which is based on allometric trophic network theory (*42*). Importantly, it derives energy fluxes in a top-down approach. The "fluxweb" tool calculates the food web's stability (*41*) by applying a predator-prey multispecies model and searching for equilibrium total biomasses of food web members. More negative stability values indicate a more stable food web, that is, the smallest equilibrium total biomass across all food web members is larger than zero, whereas a positive stability value indicates that at least one food web member is extinct under equilibrium.

Model input is census data of preserved taxa (all of which are pelagic) as members of the food web, estimated body masses, energetic demands (table S11), and potential prey (Fig. 7A and fig. S14). For modeling, we added two further members that are lowest in the food web and pool different kinds of animal taxa. We pooled taxa because we lack sufficient information on the parameter values required for modeling each taxon individually, and we aimed to keep our model as simple as possible. The first additional member is "shelled invertebrates" ("invertebrates" for short). This member is basal in the modeled food web and comprises primarily ammonoids but also halobiid bivalves and crustaceans. It pools the trophically lowest invertebrates of the Fossil Hill Fauna preserved in the fossil record. The "invertebrates" directly or indirectly provide energy to all other members of the food web. How this energy is produced in a basal member is ignored in "fluxweb" (*41*), and thus modeling of predator-prey relations within basal food web members is not possible in this tool. The second additional member is "pooled nonshelled invertebrates and fish" ("fish" for short). This member pools coleoid cephalopods such as squid and small- to medium-sized fish. It thus comprises the preserved and unpreserved taxa of the lowest trophic level on which the majority of all other trophically higher members fed (Fig. 7A and fig. S14). For the member "fish," we implemented potential within-group predator-prey relations by allowing that "fish" feed on "fish" (Fig. 7A and fig. S14) because larger fish could potentially have fed on smaller fish and squid. We further assume in our model that energy demands of all ichthyosaur taxa equaled that of modern endothermic vertebrates (*10*), whereas demands of all other taxa either equaled that of ectothermic vertebrates or of ectothermic invertebrates.

For the two members "invertebrates" and "fish," we evaluated our model for 15 different combinations of total biomasses because we lack reliable information on their total biomasses from the fossil record. Because the body masses estimated for the ichthyosaur taxa used in our model and total biomasses derived from these all have large margins of error and because the ichthyosaurs are the largest animals of the Fossil Hill Fauna, we evaluated each of the 15 combinations for standard body mass, lower limit of body mass, and upper limit of body mass based on 95% prediction intervals (table S11). A sensitivity analysis of body mass of basal "invertebrates," for which the fossil record documents a body mass variation of about five orders of magnitude, showed that potential errors had an extremely small impact on stability values and energy fluxes calculated by our model (see below and fig. S15). In the three combinations, in which the total biomass of "invertebrates" equaled that of "fish," the average energy loss between two trophic levels always turned out to be the highest across the 15 combinations, and estimated losses of around 40% were clearly unrealistic from a modern perspective (figs. S16B and S19, B and F). We thus restricted our ecological and evolutionary interpretation of modeling results to the other 12 combinations in which the total biomass of the "invertebrates" was larger than that of the "fish."

Although we assumed that energy demands of all ichthyosaurs in the Fossil Hill Fauna conformed to modern endotherms [table S11 and (*10*)], we nevertheless wanted to test model sensitivity to this assumption. We thus reran the model for all combinations assuming ectothermic and mesothermic (*54*) ichthyosaurs. Endothermy in any of the taxa in the model (table S11) results in a higher energy consumption than ectothermy and mesothermy (fig. S15). We considered mesothermy as a metabolic strategy for ichthyosaurs because several modern marine macropredators show this strategy—for example, tunas, swordfish, and lamnid sharks (*54*)—and because mesothermy was important in the evolution of elasmobranch gigantism (*55*).

The "fluxweb" tool provides different allometric equations on mass-specific metabolic rates for implementing different energetic demands (i.e., physiological losses; fig. S15). The ectothermic and the endothermic vertebrate metabolic types of "fluxweb" only differ in their use of scaling normalization constants: 19.5 for the endothermic metabolic type versus 18.18 for the ectothermic metabolic type (table S11). To implement mesothermy, we used the arithmetic mean of the two, 18.84. The scaling exponent of all three metabolic types is −0.29 (table S11). To assess the effect of the ectothermic and mesothermic metabolic types on stability values and energy fluxes, we reran the model for mesothermic and ectothermic ichthyosaurs while keeping everything else as in the standard scenario (fig. S18).

To narrow down which total biomass of the basal "invertebrates" are the most realistic for the food web of the Fossil Hill Fauna, we estimated the total biomass of ammonoids found in the Fossil Hill Member of the Augusta Mountains from field data (table S12). We are aware of the limitations of this approach because ammonoids usually accumulate in certain layers, are not evenly distributed throughout the Fossil Hill Member, and comprise different species. To estimate total ammonoid biomass, we conducted a census by shell diameter on one randomly chosen surface of 1 m^2. Recognizing five size classes, we found the following abundances: I, >23 cm diameter, one individual; II, 23 to 6 cm, 28 individuals; III, 6 to 3 cm, 49 individuals; IV, 3 to 1 cm, 49 individuals; and V, <0.5 cm, 28 individuals. To estimate the biomass of these individuals, we used an extant *Nautilus belauensis* with a 23-cm shell diameter and a mass of 1.675 kg (*75*) as a proxy and linearly downscaled its size and mass to estimate the weight of the smaller ammonoid individuals. This calculation and census of a total of 155 individuals yielded an average body mass of about 10 g. This is the rounded mean calculated from frequencies of individuals in size classes and body masses corresponding to the respective lower-size class boundaries (except for class V, for which we used a 0.5-cm shell diameter). The abundances and body masses of the five size classes further yielded about 2.7 kg as an estimate of ammonoid biomass per square meter. A field census of random samples in the Augusta Mountains suggested that 15% (0.540 km^2), 25% (0.900 km^2), or 30% (1.080 km^2) of the Fossil Hill outcrop area (3.6 km^2) is covered by ammonoids, which corresponds to a total biomass in this area of 1458 kg, 2430 kg, or 2916 kg, respectively. We used the estimated average ammonoid body mass (10 g) for the member "invertebrates" in the "fluxweb" model (table S11).

To assess a potential impact of the body mass assumed for "invertebrates," we evaluated the model with a body mass of "invertebrates" of 0.02 g (size class V) and of 1.675 kg (size class I) for the standard scenario. Our rationale was that this member provides the energy to all other trophically higher members and that their body-mass range documented in the fossil record covers nearly five orders of magnitude. However, for both body masses, the stability values and energy fluxes obtained were nearly identical to those obtained for the standard mass of 10 g. With respect to this observation, it is important that the body mass assumed for any modeled food web member (i) is used to calculate its physiological losses (model parameter X_i). Except for "invertebrates" and "fish," body masses of all members were also used to calculate their total biomasses as a product of body mass and number of counted individuals (table S11). Because the total biomass of "invertebrates" and "fish" is fixed in each model run, only physiological losses are

Downloaded from https://www.science.org at Claremont Colleges Library on December 24, 2021

altered by changing body masses. An evaluation of the equations used for physiological losses shows that whereas the body-mass range covered by the food web members spans about 10 orders of magnitude (the mass corresponding to the smallest ammonite size class V is 0.02 g, and the upper body mass limit of *C. youngorum* sp. nov. is 135.81 tonnes), the variation in losses is smaller than one magnitude over this huge range (fig. S15). For the members "fish," coelacanth fish, and *A. hagdorni*, we estimated body masses from related and similar taxa because we lack any information about their body mass and its variation in the Fossil Hill Fauna. We therefore refrained from carrying out a sensitivity analysis for body mass for these three members. Based on the arguments given above, modeling results must also be very insensitive to the body mass assumed for the members "fish" and coelacanth fish. There is only one coelacanth fish individual in the Fossil Hill Fauna, and thus its total biomass equals its body mass (table S11). However, the census for *A. hagdorni* is three individuals, and any change in the body mass assumed for this member results in a change in its total biomass. Thus, we cannot exclude the possibility that this change will alter stability values and energy fluxes. We anticipate that these values will be in the range found for ichthyosaur members with a similar body mass and total biomass.

Modeling the Fossil Hill Fauna with a hypothetical giant bulk feeder

Averaged across the 12 combinations of total biomasses of "invertebrates" and "fish," the production rate of "invertebrates" was a magnitude smaller than that of the preserved ammonoids (fig. S16C and table S12). We thus conducted a second modeling experiment (hypothesis 2) in which we added a hypothetical blue whale–sized endothermic ichthyosaur (200 tonnes, about 30 m long) to the Fossil Hill food web model while keeping everything else as in the standard scenario. This super giant bulk feeder exclusively fed on either "invertebrates" (fig. S14B) or "fish" (fig. S14C). For both feeding strategies, the hypothesized food web was again stable (fig. S19A), and for each chosen combination of total biomass of "invertebrates" and "fish," food web stability was somewhat higher than in the standard scenario (fig. S20A). When averaged across the possible combinations of total biomasses of "invertebrates" and "fish," the supergiant that fed exclusively on "invertebrates" consumed an increase in outgoing energy from "invertebrates" of 2.6×10^{-7} kJ/year and the supergiant that fed exclusively on "fish" consumed 1.7×10^{7} kJ/year (fig. S21). A detailed description of our model, a justification of model assumptions, and output variables inferred is in the supplementary materials (*10*).

REFERENCES AND NOTES

1. G. J. Vermeij, Gigantism and its implications for the history of life. *PLOS ONE* **11**, e0146092 (2016). doi: 10.1371/journal.pone.0146092; pmid: 26771527
2. N. P. Kelley, N. D. Pyenson, Vertebrate evolution. Evolutionary innovation and ecology in marine tetrapods from the Triassic to the Anthropocene. *Science* **348**, aaa3716 (2015). doi: 10.1126/science.aaa3716; pmid: 25883362
3. A. H. Knoll, M. J. Follows, A bottom-up perspective on ecosystem change in Mesozoic oceans. *Proc. Biol. Sci.* **283**, 20161755 (2016). doi: 10.1098/rspb.2016.1755; pmid: 27798303
4. J. A. Goldbogen *et al*., Why whales are big but not bigger: Physiological drivers and ecological limits in the age of ocean giants. *Science* **366**, 1367–1372 (2019). doi: 10.1126/science.aax9044; pmid: 31831666
5. W. Gearty, C. R. McClain, J. L. Payne, Energetic tradeoffs control the size distribution of aquatic mammals. *Proc. Natl. Acad. Sci. U.S.A.* **115**, 4194–4199 (2018). doi: 10.1073/pnas.1712629115; pmid: 29581289
6. G. J. Slater, J. A. Goldbogen, N. D. Pyenson, Independent evolution of baleen whale gigantism linked to Plio-Pleistocene ocean dynamics. *Proc. Biol. Sci.* **284**, 20170546 (2017). doi: 10.1098/rspb.2017.0546; pmid: 28539520
7. B. C. Moon, T. L. Stubbs, Early high rates and disparity in the evolution of ichthyosaurs. *Commun. Biol.* **3**, 68 (2020). doi: 10.1038/s42003-020-0779-6; pmid: 32054967
8. N. B. Fröbisch, J. Fröbisch, P. M. Sander, L. Schmitz, O. Rieppel, Macropredatory ichthyosaur from the Middle Triassic and the origin of modern trophic networks. *Proc. Natl. Acad. Sci. U.S.A.* **110**, 1393–1397 (2013). doi: 10.1073/pnas.1216750110; pmid: 23297200
9. P. M. Hull, Emergence of modern marine ecosystems. *Curr. Biol.* **27**, R466–R469 (2017). doi: 10.1016/j.cub.2017.04.041; pmid: 28586680
10. See supplementary materials.
11. C. v. Linnaeus, *Systema Naturae. Regnum Animale* (L. Salvius, Stockholm, ed. 10, 1758).
12. H. F. Osborn, The reptilian subclasses Diapsida and Synapsida and the early history of the Diaptosauria. *Mem. Am. Mus. Nat. Hist.* **1**, 449–507 (1903).
13. H. M. D. de Blainville, Systéme de'Herpetologie. *Nouv. Ann. Mus. Hist. Nat. Paris* **4**, 233–296 (1835).
14. J. Leidy, Notice of some reptilian remains from Nevada. *Proc. Acad. Nat. Sci. Philadelphia* **20**, 177–178 (1868).
15. P. M. Sander, The large ichthyosaur *Cymbospondylus buchseri*, sp. nov., from the Middle Triassic of Monte San Giorgio (Switzerland), with a survey of the genus in Europe. *J. Vertebr. Paleontol.* **9**, 163–173 (1989). doi: 10.1080/02724634.1989.10011750
16. N. Fröbisch, P. M. Sander, O. Rieppel, A new species of *Cymbospondylus* (Diapsida, Ichthyosauria) from the Middle Triassic of Nevada and re-evaluation of the skull osteology of the genus. *Zool. J. Linn. Soc.* **147**, 515–538 (2006). doi: 10.1111/j.1096-3642.2006.00225.x
17. N. Klein, L. Schmitz, T. Wintrich, P. M. Sander, A new cymbospondylid ichthyosaur (Ichthyosauria) from the Middle Triassic (Anisian) of the Augusta Mountains, Nevada, USA. *J. Syst. Palaeontology* **18**, 1167–1191 (2020). doi: 10.1080/14772019.2020.1748132
18. C. Monnet, H. Bucher, New middle and late Anisian (Middle Triassic) ammonoid faunas from Northwestern Nevada (USA): Taxonomy and biochronology. *Foss. Strat.* **52**, 1–121 (2005).
19. B. Moon, A new phylogeny of ichthyosaurs (Reptilia: Diapsida). *J. Syst. Palaeontology* **17**, 129–155 (2019). doi: 10.1080/14772019.2017.1394922
20. J. A. Massare, Tooth morphology and prey preference of Mesozoic marine reptiles. *J. Vertebr. Paleontol.* **7**, 121–137 (1987). doi: 10.1080/02724634.1987.10011647
21. R. Motani, Evolution of fish-shaped reptiles (Reptilia: Ichthyopterygia) in their physical environments and constraints. *Annu. Rev. Earth Planet. Sci.* **33**, 12.11–12.26 (2005).
22. C. McGowan, Giant ichthyosaurs of the Early Jurassic. *Can. J. Earth Sci.* **33**, 1011–1021 (1996). doi: 10.1139/e96-077
23. T. M. Scheyer, C. Romano, J. Jenks, H. Bucher, Early Triassic marine biotic recovery: The predators' perspective. *PLOS ONE* **9**, e88987 (2014). doi: 10.1371/journal.pone.0088987; pmid: 24647136
24. S. Gutarra *et al*., Effects of body plan evolution on the hydrodynamic drag and energy requirements of swimming in ichthyosaurs. *Proc. Biol. Sci.* **286**, 20182786 (2019). doi: 10.1098/rspb.2018.2786; pmid: 30836867
25. R. Motani *et al*., A basal ichthyosauriform with a short snout from the Lower Triassic of China. *Nature* **517**, 485–488 (2015). doi: 10.1038/nature13866; pmid: 25383536
26. S. Nummela, T. Hussain, J. G. M. Thewissen, Cranial anatomy of Pakicetidae (Cetacea, Mammalia). *J. Vertebr. Paleontol.* **26**, 746–759 (2006). doi: 10.1671/0272-4634(2006)26[746:CAOPCM]2.0.CO;2
27. J. G. M. Thewissen, J. D. Sensor, M. T. Clementz, S. Bajpai, Evolution of dental wear and diet during the origin of whales. *Paleobiology* **37**, 655–669 (2011). doi: 10.1666/10038.1
28. M. A. MacIver, L. Schmitz, U. Mugan, T. D. Murphey, C. D. Mobley, Massive increase in visual range preceded the origin of terrestrial vertebrates. *Proc. Natl. Acad. Sci. U.S.A.* **114**, E2375–E2384 (2017). doi: 10.1073/pnas.1615563114; pmid: 28270619
29. J. M. Fahlke, K. A. Bastl, G. M. Semprebon, P. D. Gingerich, Paleoecology of archaeocete whales throughout the Eocene: Dietary adaptations revealed by microwear analysis. *Palaeogeogr. Palaeoclimatol. Palaeoecol.* **386**, 690–701 (2013). doi: 10.1016/j.palaeo.2013.06.032
30. L. N. Cooper *et al*., Aquatic habits of cetacean ancestors: Integrating bone microanatomy and stable isotopes. *Integr. Comp. Biol.* **56**, 1370–1384 (2016). doi: 10.1093/icb/icw119; pmid: 27697778
31. L. J. Revell, Phytools: An R package for phylogenetic comparative biology (and other things). *Methods Ecol. Evol.* **3**, 217–223 (2012). doi: 10.1111/j.2041-210X.2011.00169.x
32. J. C. Uyeda, L. J. Harmon, A novel Bayesian method for inferring and interpreting the dynamics of adaptive landscapes from phylogenetic comparative data. *Syst. Biol.* **63**, 902–918 (2014). doi: 10.1093/sysbio/syu057; pmid: 25077513
33. C. M. Peredo, N. D. Pyenson, C. D. Marshall, M. D. Uhen, Tooth loss precedes the origin of baleen in whales. *Curr. Biol.* **28**, 3992–4000.e2 (2018). doi: 10.1016/j.cub.2018.10.047; pmid: 30503622
34. J. D. Walker, J. W. Geissman, S. A. Bowring, L. E. Babcock, "Geologic time scale v. 5.0" (Geological Society of America, 2018).
35. K. M. Nichols, N. J. Silberling, Stratigraphy and depositional history of the Star Peak Group (Triassic), northwestern Nevada. *Spec. Pap. Geol. Soc. Am.* **178**, 1–73 (1977).
36. G. Cuny, O. Rieppel, P. M. Sander, The shark fauna from the Middle Triassic (Anisian) of North-Western Nevada. *Zool. J. Linn. Soc.* **133**, 285–301 (2001). doi: 10.1111/j.1096-3642.2001.tb00627.x
37. O. Rieppel, *Handbook of Paleoherpetology / Sauropterygia I.: Placodontia, Pachypleurosauria, Nothosauroidea, Pistosauroidea* (Friedrich Pfeil, 2000).
38. J. C. Merriam, *Triassic Ichthyosauria, with Special Reference to the American Forms* (Memoirs of the University of California, The University Press, 1908).
39. L. Schmitz, P. M. Sander, G. W. Storrs, O. Rieppel, New Mixosauridae (Ichthyosauria) from the Middle Triassic of the Augusta Mountains (Nevada, USA) and their implications for mixosaur taxonomy. *Palaentographica A* **270**, 133–162 (2004).
40. J. C. Merriam, Preliminary note on a new marine reptile from the Middle Triassic of Nevada. *Univ. Calif. Publication Bull. Dept. Geol.* **5**, 5–79 (1906).
41. B. Gauzens *et al*., Fluxweb: An R package to easily estimate energy fluxes in food webs. *Methods Ecol. Evol.* **10**, 270–279 (2018). doi: 10.1111/2041-210X.13109
42. N. D. Martinez, Allometric trophic networks from individuals to socio-ecosystems: Consumer-resource theory of the ecological elephant in the room. *Front. Ecol. Evol.* **8**, 92 (2020). doi: 10.3389/fevo.2020.00092
43. R. Motani, D.-Y. Jiang, A. Tintori, C. Ji, J.-D. Huang, Pre- versus post-mass extinction divergence of Mesozoic marine reptiles dictated by time-scale dependence of evolutionary rates. *Proc. Biol. Sci.* **284**, 20170241 (2017). doi: 10.1098/rspb.2017.0241; pmid: 28515201
44. J. H. Brown, J. F. Gillooly, A. P. Allen, V. M. Savage, G. B. West, Toward a metabolic theory of ecology. *Ecology* **85**, 1771–1789 (2004). doi: 10.1890/03-9000
45. E. L. Nicholls, M. Manabe, Giant ichthyosaurs of the Triassic – A new species of *Shonisaurus* from the Pardonet Formation (Norian, Late Triassic) of British Columbia. *J. Vertebr. Paleontol.* **24**, 838–849 (2004). doi: 10.1671/0272-4634(2004)024[0838:GIOTTN]2.0.CO;2
46. C. R. McClain *et al*., Sizing ocean giants: Patterns of intraspecific size variation in marine megafauna. *PeerJ* **3**, e715 (2015). doi: 10.7717/peerj.715; pmid: 25649000
47. A. Brayard *et al*., Unexpected Early Triassic marine ecosystem and the rise of the Modern evolutionary fauna. *Sci. Adv.* **3**,

Downloaded from https://www.science.org at Claremont Colleges Library on December 24, 2021

e1602159 (2017). doi: 10.1126/sciadv.1602159; pmid: 28246643
48. H. Song, P. B. Wignall, A. M. Dunhill, Decoupled taxonomic and ecological recoveries from the Permo-Triassic extinction. *Sci. Adv.* **4**, eaat5091 (2018). doi: 10.1126/sciadv.aat5091; pmid: 30324133
49. P. M. Sander *et al*., Biology of the sauropod dinosaurs: The evolution of gigantism. *Biol. Rev. Camb. Philos. Soc.* **86**, 117–155 (2011). doi: 10.1111/j.1469-185X.2010.00137.x; pmid: 21251189
50. M. J. Benton *et al*., Exceptional vertebrate biotas from the Triassic of China, and the expansion of marine ecosystems after the Permo-Triassic mass extinction. *Earth Sci. Rev.* **137**, 85–128 (2014). doi: 10.1016/j.earscirev.2014.08.004
51. M. J. Orchard, Conodont diversity and evolution through the latest Permian and Early Triassic upheavals. *Palaeogeogr. Palaeoclimatol. Palaeoecol.* **252**, 93–117 (2007). doi: 10.1016/j.palaeo.2006.11.037
52. R. Motani, B. M. Rothschild, W. J. Wahl Jr., Large eyeballs in diving ichthyosaurs. *Nature* **402**, 747 (1999). doi: 10.1038/45435
53. D.-E. Nilsson, E. Warrant, S. Johnsen, Computational visual ecology in the pelagic realm. *Philos. Trans. R. Soc. London Ser. B* **369**, 20130038 (2014). doi: 10.1098/rstb.2013.0038; pmid: 24395965
54. J. M. Grady *et al*., Metabolic asymmetry and the global diversity of marine predators. *Science* **363**, eaat4220 (2019). doi: 10.1126/science.aat4220; pmid: 30679341
55. C. Pimiento, J. L. Cantalapiedra, K. Shimada, D. J. Field, J. B. Smaers, Evolutionary pathways toward gigantism in sharks and rays. *Evolution* **73**, 588–599 (2019). doi: 10.1111/evo.13680; pmid: 30675721
56. A. T. Boersma, N. D. Pyenson, *Albicetus oxymycterus*, a new generic name and redescription of a basal physeteroid (Mammalia, Cetacea) from the Miocene of California, and the evolution of body size in sperm whales. *PLOS ONE* **10**, e0135551 (2015). doi: 10.1371/journal.pone.0135551; pmid: 26651027
57. R. W. Boessenecker, M. Churchill, E. A. Buchholtz, B. L. Beatty, J. H. Geisler, Convergent evolution of swimming adaptations in modern whales revealed by a large macrophagous dolphin from the Oligocene of South Carolina. *Curr. Biol.* **30**, 3267–3273.e2 (2020). doi: 10.1016/j.cub.2020.06.012; pmid: 32649912
58. J. H. Geisler, M. W. Colbert, J. L. Carew, A new fossil species supports an early origin for toothed whale echolocation. *Nature* **508**, 383–386 (2014). doi: 10.1038/nature13086; pmid: 24670659
59. J. A. Goldbogen, P. T. Madsen, The evolution of foraging capacity and gigantism in cetaceans. *J. Exp. Biol.* **221**, jeb166033 (2018). doi: 10.1242/jeb.166033; pmid: 29895582
60. E. E. Maxwell, D. Y. Cortés, P. Patarroyo, M. L. P. Ruge, A new specimen of *Platypterygius sachicarum* (Reptilia, Ichthyosauria) from the Early Cretaceous of Colombia and its phylogenetic implications. *J. Vertebr. Paleontol.* **39**, e1577875 (2019). doi: 10.1080/02724634.2019.1577875
61. W. P. Maddison, D. R. Maddison, Mesquite: A modular system for evolutionary analysis. Version 3.02 (2015); www.mesquiteproject.org.
62. P. A. Goloboff, J. S. Farris, K. C. Nixon, TNT, a free program for phylogenetic analysis. *Cladistics* **24**, 774–786 (2008). doi: 10.1111/j.1096-0031.2008.00217.x
63. J.-D. Huang *et al*., The new ichthyosauriform *Chaohusaurus brevifemoralis* (Reptilia, Ichthyosauromorpha) from Majiashan, Chaohu, Anhui Province, China. *PeerJ* **7**, e7561 (2019). doi: 10.7717/peerj.7561; pmid: 31565558
64. D. Swofford, *PAUP* Phylogenetic Analysis Using Parsimony (* and Other Methods). Version 4.0b10* (Sinauer Associates, 2002).
65. R Core Team, R software, version 3.5.2 (R Foundation for Statistical Computing, Vienna, Austria, 2020); www.R-project.org/.
66. J. H. Geisler, A. E. Sanders, Morphological evidence for the phylogeny of Cetacea. *J. Mamm. Evol.* **10**, 23–129 (2003). doi: 10.1023/A:1025552007291
67. G. T. Lloyd, G. J. Slater, A total-group phylogenetic metatree for Cetacea and the importance of fossil data in diversification analyses. *Syst. Biol.* **70**, 922–939 (2021). doi: 10.1093/sysbio/syab002; pmid: 33507304
68. S. Bajpai, P. D. Gingerich, A new Eocene archaeocete (Mammalia, Cetacea) from India and the time of origin of whales. *Proc. Natl. Acad. Sci. U.S.A.* **95**, 15464–15468 (1998). doi: 10.1073/pnas.95.26.15464; pmid: 9860991
69. A. E. Hernández Cisneros, J. Velez-Juarbe, Paleobiogeography of the North Pacific toothed mysticetes (Cetacea: Aetiocetidae): A key on the Oligocene cetacean distributional patterns. *Palaeontology* **64**, 51–61 (2021). doi: 10.1111/pala.12507
70. M. Viglino, M. R. Buono, R. E. Fordyce, J. I. Cuitiño, E. M. G. Fitzgerald, Anatomy and phylogeny of the large shark-toothed dolphin *Phoberodon arctirostris* Cabrera, 1926 (Cetacea: Odontoceti) from the early Miocene of Patagonia (Argentina). *Zool. J. Linn. Soc.* **185**, 511–542 (2019). doi: 10.1093/zoolinnean/zly053
71. C. M. Peredo, M. D. Uhen, M. D. Nelson, A new kentriodontid (Cetacea: Odontoceti) from the early Miocene Astoria Formation and a revision of the stem delphinidan family Kentriodontidae. *J. Vertebr. Paleontol.* **38**, e1411357 (2018). doi: 10.1080/02724634.2017.1411357
72. M. R. McGowen *et al*., Phylogenomic resolution of the cetacean tree of life using target sequence capture. *Syst. Biol.* **69**, 479–501 (2020). doi: 10.1093/sysbio/syz068; pmid: 31633766
73. N. D. Pyenson, S. N. Sponberg, Reconstructing body size in extinct crown Cetacea (Neoceti) using allometry, phylogenetic methods and tests from the fossil record. *J. Mamm. Evol.* **18**, 269–288 (2011). doi: 10.1007/s10914-011-9170-1
74. N. Cooper, G. H. Thomas, C. Venditti, A. Meade, R. P. Freckleton, A cautionary note on the use of Ornstein Uhlenbeck models in macroevolutionary studies. *Biol. J. Linn. Soc. Lond.* **118**, 64–77 (2016). doi: 10.1111/bij.12701; pmid: 27478249
75. D. L. Pisor, *Registry of World Record Size Shells* (ConchBooks, ed. 5, 2008).

ACKNOWLEDGMENTS

We thank D. Goodreau and E. Durazo [all from Dinosaur Institute (DI), Natural History Museum of Los Angeles County (LACM)] for preparation of the specimen; M. Walsh (DI) for curation; and S. Abramowicz (DI) and G. Oleschinski (Bonn) for photography. S. Abramowicz is acknowledged for drafting the summary figure. E. Maxwell (Stuttgart) kindly made the data matrix from (*60*) available before final publication and provided helpful technical advice. The specimen was collected under Bureau of Land Management (BLM) Paleontological Resources Use Permit N-92625. The help of BLM staff at the Winnemucca field office is gratefully acknowledged. We thank the reviewers for their constructive comments. T. and B. Young and their Great Basin Brewery (Reno, NV, USA) generously supported our fieldwork by contributions in kind and monetary contributions. **Funding:** This research was funded in part by grants from the Deutsche Forschungsgemeinschaft (project numbers 388659338 and 264173172) to P.M.S. and by the National Geographic Society (grant number 9599-14) and the W. M. Keck Science Department to L.S. Great Basin Brewery (Reno, NV) supported our fieldwork and the preparation of the specimen at the LACM. Additional support was provided by the DI under the direction of L. Chiappe. The work of L.J.R. on phytools is supported by the National Science Foundation (DEB-1350474 and DBI-1759940). **Author contributions:** The overall idea, concept, and approach were developed by P.M.S., L.S., and T.W. Morphological descriptions and phylogenetic analysis were performed by P.M.S., N.K., T.W., and L.S. Evolutionary rate analysis was performed by L.S., J.V.J., and L.J.R. Energy-flux modeling was performed by E.M.G., N.K., and P.M.S. The manuscript was written by P.M.S. and L.S. with contributions from E.M.G., J.V.J., L.J.R., N.K., and T.W. All authors read, edited, and discussed the manuscript and participated in data collection. **Competing interests:** The authors declare no competing interests. **Data and materials availability:** The holotype specimen of *C. youngorum* sp. nov. is owned by the US Department of the Interior and housed in the collections of the Dinosaur Institute, Natural History Museum of Los Angeles County (Los Angeles, CA, USA) as LACM DI 157871. All data analyzed in this study are available in the main text and supplementary materials. R scripts are available at data S6 and S8.

SUPPLEMENTARY MATERIALS

science.org/doi/10.1126/science.abf5787
Supplementary Text
Figs. S1 to S21
Tables S1 to S14
References (*76*–*178*)
MDAR Reproducibility Checklist
Data S1 to S8

6 November 2020; accepted 26 October 2021
10.1126/science.abf5787

Downloaded from https://www.science.org at Claremont Colleges Library on December 24, 2021

Science

Early giant reveals faster evolution of large body size in ichthyosaurs than in cetaceans

P. Martin SanderEva Maria GriebelerNicole KleinJorge Velez JuarbeTanja WintrichLiam J. RevellLars Schmitz

Science, 374 (6575), eabf5787. • DOI: 10.1126/science.abf5787

Early marine giant

The largest animals to have ever lived occupied the marine environment. Modern cetaceans evolved their large size over tens of millions of years in response to the increased productivity of cold marine waters. However, whales were not the first marine giants to evolve. Sander *et al*. describe a 244-million-year-old fossil ichthyosaur that would have rivaled modern cetaceans in size (see the Perspective by Delsett and Pyenson). The animal existed at most 8 million years after the emergence of the first ichthyosaurs, suggesting a much more rapid size expansion that may have been fueled by processes after the Permian mass extinction. —SNV

View the article online
https://www.science.org/doi/10.1126/science.abf5787
Permissions
https://www.science.org/help/reprints-and-permissions

Downloaded from https://www.science.org at Claremont Colleges Library on December 24, 2021

Use of think article is subject to the Terms of service

Science (ISSN) is published by the American Association for the Advancement of Science. 1200 New York Avenue NW, Washington, DC 20005. The title *Science* is a registered trademark of AAAS.
Copyright © 2021 The Authors, some rights reserved; exclusive licensee American Association for the Advancement of Science. No claim to original U.S. Government Works

Science
AAAS

Supplementary Materials for

Early giant reveals faster evolution of large body size in ichthyosaurs than in cetaceans

P. Martin Sander *et al.*

Corresponding authors: P. Martin Sander, martin.sander@uni-bonn.de; Eva Maria Griebeler, em.griebeler@uni-mainz.de; Lars Schmitz, lschmitz@kecksci.claremont.edu

Science **374**, eabf5787 (2021)
DOI: 10.1126/science.abf5787

The PDF file includes:

Other Supplementary Material for this manuscript includes the following:

Supplementary Methods

Provenance, discovery and preparation, and differential diagnosis

Provenance. The specimen described in this publication, LACM DI 157871, comes from the Anisian age Fossil Hill Member of the Favret Formation at Favret Canyon, Augusta Mountains, Pershing County, Nevada, USA. The specimen is accessioned to the collections of the Dinosaur Institute (DI) which is part of the Natural History Museum of Los Angeles County (LACM) as LACM DI 157871. The LACM has Federal Repository status for fossils. The type locality is LACM 8025. Exact coordinates are on file at the repository. The specimen was discovered by author P. Martin Sander in 1998 and given the field number RS 1998/11. The specimen was excavated by him and his crews in 2014 and 2015. The specimen was collected under BLM Paleontological Resources Use Permit N-92625. The determination of the geologic age of LACM DI 157871 is described in section "Horizon and locality".

Discovery and preparation. The discovery situation in 1998 consisted of several articulated large cymbospondylid-type dorsal vertebrae which are distinctly taller than long and have elongate rib articular facets that are slanted anteroventrally and appear truncated by the anterior surface of the centrum. At the time of discovery, it was recognized from the orientation of the rib articular facets that the anterior face of the vertebrae was directed into the hillside. However, it was not apparent that the skeleton would comprise the skull, shoulder girdle, and forelimbs. A test pit in 2011 exposed the back of the skull. Full-scale excavation was conducted in 2014 and 2015, and the specimen was recovered in 13 plaster jackets. A popular account of the excavation was published by Montanari (*76*). The skull was contained in jackets 11 to 13 and prioritized for preparation at the LACM.

Before jacketing, the skeleton was documented photographically (Fig. S1), and a 3D model was captured using photogrammetry. These field observations indicate that the skeleton is articulated and complete from the anterior to the middle dorsal region forward but that some loss of distal limb elements may have occurred. The skeleton is preserved ventral-side up, with the skull in left ventrolateral position and the postcranial skeleton exposed fully ventrally. Despite careful excavation, only one limb bone distal to the right humerus was encountered during

excavation, none distal to the left humerus. Some observations concerning the morphology of the anterior dorsal vertebrae were made before jacketing as well.

The specimen is only partially prepared to date. The skull has been fully prepared from both sides. Field top (stratigraphic up) exposes a ventrolateral view of the left side of the skull, and field bottom (stratigraphic down) exposes a dorsolateral view of the right side of the skull. However, the skull is strongly compressed, particularly so posterior to the rostrum. The bones of the rostrum appear to have withstood sediment compaction better than the region behind the external nares. Only two of eleven postcranial blocks are prepared to date, revealing the right scapula, a partial right coracoid, a right clavicle, four posterior cervical vertebrae, and the right humerus. The latter is very well and three-dimensionally preserved (Fig. 2)

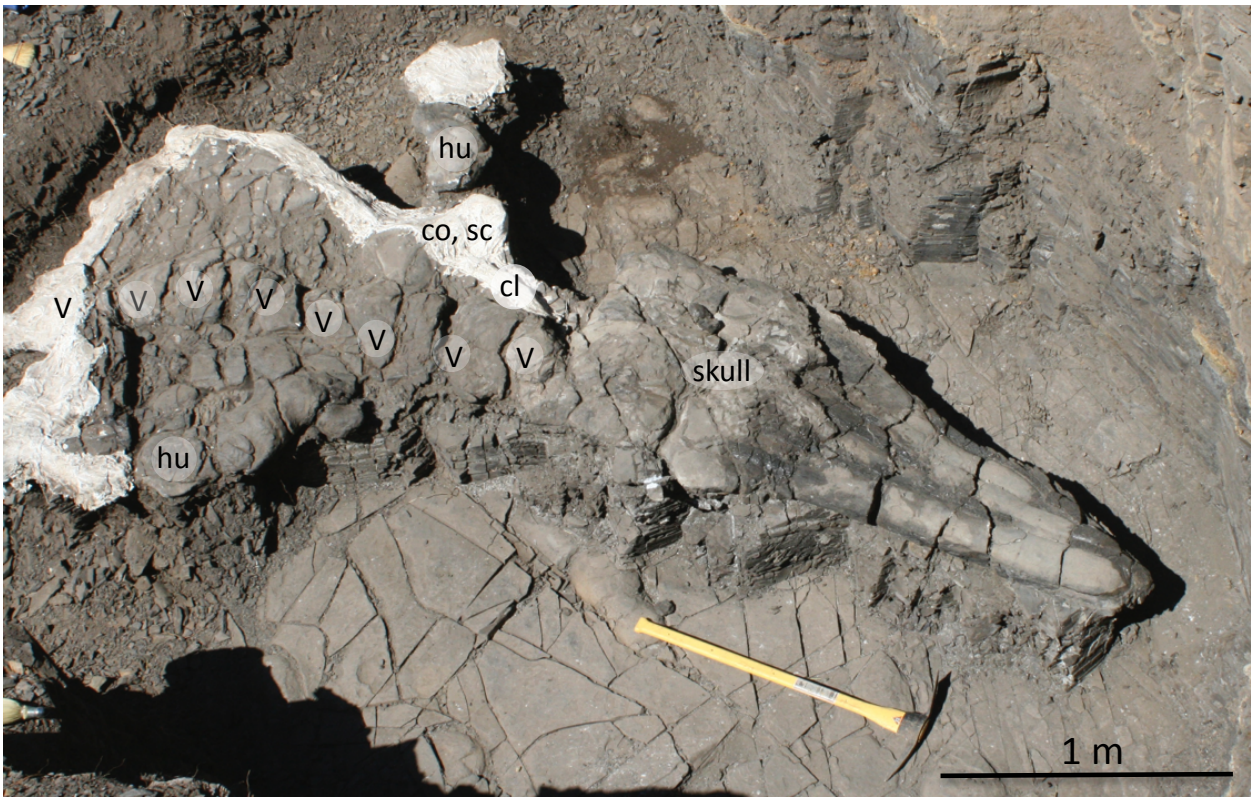

Fig. S1. The holotype of *Cymbospondylus youngorum* sp. nov. LACM DI 157871. Field situation of the skeleton before jacketing on August 12, 2015. The skeleton is positioned with the ventral side up. See Fig. 1C for a comparison with the prepared skull in the same view. Abbreviations: cl, clavicle; co, coracoid; hu, humerus; sc, scapula; v, vertebral column.

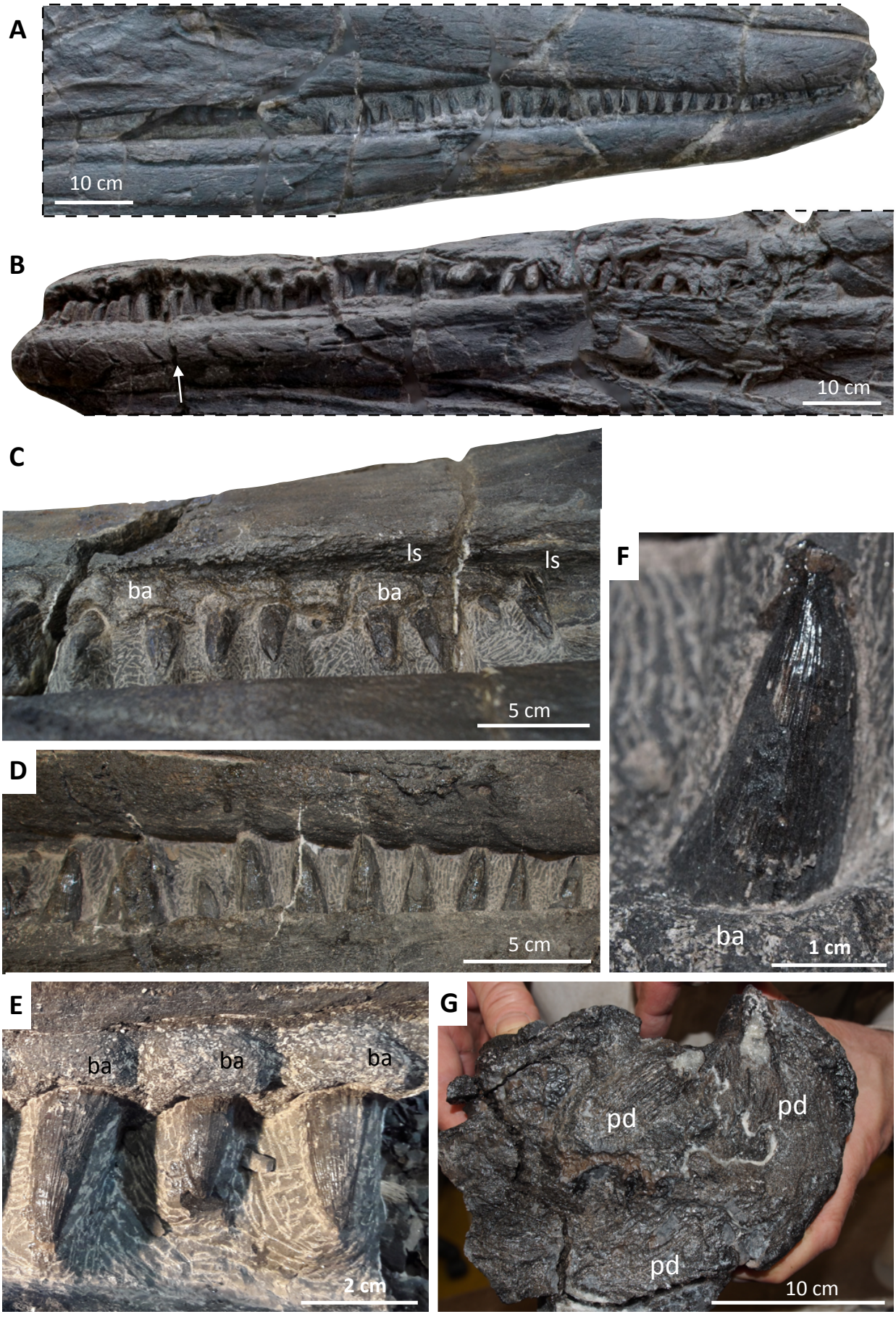
A
10 cm
B
10 cm
C
ba
ba
ls
ls
5 cm
D
5 cm
F
ba
1 cm
E
ba
ba
ba
2 cm
G
pd
pd
pd
10 cm

Fig. S2. Dental features of the holotype of *Cymbospondylus youngorum* sp. nov. LACM DI 157871. (**A**) Right tooth row, only exposing dentary teeth. Cut-out from an image of the complete skull. (**B**) Left tooth row,. Cut-out from an image of the complete skull. Arrow indicates location of cross section in (**G**). (**C**) Posterior part of right dentary, showing labial shelf and teeth set in bone of attachment. (**D**) Middle part of right tooth row. (**E**) Teeth from middle of right dentary. Note the bone of attachment. (**F**) Single dentary tooth, leftmost tooth in (E). (**G**) Cross section of tip of snout visible during preparation. Note the plicidentin of the teeth. Abbreviations: ba, bone of attachment; ls, labial shelf; pd, plicidentin.

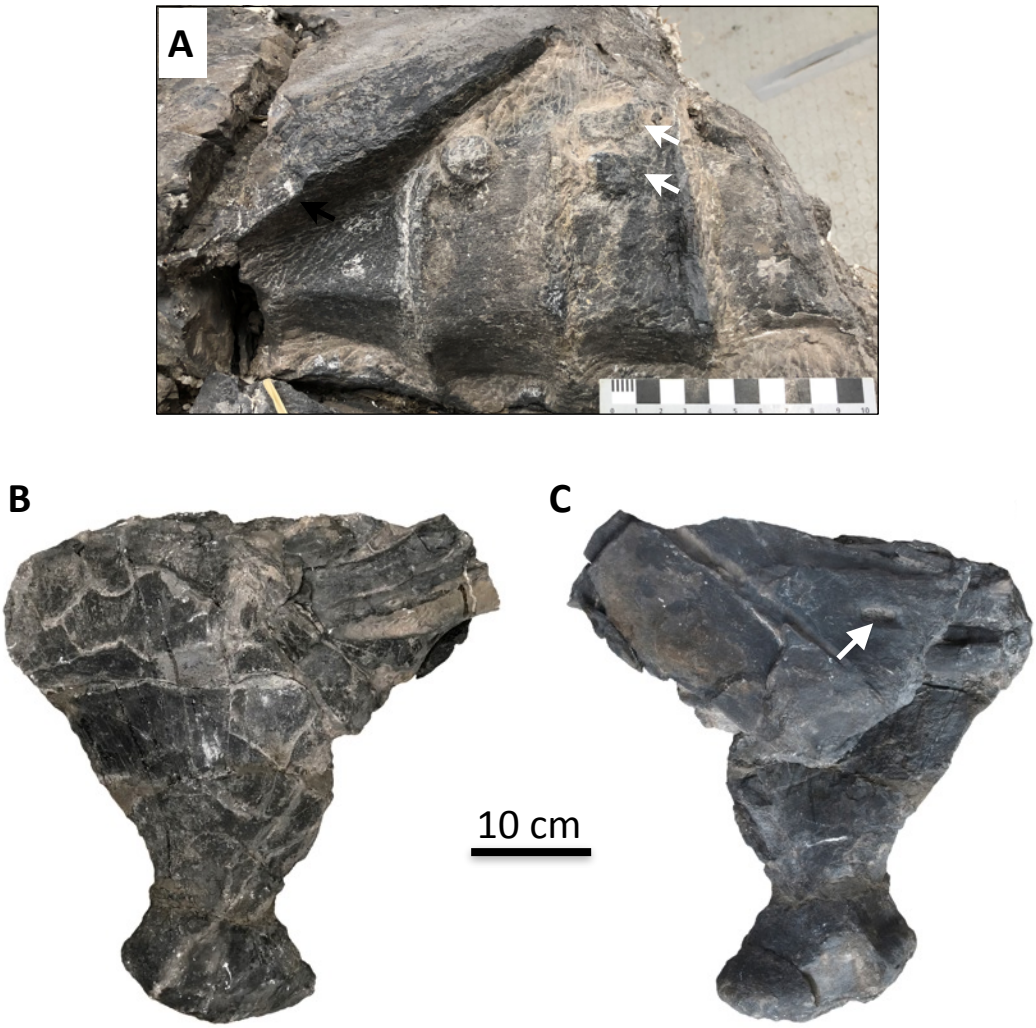

Fig. S3. Cervical vertebra, scapula, and coracoid of the holotype of *Cymbospondylus youngorum* sp. nov. LACM DI 157871. (**A**) Posterior cervical vertebrae in left lateral view. Note the proximity of diapophysis and parapophysis (arrows). (**B**) Right scapula in lateral view. (b) Right scapula in medial view and part of the right coraoid with the coracoid foramen (arrow).

Differential Diagnosis. The skull of *C. youngorum* sp. nov. lacks the high sagittal crest seen in all other species of *Cymbospondylus* but also lacking in *Thalattoarchon*. *Cymbospondylus youngorum* differs from *C. duelferi* and *C. buchseri* in the posteroventral process of the jugal which is also seen in *C. petrinus* and *C. nichollsi* (Fig. S4).

Cymbospondylus youngorum sp. nov. differs from the other species of *Cymbospondylus* for which this is known in the high number of tooth positions per jaw ramus (>40). *Cymbospondylus duelferi* has only >21 and *C. petrinus* has 30-35 (table S2). The teeth are also absolutely and relatively much smaller than those of *Thalattoarchon saurophagis* (Fig. S5), the only other Middle Triassic ichthyosaur approaching the new species in size, and differ in their lack of cutting edges. The teeth of the new species are supported by a thick base of bone of attachment, lacking in any of the other species and not seen in any other ichthyosaur (Fig. 2).

The scapula differs substantially in shape from all other species of *Cymbospondylus* for which it is known (*C. petrinus*, *C. duelferi, C. buchseri*) in having only a small dorsal expansion and a much wider ventral part (Fig. S6). The clavicle lacks the blade that is present in *C. petrinus* and *C. nichollsi*. The humerus of *C. youngorum* sp. nov. differs from that of *C. duelferi* in having a less constricted shaft and a proximal end that is wider than the distal end (Fig. 2, Fig. S6). It differs from that of *C. petrinus*, *C. duelferi,* and *C. buchseri* in the rounded proximal and distal margins, with indistinct articular facets for the radius and ulna, and the lack of an anterior flange (Fig. S6). It differs from that of *C. buchseri* in proportions, in being more than twice as long as wide. The humeri of *C. nichollsi* and *Thalattoarchon* are unknown.

Cymbospondylus youngorum sp. nov. has the same skull to preorbital length ratio as *C. petrinus*, and both differ distinctly from *C. duelferi*, resulting in a slightly shorter preorbital length in *C. duelferi* (56%) when compared to the other two (61%/61.5% of skull length in *C. youngorum* sp. nov. and *C. petrinus*). The postorbital length in relation to skull length is relatively greater (22.8%) in *C. youngorum* sp. nov. than in *C. petrinus* (17.6%), *C. duelferi* (18.5%), and *C. nichollsi* (20.0%). The orbit to skull length ratio is greatest in *C. duelferi* (21.5%) and smallest in *C. youngorum* sp. nov. (14.7%). The value for *C. petrinus* is 17.0%. In fact, the ratio of *C. youngorum* sp. nov. is the smallest known for ichthyosaurs, likely a result of scaling effects (table S2).

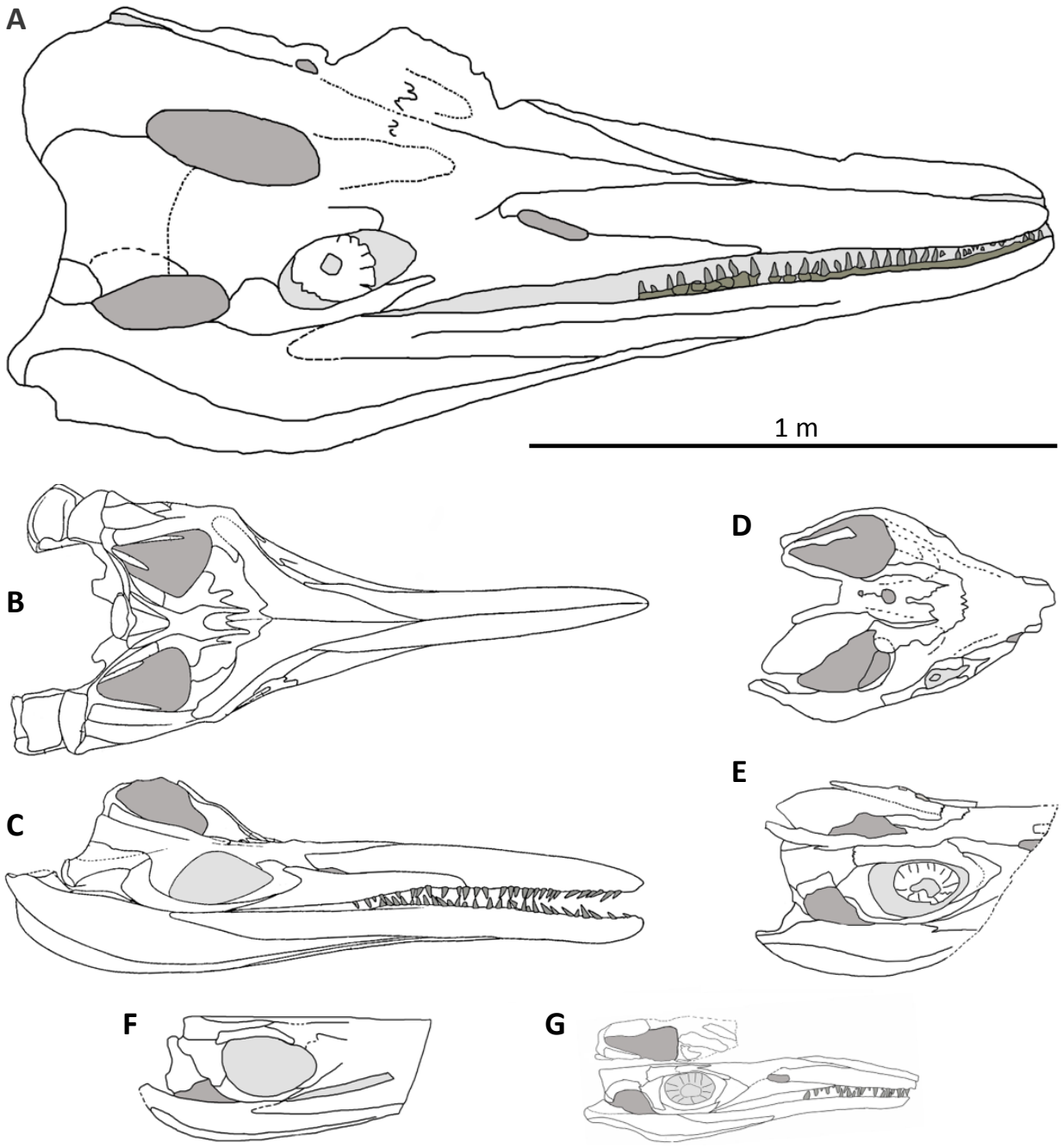

Fig. S4. Comparison of skulls of the species of *Cymbospondylus*. All images are to the same scale, taxa are arranged by decreasing size. (**A**) *C. youngorum* sp. nov., dorsolateral view. (**B**) *C. petrinus*, dorsal view. (**C**) *C. petrinus*, lateral view. Both views are modified from Merriam (1908)(*38*). (**D**) *C. nichollsi*, dorsal view. (**E**) *C. nichollsi*, lateral view. Both views are modified from Fröbisch et al. (2006)(*16*). (**F**) *C. buchseri*, dorsal view modified from Sander (1989). (**G**) *C. duelferi*, dorsolateral view modified from Klein et al. (2020)(*17*).

Supplementary Anatomical Description: Skull

The right half of the skull is exposed from the field bottom and is seen in dorsolateral view. Most of the bones of the snout, cheek, and skull roof are thus described from the right side of the skull. The lower jaws are tightly articulated. The right lower jaw is fully exposed in lateral view and is 1965 mm long from the tip of the dentary to the tip of the retroarticular process. The left half of the skull and the palate is seen in field-top view but largely covered by the lower jaws. The skull is highly ossified and sutures are only well visible in the preorbital region. Sutures are additionally obscured by numerous cracks, intertwined and telescoped skull elements, and shifted cervical vertebrae as a result of dorsoventral compaction of the skull as well as disarticulation of the neck.

The snout, dominated by the premaxillae and nasals, appears relatively massive compared to the other species of *Cymbospondylus* (Fig. 2, Fig. S4) and most later ichthyosaurs. It is wedge-shaped and evenly tapering. However, the preorbital region measures 61.4% of the entire skull length. The maxilla is long (62.9 % of preorbital length and 38.6% of entire skull length) compared to more derived ichthyosaurs. The maxillary tooth row is restricted to the anterior half of the maxillary and does not reach posterior to the external naris. At 43, the total number of tooth positions in the upper and lower jaw is higher than in any other *Cymbospondylus* species for which it is known; Fig. S4, table S2). The postorbital region is 22.75% of the entire skull length and 47.25% of the postnarial length. The postorbital region is longer than the orbit. The latter is 14.7% of entire skull length and 32.4% of the postnarial length. The postorbital region (cheek region) is slightly less than 1/3 of the preorbital length (61.4% of entire skull length). See table S2 for further ratios.

The orbit is elliptical and wider than high. The length of the orbit is only 14.7% of skull length and 14.1% of lower jaw length. These are very low values for an ichthyosaur and probably reflect negative interspecific allometry of the orbit during evolutionary body size increase. The diameter of the eye, as indicated by the scleral ossicles, was perhaps even smaller than the height of the orbit, similar to other species of *Cymbospondylus*. The number of scleral plates supporting the eyeball is not countable due to preservation. The orbit is nearly as long as the upper temporal opening (table S1). The anterior orbital margin is the shape of a half ellipse.

A distinct anterior terrace is visible in front of the upper temporal opening. This anterior terrace is anteriorly tapering and elongated, extending as far anterior as to the level of the posterior external naris (Fig. 2). Sutures are highly ossified here and elements contributing to the anterior terrace cannot be identified with confidence. The posterodorsal part of the parietals forms a low parietal (sagittal) crest. The lower temporal embayment is of a similar length as the orbit and slightly shorter than the upper temporal opening (table S1). For further measurements, see table S1, and for skull ratios see table S2.

Premaxilla. Both premaxillae meet anteriorly at a distinctive midline suture, the anteriormost part of which has split open a bit during fossilization. Posteriorly, the premaxillae are divided by anterior processes of the tapering nasals. Posterolaterally, the premaxilla reaches shortly beyond the posterior end of the external naris (Fig. 2). The bone forms the dorsal margin and surrounds the anterodorsal part of the external naris. The suture to the maxilla is obscure. In the right premaxilla, teeth are hidden from view due to skull deformation. The field-top view of the specimen provides the occlusal view of the teeth of the left premaxilla, displaying a bulging mass of bone of attachment (see below) and 36 tooth positions, including 10 empty alveoli.

Maxilla. The right maxilla is seen in lateral view and the left one in ventrolateral view. Most of the description is based on the right maxilla. The maxilla is relatively large, reaching 62.9% of the preorbital length. Although the dorsomedial sutures of the maxilla to the lacrimal and the nasal are obscured by damage to the bone surface, overall, the maxilla resembles an elongate triangle with the ventral part forming the longest side and the dorsal part having the widest angle. The anterodorsal part tapers and shares a suture with the premaxilla (Fig. 2). Posteroventrally, the maxilla contacts the lacrimal and ventrally it has a suture with the jugal. The maxilla forms the ventral margin of the external naris. No teeth are exposed on the right maxilla, but the left maxilla can be seen to carry seven functional teeth which are visible in medial (field top) view only. The combined information of field top and field bottom view revealed that the maxillary tooth row extends posteriorly to the level of the posterior margin of the external naris and thus stops well before the orbit. This can be seen when overlaying images of the dorsal and ventral view of the skull, revealing the position of the orbit even in ventral view.

Lacrimal. The lacrimal forms the anterior margin of the orbit. However, only the ventral suture along the orbit margin of the lacrimal is well visible (Fig. 2), where the lacrimal contacts the jugal and maxilla.

Nasal. The nasal is a large element that makes up most of the preorbital skull in dorsal view and contributes also to the lateral part of the skull where the nasals contact the maxilla. The anterior processes are distinctly separated along a midline suture (Fig. 2). The nasals reach well anterior to the external naris and deeply divide the premaxillae. The nasals are excluded from the dorsal margin of the external naris and probably from the entire external naris because they do not seem to enter the naris along its posterior margin, either. The nasals appear to broaden posteriorly to the external naris by forming a ventrolateral process, which contacts the maxilla. No sutures are discernable further posteriorly. The nasal is likely separated from the orbit margin by the pre- and postfrontals. The posterior extent of the nasals remains unknown.

Prefrontal and postfrontal. No sutures are visible in the region of these bones except for that between the lacrimal and the prefrontal. However, both elements are most likely fused to each other and must form the dorsal margin of the orbit.

Frontal and parietal. Sutures of both elements are not discernable except for the dorsal interdigitating nasal-frontal suture. This is located anterior to the upper temporal fenestra at the height of the middle of the anterior terrace and orbit. Most likely the frontal borders the anterolateral part of the upper temporal fenestra, but it is excluded from the orbit by the fused pre- and postfrontals. Medially, the frontal has contact to the parietal. Most likely, the parietal forms the anteromedial and entire medial margin of the upper temporal fenestra. The posterior part of the skull roof is formed by the parietals, which are separated by a deep slit along the skull midline (Fig. 2). A thin medial parietal ridge is present, different from the low to high parietal crests of the other species of *Cymbospondylus*. However, the presence of a crest may have been obscured by heavy compaction of the skull in this region.

Supratemporal. Again, because of compaction, the supratemporal is not well delimited, but we assume its presence in the posterior skull region. The bone must form the posterior margin of the upper temporal fenestra as suggested by the suture ventrally separating it from the squamosal.

Jugal. The jugal forms the ventral and posteroventral margin of the orbit. Anteriorly, the jugal ascends slightly, but it is separated from the anterior margin of the orbit by the ventral process of the lacrimal. The posteroventral part of the jugal forms the anterior margin of the lower temporal embayment. At its posteroventral part, the jugal has a short posterior process that is directed into the lower temporal embayment. Dorsally, the jugal contacts the postorbital in a dorsally convex suture (Fig. 2).

Postorbital. There are no clear sutures indicating the size and shape of the postorbital except for the ventral suture with the jugal (Fig. 2). The postorbital likely forms the mid-posterior margin of the orbit. It is unclear whether the postorbital extends dorsally as far as to the lateral margin of the upper temporal fenestra. However, the postorbital contributes to the anterodorsal margin of the lower temporal embayment with its posterior part as evidenced by the suture with the quadratojugal

Squamosal. The sutures delimiting the squamosal are not discernable, except for the dorsal one. However, the squamosal must form most of the area of the cheek region. The dorsal suture extends posteriorly from the posterior margin of the upper temporal opening, indicating that the squamosal contributes to the margin of the upper temporal opening (Fig. 2), although the extent of this contribution is unclear. The squamosal probably contacts the postorbital anteriorly (and maybe also the postfrontal), the quadratojugal and quadrate ventrally, and the supratemporal dorsally in a deep suture. The extent of the contribution of the squamosal to the upper temporal opening is unclear.

Quadratojugal. This bone makes the most extensive contribution to the dorsal margin of the lower temporal embayment. It has sutural contacts with the quadrate posteriorly and the postorbital anteriorly. Dorsally, the squamosal must have bordered the squamosal but a clear suture is lacking.

Quadrate. In lateral view, this bone is incompletely exposed, as in most ichthyosaurs but in posterior view, it has a fairly large dorsal extent. The quadrate forms the condyle of the jaw joint, the ventral-most part of the posterior skull margin, and contributes to the posterodorsal end of the lower temporal embayment. In anterior direction, the quadrate is bordered by the quadratojugal.

Occipital region. The occipital region provides no information because of the strong compaction of the skull in its posterior half.

Palatal region. The palatal region is largely covered by the lower jaws, primarily the left one. In between the jaw rami, the palate remains obscured by matrix, and in the posterior palatal region, compaction has obliterated any morphology.

Lower jaw. The lower jaws are in tight contact with the skull and to each other but seemingly somewhat separated at the symphysis (Fig. 2). The left lower jaw is exposed in lateral and the right one in medial view, both revealing different elements and/or different views on the same elements. The right lower jaw is well preserved and articulated but the left one appears more crushed and is somewhat disarticulated posteriorly. The ventral border of the right lower jaw is anteriorly very slightly concave but below the eye forms a distinctive convex line. The retroarticular process is short, terminating slightly posterior to the occipital region and jaw joint. As mentioned above, the total length of the right lower jaw is 1970 mm.

Dentary. The right dentary is completely exposed in lateral view. Mainly the left dentary is visible in the ventral view of the skull. The right dentary reaches posterior to the posterior orbital margin and thus forms over two thirds of the length of the lower jaw. The preserved teeth stop

well before the external naris (check as can be seen in the overlay of the ventral and dorsal skull images. The surface of the anterior part of the dentary carries six deep slanted foramina (Fig. 2) that continue into a distinctive groove in the dorsoventral center of the bone. The groove continues nearly to the posterior end of the dentary, well beyond the end of the tooth row. The left dentary reveals 31 tooth positions of which 21 hold functional teeth, whereas the right dentary carries approximately 29 teeth. The teeth in both dentaries are set in a thick rim of porous bone of attachment which is particularly pronounced in the posterior part of the tooth row (Fig. 2). *Cymbospondylus youngorum* sp. nov. exhibits a labial shelf on the dentary, which means that the dentary teeth are positioned lingually, exposing labially a broad horizontal surface as defined in reference (*77*) (Fig. S2C).

Surangular. The well exposed right surangular extends anteroventrally from the anterior margin of the external naris to the posterior end of the lower jaw, reaching half of the jaw length. The bone borders anterodorsally on the dentary and ventrally on the angular, resulting in a wedge-shaped anterior part. The posterior end appears curved downward in the retroarticular process. The suture to the articular is not visible, suggesting that there is no lateral exposure of the articular. However, the dorsal margin of the surangular in this regions is deeply concave, indicating a deeply excavated glenoid. The left surangular is less well preserved but equally large.

Angular. In lateral view of the right lower jaw, the angular runs parallel to the surangular, expanding posteriorly in height, exceeding that of the surangular in this region. The exposure of the angular is also extensive in the retroarticular process, to which the angular contributes more than the surangular. The angular forms at least the posterior half of the ventral margin of the lower jaw. In anterior direction, the angular thus extends much further than the surangular (well anterior to the external naris). The angular has a pointed anterior process and contacts the dentary in a long suture. In the medial view of the right lower jaw, a short part of the suture between surangular and angular is visible through the Meckelian fossa (Fig. 2).

Articular and prearticular. The articular and prearticular are exposed in medial view in the right lower jaw. The articular forms the posterior tip of the lower jaw and is ventrally bordered by the prearticular, which has an anterior pointed process that apparently contacts the dentary in the coronoid region. However, there is no evidence for a coronoid (Fig. 2). The dorsal margin of the prearticular and the anterior margin of the articular encompass a large Meckelian fossa.

Splenial. The right splenial is extensively developed and probably the longest bone of the lower jaw. It forms most of the medial wall of the lower jaw and contributes clearly to the mandibular symphysis. The splenial here has a wedge-shaped suture to the dentary. Posteriorly, the splenial terminates in a pointed tip that extends considerably below the prearticular.

Dentition. Although the right side of the skull is better exposed, the left side offers a more comprehensive view on the dentition and count of the number of teeth (table S1). In particular, the premaxilla is well exposed in occlusal view. As noted above, the left premaxilla carries 36 tooth positions, of which 26 hold functional teeth and ten represent empty alveoli (Fig. 2, Fig. S2). The left maxilla has seven functional teeth and no empty alveoli. The total of tooth positions thus is 43 in the upper jaw. As noted, the left dentary reveals 31 tooth positions of which 21 hold functional teeth, whereas the right dentary carries approximately 29 teeth. Six of these are smaller, representing replacement teeth which can be recognized by their distinctly smaller size (Fig. 2, Fig. S2). The dentary tooth rows appear to extend less far posteriorly than the tooth rows of the upper jaws. This is likely an artifact of preservation in that the posterior teeth of both dentaries are hidden from view by compactional rotation of the dentaries. Given that the teeth of the upper and the lower jaw are of equal size, there is no reason to assume that the lower tooth count was substantially different from the upper count.

The individual teeth are relatively uniform in size and shape, neither of which differ between the upper and the lower jaw. Maximum measured crown height is 37 mm in the middle of the right lower jaw. This is slightly larger than average relative tooth size for ichthyosaurs (Fig. S5, table S3) and very different from the very large teeth of the somewhat smaller ichthyosaur *Thalattoarchon* (crown height in posterior maxillary teeth of 50 mm, *8*). The tooth

crowns are conical with bluntly pointed tips and coarsely striated enamel similar to other ichthyosaurs (*20*). The base of the enamel cap is well defined (Fig. 2F, Fig. S2). The horizontal section of the teeth is circular at the root but becomes more triangular in the crown but without distinct carinae marking the triangle (Fig. 2F, Fig. S2). The crowns are slightly curved inwards (towards lingual, Fig. 2E, F, Fig. S2). Prominent grooves and ridges basal to the crown in the apical third of the root are visible at the basis of the tooth crown, indicating the presence of plicidentine, although the root is covered by bone of attachment in most teeth. Plicidentine was also observed in the fracture planes crossing the snout before preparation of the skull during excavation (Fig. S2G).

Tooth implantation and tooth replacement are not fully understood, but we offer the following observation. The anchoring of the teeth involves a thick bone of attachment which means that teeth are sitting on a bulge or rim of porous bone tissue (Fig. 2, Fig. S2E). The bone of attachment separates each individual tooth and its roots from the neighboring teeth in the posterior part of the jaw but less so in the anterior part where the teeth appear more densely spaced as well (Fig. 2, Fig. S2). Alveoli appear closed and not open to the labial side as in *C. duelferi* (*17*). The replacement tooth seems to develop below a functional tooth, eventually displacing its predecessor. This pattern is again different from *C. duelferi* where there is an alternate pattern of tooth replacement (*17*).

The species of *Cymbospondylus* differ in various aspects of their dentition such as number of teeth, size of teeth, spacing of teeth (Fig. S4), tooth implantation and tooth replacement. This statement is based on the evidence from the holotypes of *C. youngorum* sp. nov. (this study), *C. duelferi* (LACM DI 158109; *17*), and specimens UCMP 9913 and UCMP 9950 of *C. petrinus* (*40*). The dentition of *C. nichollsi* remains unknown (*16*). The dentition of *C. buchseri* (*15*) is too poorly known for a direct comparison but its teeth are in general similar, being conical in the middle part of the rostrum and lower jaw.

At 43 upper jaw tooth positions, *C. youngorum* sp. nov. has more teeth than *C. petrinus* (30-35) and *C. duelferi* (25 - 30). Compared to the other species of the genus, the relative tooth size of *C. youngorum* sp. nov. is similar to that of *C. petrinus* and average for ichthyosaurs in general (Fig. S4). A qualitative assessment suggests the teeth of *C. youngorum* sp. nov. are relatively smaller than the teeth of *C. duelferi* and possibly *C. buchseri* (Fig. S4). Although we

did not quantify tooth spacing directly, the teeth of *C. youngorum* sp. nov. are more densely spaced than in the other species, especially *C. duelferi* (Fig. S4). The relatively closer spacing of the teeth results from their higher number but average size (Fig. S5). There is a low number of empty alveoli, indicating that tooth formation was relatively faster and residence time of functional teeth was relatively longer than in the other species. In *C. youngorum* sp. nov. and *C. petrinus*, tooth replacement was more irregular as opposed to the alternating replacement in *C. duelferi*. *Cymbospondylus youngorum* sp. nov. and *C. duelferi* both show distinctive bone of attachment which is lacking in *C. petrinus* and *C. buchseri.*

Table S1. Skull and postcranial measurements (in mm, unless noted otherwise) of *Cymbospondylus youngorum* sp. nov. Measurements are from the right side of the skull unless noted otherwise (see pictures to document the exact placement of the measurements).

Skull length	1890
Lower jaw length	1970
Skull height along the quadrate	510
Skull length posterior to nares (postnarial length)	910
Skull length anterior to nares (prenarial length)	850
Preorbital length	1160
Length of cheek (postorbital) region	430
Length of orbit	278
Height of orbit	125
Length of upper temporal opening	325
Width of upper temporal opening	ca. 135
Length of lower temporal embayment	272
Width of lower temporal embayment	103
Length of maxilla	730
Postdentary length of lower jaw	580
Length of right splenial Length of left splenial	1610 1400
Number of pmx teeth	left pmx: 36 positions, 10 empty alveoli
Number of mx teeth	left mx: 7 positions, none empty
Number of dentary teeth	left dentary: 31 positions, 21 functional teeth
Tooth crown height emerging from bone of attachment	max. is 37 mm, at pos. 9 and pos. 20 of right dentary
Weight of skull (kg)	173
Length of right humerus	453

Table S2. Comparison of measurements, counts, and ratios of the Nevada species of *Cymbospondylus*. Body length for *C. duelferi*, *C. petrinus*, and *C. youngorum* sp. nov. is based on the regression of body length on humerus length described below (Fig. S8). Body length for *C. nichollsi* is from reference (*16*). Total skull length is estimated for *C. nichollsi* and *C. duelferi*. nm = not measurable; UTF = upper temporal fenestra. Linear dimensions are in mm.

Species	***C. duelferi***	***C. nichollsi***	***C. petrinus***	***C. youngorum* sp. nov.**
Specimen number	**LACM DI 158109**	**FMNH PR2251**	**UCMP 9950**	**LACM DI 157871**
Length (mm)				
Body length (estimated)	4996	7600	12563	17648
Skull length	>610 (~650)	~975	1166	1890
Humerus length	132	-	325	453
Counts in skull				
Number of scleral ossicles	12	14	16-18	-
Tooth positions in upper jaw/ dentary	>21/-	-	30-35/30-35	43/>31
Ratios in skull				
Skull length/preorbital length	1.78	-	1.63	1.63
Skull length/postorbital length	5.4	4.97	5.69	4.4
Skull length/UTF length	4.3	4.3	6.1	5.8
Skull length/maxilla length	3.4	-	2.84	2.59
Postnarial length/postorbital length	2.95	2.26	2.56	2.1
Postnarial length/maxilla length	1.63	-	1.54	1.25
Postnarial length/UTF length	2.06	1.95	2.8	2.8
Postnarial length/orbit length	2.2	2.2	2.7	3.08
Preorbital length/maxilla length	1.93	-	2.08	1.59
Orbit length/orbit height	1.73	1.56	1.72	2.36
Orbit length/skull length	0.215	0.215	0.170	0.147
Orbit length/preorbital length	0.38	-	0.28	0.25

Orbit length/postorbital length	1.17	0.7	0.9/0.64	0.69
Orbit length/length of cheek region	1.31	0.83	0.79	0.69
Orbit length/maxilla length	0.74	-	0.5	0.4
Orbit length/postdentary length	0.9	0.55	0.62	0.51

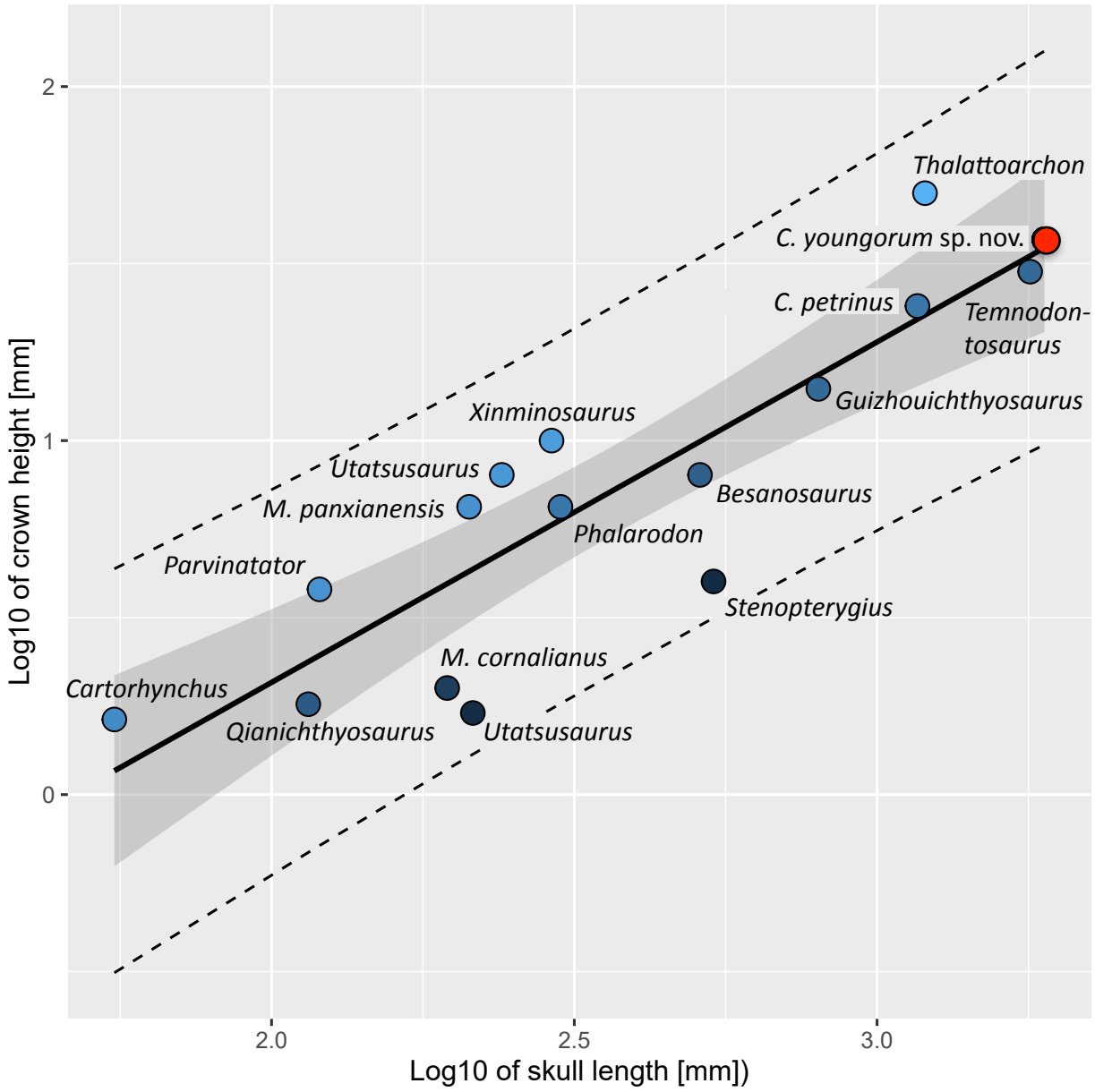

Fig. S5. Relative tooth size in *Cymbospondylus youngorum* sp. nov. Linear regression of skull length vs. tooth crown height for selected ichthyosaurs for which both measurements are available. Tooth crown height in *Cymbospondylus youngorum* sp. nov. is average and similar to *C. petrinus*. Shaded area indicates 95% confidence interval. The dashed lines delimit the 95% prediction interval. The color of the data points is coded to the regression residuals. Data is from Table S3.

Table S3. Skull length and tooth size of *Cymbospondylus youngorum* sp. nov. compared to other ichthyosaurs. This table contains the source data for the graph of relative tooth size in Fig. S5. PIMUZ, Paläontologisches Institut und Museum Universität Zürich, Switzerland; UCMP, University of California Museum of Paleontology.

Taxon	Skull length (mm)	Crown height (mm)	Source skull length	Source crown height
Besanosaurus leptorhynchus	510	8	*78*	*78*
Cartorhynchus lenticarpus	55	1,63	*79*	*79*
Chaohusaurus brevifemoralis	115	1,8	*63*	Measured from photo of holotype in *63*
Cymbospondylus petrinus	1166	24	*38*	Measured from photo of UCMP 9950
Cymbospondylus youngorum sp. nov.	1890	37	This study	This study
Guizhouichthyosaurus tangae	800	14	*80*	*80*
Mixosaurus cornalianus	195	2	Personal observation PMS on PIMUZ T 4376	Personal observation PMS on PIMUZ T 4376
Mixosaurus panxianensis	212	6.5	*77*	*77*
Parvinatator wapitiensis	120	3.8	*81*	*81*
Phalarodon callawayi	300	6.5	*39*	*39*
Qianichthyosaurus zhoui	240	8	*82*	Measured from figures in the same paper.

Stenopterygius quadriscissus	537	4	Personal observation PMS on spec. no IGPB R364	Personal observation PMS on spec. no IGPB R364
Temnodontosaurus platyodon	1790	30	*22*	*22*
Thalattoarchon saurophagis	1200	50	*8*	*8*
Utatsusaurus hataii	215	1.7	*83*, *84*	*84*
Xinminosaurus catactes	290	10	*85*	Measured from photo of holotype

Supplementary Anatomical Description: Postcranial skeleton

Vertebral column. Vertebrae currently can be studied in two regions of the skeleton: cervical, and middle dorsal vertebrae are all vertebrae that retain the parapophysis (*15*, *16*). Two or three anterior cervical vertebrae were dislocated to the right upper temporal opening (Fig. 2A), but these vertebrae are too deformed for description. Another three heavily deformed cervicals are seen in the field-top view of the skull, being crushed against the occiput (Fig. 2C, D). Four posterior cervical vertebrae are preserved in block 10. The minimum count of cervicals in *C. youngorum* sp. nov. thus is nine or ten, comparable to *C. petrinus* (*38*) and *C. nichollsi* (*16*)(eight to ten), but higher than in *C. buchseri* which has only six (*15*, *16*).

Dimensions of the posterior cervicals as measured along the ventral midline are between 59 mm and 62 mm, the minimum dorsoventral height is 130 mm. The centra have a flat ventral surface, clearly different from the nearly round ventral surfaces of *Thalattoarchon* (*8*). The second-to-last cervical centrum has two rib articular facets, a round parapophysis and an incompletely exposed diapophysis. In the last cervical centrum, there is a very small parapophysis, suggesting that this centrum represents the posteriormost cervical (Fig. S3A).

Articulated middle dorsal vertebrae were the only bones initially visible of the skeleton upon discovery. The centra of these vertebrae are distinctly taller than wide and long. The rib articular facets are elongate, extending in an anteroventral direction. The facets are truncated by the anterior face of the centrum, as is typical for the dorsal vertebrae of *Cymbospondylus* (*15*, *38*, *86*).

Scapula. The right scapula is preserved completely albeit with some crushing. The ventral part of the scapula forms a thickened head for the articulation with the coracoid and formation of the glenoid. However, there is no apparent separation between the coracoid facet and the glenoid facet. The ventral part continues into a narrow blade that asymmetrically widens dorsally, with the posterior part of the blade being more developed than the anterior part. The blade ends dorsally in a rounded margin. The greatest dimension of the scapula along the longitudinal axis of Motani (*87*) is 425 mm. This scapula morphology lacks a close match in any other ichthyosaur scapulae (see illustrations in *87* and Fig. S6) although homologous parts such as the dorsal blade and the facets for the coracoid and glenoid are recognizable.

Coracoid. The right coracoid is incompletely exposed, with only the lateral part being visible. There is a greatly thickened articular facet for the scapula and distinctive coracoid foramen (Fig. S3), like in all the other species of the genus except for *C. duelferi* (*17*) which lacks a foramen. The glenoid margin is thick (85 mm) and 230 mm long. The coracoid foramen in *C. youngorum* sp. nov. is 30 mm long. The posterior margin is nearly straight, but the anterior and medial portions are absent and may be preserved in adjacent blocks 5, 6, and 8.

Clavicle. Both clavicles are present but incompletely exposed. The better exposed one has a preserved length of 410 mm, and increases in maximum diameter in posterior direction from 40 mm to 65 mm. The anterior region has roundish-squarish cross section which changes posteriorly into a triangular one via a crest that gradually develops. Little can be said about the other clavicle because it is still mostly covered by a concretionary matrix. The bone also has a sharp keel or edge to it but no blade, like *C. buchseri* but unlike *C. petrinus, C. nichollsi*, and *C. duelferi.*

Humerus. Both humeri are preserved but only the right one is currently prepared. The humerus of LACM DI 157871 shows a simplified morphology (Fig. 2G-K), lacking any pronounced flanges, crests, trochanters, and tuberosities. The humerus is more than twice as long proximodistally than anteroposteriorly wide, and the proximal end is wider than the distal end. Total length is 453 mm, the proximal end is 252 mm wide, and the distal end is 232 mm wide. The proximal head is not set off, a dorsal trochanter, and a dorsal ridge are not visible. The proximal articular facet is distinctly triangular (Fig. 2G), resulting from a shallow deltopectoral crest. The anterior margin is concave and sharp but it lacks an anterior flange. The posterior margin is also concave but more rounded than the anterior margin, resulting in an uneven triangular shaft cross section. The indistinct distal facets are terminal with the radial facet being larger than that of the ulnar facet. An anterodistal or posteriodistal facet for a sesamoid is absent. The proximal and distal margins of the periosteal bone show distinctive low ridges oriented longitudinally.

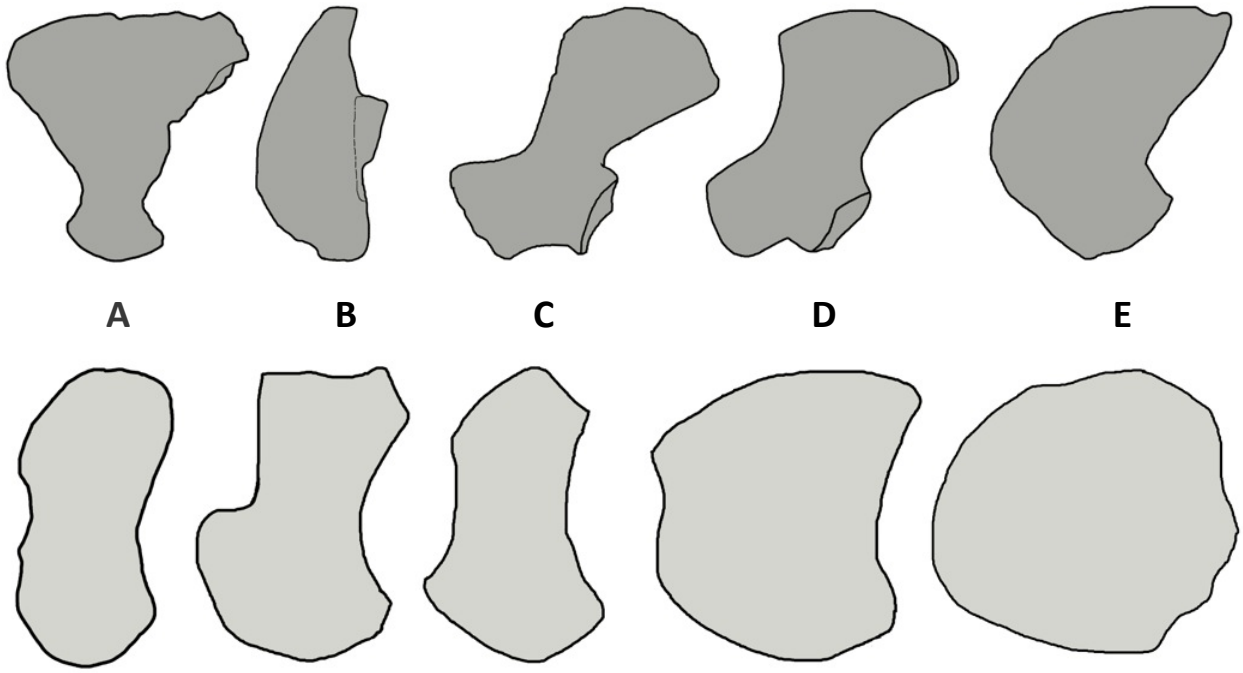

Fig. S6. Comparison of shape shape of the scapula (top) and humerus (bottom) of large Middle Triassic ichthyosaurs. (**A**) *Cymbospondylus youngorum* nov. spec. (**B**) *C. duelferi*, modified from Klein et al. (2020)(*17*). (**C**) *C. petrinus*, modified from Merriam (1908)(*38*). (**D**) *C. buchseri*, modified from Sander (1989)(*15*). (**E**) *Besanosaurus leptorhynchus*, modified from Dal Sasso & Pinna (1996)(*78*). Images are not to scale.

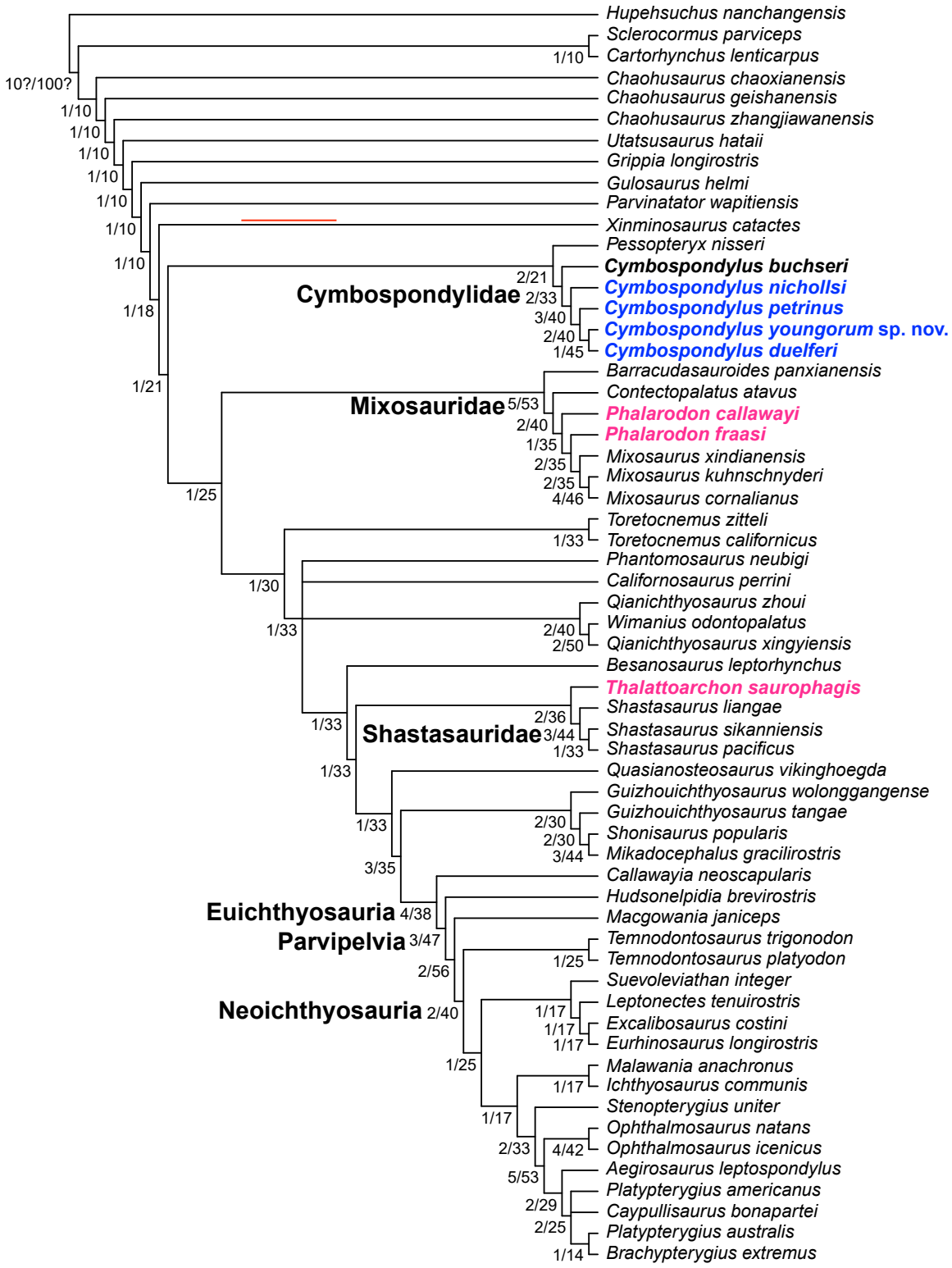

Fig. S7. Phylogenetic hypothesis for Ichthyosauria based on Analysis I. The new taxon Cymbospondylus youngorum sp. nov. is part of the Fossil Hill Member Cymbospondylus clade (blue lettering). Species set in magenta are also part of the FHF. Numbers at nodes indicate absolute and relative Bremer support values.

Table S4. Comparison of the the four phylogenetic analyses. CI, consistency index; PAUP, PAUP software for phylogenetic analysis (*64*); MPTs, most parsimonious trees; RI, retention index; TNT, TNT software for phylogenetic analysis (*62*).

	Analysis I	**Analysis II**	**Analysis III**	**Analysis IV**
Search	TNT, new tech	TNT, traditional	TNT, new tech	PAUP, heuristic
# Taxa	60	60	39	39
Tree length	1225	1225	851	843
# MPTs	4	3286	2	308
CI	0.259	0.259	0.329	0.331
RI	0.627	0.627	0.545	0.533

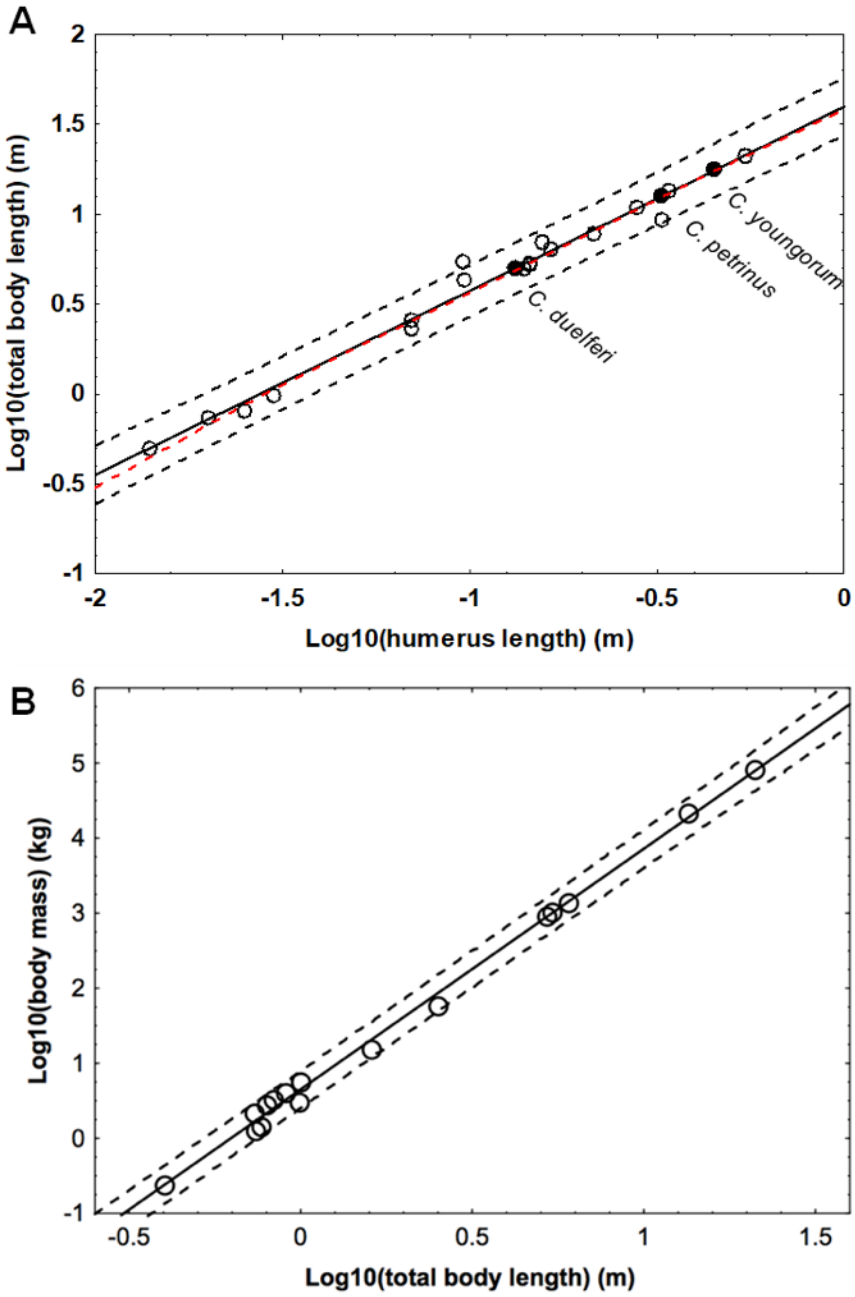

Fig. S8. Linear regression analyses on the relationship between humerus length, total body length and body mass of Triassic ichthyosaurs. Prior to both analyses, humerus length (HL), total body length (TL) and body mass (BM) of ichthyosaurs were log10-transformed. (**A**) Regression of log10(TL) on log10(HL). The ichthyosaur sample analyzed (N = 18) is the compilation from Scheyer et al. (*23*). The regression relationship is log10(TL) = 1.599 (s.e.=0.038) + 1.023 (s.e.=0.035) * log10(HL), with $R^2 = 0.9801$. The red dashed curve is the inverse of that published in Scheyer et al. (*23*). Scheyer et al. (*23*) predicted humerus length from total body length without log transformation and gave no prediction interval. Note that their curve only underestimates total body lengths for small humerus lengths compared to our function. (**B**) Regression of log10(BM) on log10(TL). The ichthyosaur sample analyzed is found in table S4 and is from Gutarra et al. (*24*). The regression relationship is log10(BM) = 0.6529 (s.e.=0.0312) + 3.2064 (s.e.=0.0552) * log10(TL), with $R^2 = 0.9956$. Black dashed lines indicate 95% prediction intervals of regressions in both panels.

Table S5. List of Triassic ichthyosaur total body lengths and body mass estimates. This length data set was compiled by Gutarra et al. (*24*) and used by us for establishing a length vs. mass regression in order to estimate body masses of the Fossil Hill Member ichthyosaurs. Gutarra et al. (*24*) provided body mass estimates for 1 m-sized ichthyosaurs (V (m^3) + limbs) from different Triassic genera. They reconstructed this standardized body mass of specimens from digital models erected for different genera (V (m^3) +limbs). We up- or down-scaled the respective 'V (m^3) +limbs' value to the total body length of each listed specimen in order to estimate its body mass. See Gutarra et al. (*24*) for details of specimens and collections acronyms.

Genus	Species	Total body length (m)	Specimen	Reference	V (m +limbs	Body mass (kg)
Cartorhynchus	*lenticarpus*	0.4	AGM CH-628-16	*25*	0.0037	0.237
Sclerocormus	*parviceps*	1.6	AGB6265	*88*	0.0037	15.155
Chaohusaurus	sp.	0.763	AGM I-1 CHS-5 composite	*89*	0.0032	1.421
Chaohusaurus	sp.	0.99	AGM L-4	*88*	0.0032	3.105
Chaohusaurus	*zhangjiawanenesis*	0.74	WHGMR V26001	*90*	0.0032	1.297
Utatsusaurus	*hataii*	2.5	Reconstruction	*91*	0.0037	57.813
Mixosaurus	*cornalianus*	0.795		*8*	0.0057	2.864
Mixosaurus	*cornalianus*	0.83	PIMUZ T4376	*39*	0.0057	3.259
Mixosaurus	*cornalianus*	0.9	PIMUZ T2420	*92*	0.0057	4.155
Mixosaurus	*panxianensis*	0.73	GMPKU-P-1039	*77*	0.0057	2.217
Mixosaurus	*xindianensis*	1	YIGM SPC V-0732	*93*	0.0057	5.700
Shonisaurus	*popularis*	13.5	Reconstruction	*94*	0.0088	21651.300
Shonisaurus	*sikanniensis*	21	TMP 94.378.2	*45*	0.0088	81496.800
Guizhouichthyosaurus	*tangae*	5.4	TR 00001	*95*	0.0065	1023.516
Guizhouichthyosaurus	*tangae*	5.2	IVPP V 11853	*96*	0.0065	913.952
Guizhouichthyosaurus	*tangae*	6	Various specimens GNG	*80*	0.0065	1404.000

Comparative Body Size Evolution Analysis: Supplementary Information

Phylogenies for ichthyosaurs and cetaceans. For the size evolution analysis, we used the phylogeny from this study for ichthyosaurs (Methods of main text, Figs. 2 and S7). For cetaceans, we compiled a comprehensive phylogeny with a special focus on early whales. This phylogeny (Fig. S9) includes 250 taxa from the earliest cetaceans to representative extant species. Most large morphological or combined phylogenetic analyses of cetaceans derive from the character/ state matrix first published by Geisler and Sanders (*66*), with modifications made in subsequent works (e.g., *97-101*). While taxon sampling sometimes varies amongst these works, the relationships between different cetacean groups are generally stable and consistent. For the sources of this phylogeny, we followed McGowen et al. (7*2*) for extant taxa, Martínez-Cáceres et al. (*102*), Gibson et al. (*103*), and Lambert et al. (*104*) for early cetaceans outside of the odontocete-mysticete dichotomy, Marx and Kohno (*105*), Bisconti et al. (*106*, *107*), Buono et al. (*108*), Slater et al. (*6*), Fordyce and Marx (*109*), Peredo et al. (*33*), Muizon et al. (*110*), and Hernández-Cisnero and Velez-Juarbe (*69*) for mysticetes, and Aguirre-Fernández et al. (*111*), Murakami et al. (*112*), Ramassamy (*113*), Tanaka and Ishichima (*114*), Bianucci et al. (*115 - 117*), Tanaka et al. (*118*), Velez-Juarbe (*119*), Peredo et al. (*71*), Viglino et al. (*70*) and Benites-Palomino et al. (*120*) for odontocetes.

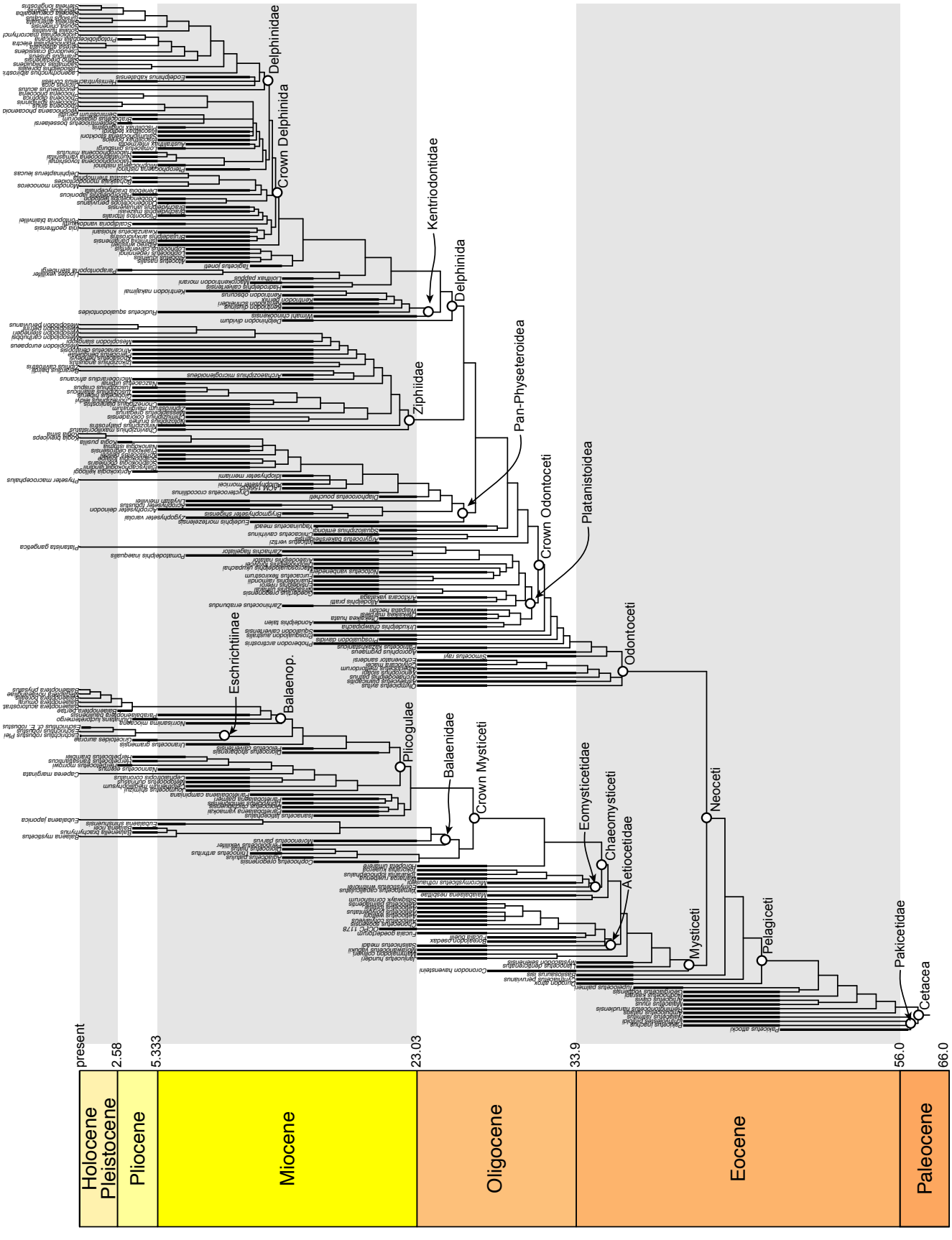

Fig. S9. Composite cetacean phylogeny and time calibration. For details see text. References to taxa, phylogenies, and temporal occurrences are found in supplementary Data S5.

Stratigraphic ranges for time calibration of phylogenies. For time calibration of our phylogenies we relied initially on the Paleobiology Database (http://fossilworks.org/?a=home) with subsequent verification from the primary literature. Our first and last appearance dates are then based on the geologic stages that apply to each taxon following the GSA Geologic Time Scale (*34*). Most of our dates agree with those in the PBDB and with the dates used by Lloyd and Slater (*67*) for the cetaceans. One notable difference, however, is that our range for *Pakicetus attocki* differs by being older, encompassing the Ypresian, instead of Lutetian as listed in the Paleobiology Database. Our justification for the older stratigraphic is the occurrence of *P. attocki* in the Kuldana Fm. (Pakistan) and the Subathu Fm. (India) which seem to span across these two stages (e.g., *68*, *121*, *122*, *123*). However, the justifications used to correlate these formations and restrict the age of *P. attocki* to either the Ypresian or Lutetian have been criticised (*122*, *123*) and thus the age remains controversial (*124*), although other authors seem to favor a Ypresian age for Pakicetidae (e.g., *125*: fig. 1, *126*: fig. 1) while others show their range spanning across the Ypresian-Lutetian (e.g., *127*: fig. 7.2). We account for this uncertainty by assigning *P. attocki* to the Ypresian while placing all other pakicetids into the Lutetian, so that Pakicetidae as a whole comprise the full range of Ypresian-Lutetian.

Image credits for vectorized outlines of ichthyosaurs and cetaceans. Ichthyosaur silhouettes are modified from PhyloPic, please see table S6 for full credits, while silhouettes of cetaceans are based on life restoration work of Carl Buell (*127*, *128*).

Table S6. Image credits for ichthyosaur silhouettes

Taxon	Artist	Image source	License	Modifications
Hupehsuchus	Neil Kelley	http://phylopic.org/image/16289b28-9d75-4a3d-9f9e-e77bd2e3e29f/	https://creativecommons.org/publicdomain/zero/1.0/	opacity, shadow
Chaohusaurus	Gareth Monger	http://phylopic.org/image/3bc49ba6-9956-4654-ae1f-a70f0e1ed442/	https://creativecommons.org/licenses/by/3.0/	reflected, opacity, shadow
Utatsusaurus	Nobu Tamura (vectorized by T. Michael Keesey)	http://phylopic.org/image/cf07f025-6977-430a-8ea1-a2297f3f864c/	https://creativecommons.org/licenses/by-sa/3.0/	reflected, opacity, shadow
Cymbospondylus	Gareth Monger	http://phylopic.org/image/8162d84e-4578-4adf-98d5-2faad56bba19/	https://creativecommons.org/licenses/by/3.0/	reflected, opacity, shadow
Mixosaurus	Gareth Monger	http://phylopic.org/image/cd989aa0-9d3d-44a7-847e-e1a9fb83f946/	https://creativecommons.org/licenses/by/3.0/	reflected, opacity, shadow
Shastasaurus	Gareth Monger	http://phylopic.org/image/83c83962-d551-42dd-a3b2-99346a89fc99/	https://creativecommons.org/licenses/by/3.0/	reflected, opacity, shadow
Ichthyosaurus	Scott Hartman	http://phylopic.org/image/cf4136a7-2d32-454b-b3e8-f376e6da0d93/	https://creativecommons.org/licenses/by/3.0/	reflected, opacity, shadow
Thalattoarchon	Lars Schmitz, after Gareth Monger's *Cymbo-spondylus*	not applicable	not applicable	not applicable

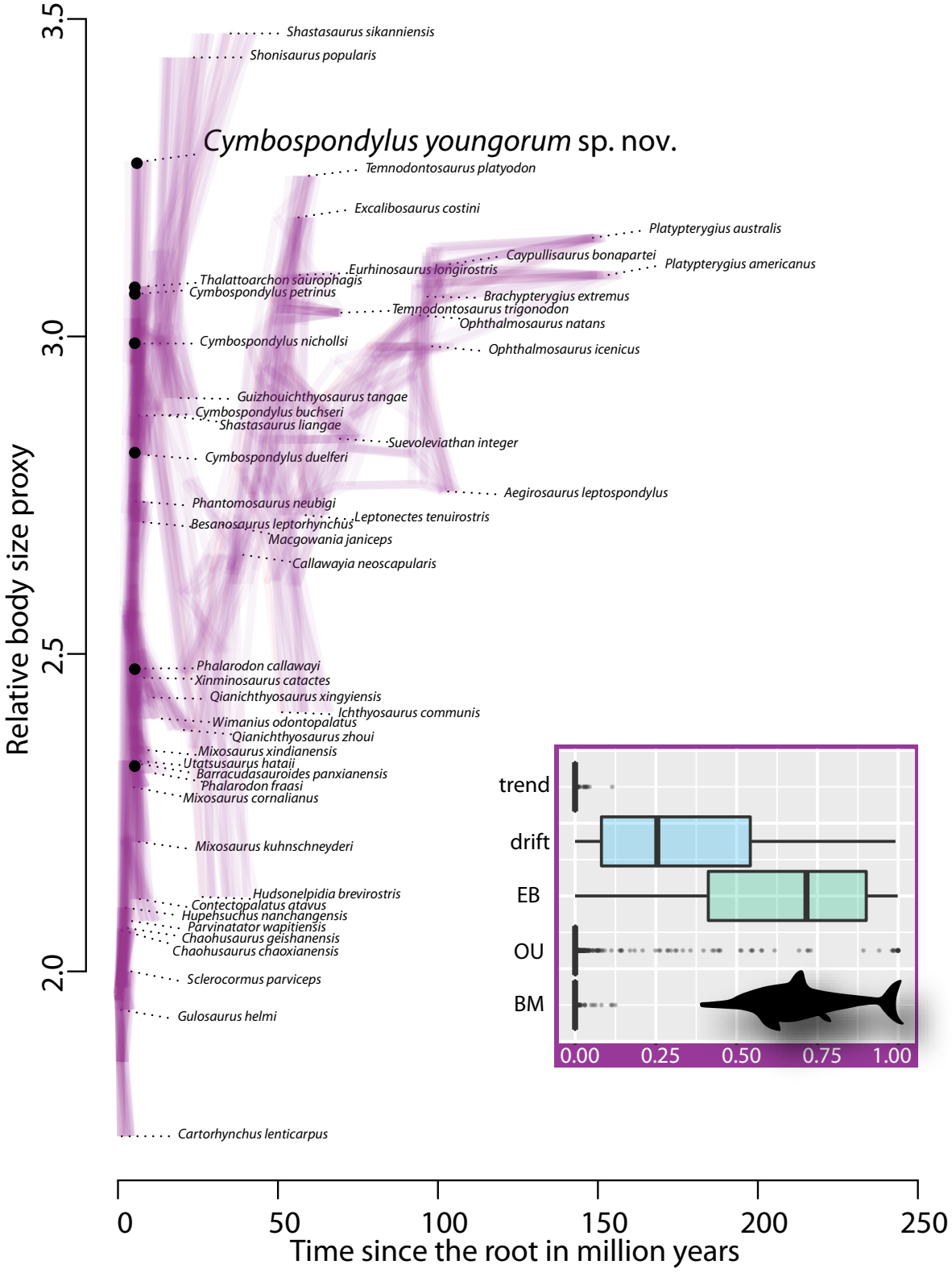

Fig. S10. Evolutionary traitgram of ichthyosaur skull length. Body size optimization plot as traitgram for ichthyosaurs on a traitgram with absolute sizes, i.e., skull length (see Data S4). Filled circles denote ichthyosaur species from the Fossil Hill Fauna. Inset: Model-fitting results for ichthyosaurs using Akaike weights for five different models. The best model is EB. Abbreviations for models: BM, Brownian motion; OU, Ornstein-Uhlenbeck; EB, early burst.

Evolutionary models for clade-wide analysis. We evaluated the fit of trait evolution models to the data for the given phylogenies with a Maximum Likelihood approach, using the "fitContinuous" function of the R package 'geiger' (*129*, *130*)(Data S6). We fit five different models, all of which are considered to have macroevolutionary relevance (table S7).

Table S7. Descriptions of the evolutionary models used in clade-wide analyses.

Model	**Description**
Brownian Motion (BM)	The Brownian Motion (BM; *131*) model simulates a random walk where the correlation structure of the continuous trait values is proportional to the amount of shared history.
Ornstein-Uhlenbeck (OU)	In its simplest form, the Ornstein-Uhlenbeck (OU; *132*), assumes a random walk coupled with the tendency of trait values to stay in proximity of a single stationary peak.
Early Burst (EB)	The Early burst (EB; *133*) model assumes high rates of evolution in the early phase of a clade, followed by a subsequent slow-down. THis model is also known as the accelerating-decelerating (ACDC) model of Blomberg et al. (*134*).
Trend	A diffusion model similar to BM but with a linear trend toward faster or slower rates through time.
Drift	A trait evolution model also similar to BM but featuring a directional change toward larger or smaller trait values over time. Confusingly, this model is often referred to as a 'trend' model in the literature.

Resampling approaches. To account for any artifactual or other non-biological differences between our ichthyosaur and cetacean datasets, we not only performed model fitting for the entire dataset but also carried out several re-sampling approaches of the cetacean data. Altogether we completed 9 different model fitting approaches:

i. Original analysis: full dataset for both ichthyosaurs and cetaceans. [1,000 iterations, Fig. 3, Fig. S11A, B]

ii. Resampling 1: The cetacean dataset (*N*=250) is much larger than the one for ichthyosaurs (*N*=48), hence we tested whether random down-sampling to the N of the ichthyosaur dataset influenced the model-fitting results. [100 iterations, Fig. S11C]

iii. Resampling 2: The cetacean dataset consists of both extant and extinct lineages, a composition different from the entirely extinct ichthyosaur clade. We therefore tested whether model-fitting results changed when all extant lineages were excluded. [100 iterations, Fig. S11D]

iv. Resampling 3: Cetaceans include a large radiation (Mysticeti) of giant filter feeders, of which there is no evidence in ichthyosaurs, even though filter feeding may have been present in Upper Triassic taxa. If the absence of filter feeding in ichthyosaurs is a true signal, the comparison of cetaceans with ichthyosaurs would be more complicated than accounted for by an undifferentiated analysis. We therefore explored whether the model-fitting results for cetaceans changed when we removed all filter feeders from the analysis. [100 iterations, Fig. S11E]

v. Resampling 4: Given that both the presence of extant species and the presence of filter feeders in the data may influence the model fitting, we removed both and repeated the analysis. [100 iterations, Fig. S11F]

vi. Resampling 5: To account for both unequal N and the presence of extant species in the cetacean data, we excluded extant species and subsequently down-sampled to match the N of ichthyosaurs. [100 iterations, Fig. S11G]

vii. Resampling 6: For this resampling approach, we removed filter feeders and then randomly down-sampled to match *N* of ichthyosaurs. [100 iterations, Fig. S11H]

viii. Resampling 7: To account for presence/absence of filter feeders, extant species, and uneven sample size, we removed filter feeders and extant species, and after that down-sampled randomly to match N of ichthyosaurs. [100 iterations, Fig. S11I]

ix. Resampling 8: The degree of aquatic specialization of early cetaceans and ichthyosaurs varies to the extent described in the main text. We therefore tested if the model fitting results changed when we only included the Pelagiceti in the analysis. [100 iterations, Fig. S11J]

Results of model fitting. In our initial model-fitting results to the full datasets, the early burst and trend models are strongly preferred over all other models for ichthyosaurs. By contrast, no strong preference is indicated for any of the 5 tested models in cetaceans (Fig. 3). For ichthyosaurs, the lowest AICc scores were found for the EB and trend model (Fig. 3, Figs. S10, S11a), indicating that these two models fit the data better than any of the other tested models. .he mean of the Akaike weights of the EB model for 1,000 iterations was 0.63 (median=0.72), while the mean Akaike weight of the next best fitting model, the trend model, was 0.34 (median=0.25). The slope estimates of the trend model indicate a deceleration of rates over time, in which case the trend model becomes similar to an EB model. Therefore, models that describe an early burst pattern in the data receive a combined conditional probability of, on average, 0.97. Given that small tree sizes tend to make it more difficult to estimate evolutionary model parameters (*135*), the strong support for early burst processes in ichthyosaurs (N=48) is surprising.

Among cetaceans (N=250), AICc scores were highly similar across the five tested models (Fig. 3, Fig. S11B), a pattern that is also reflected in their corresponding Akaike weights. The EB model received the highest Akaike weight (mean=0.324, median=0.21), but is followed closely by the drift (mean=0.317, median=0.25), trend (mean=0.18, median=0.16), and BM models (mean=0.12, median=0.1). The OU model earned the lowest degree of support in the set (mean=0.06, median=0.04). Down-sampling of the cetacean data set to the N of ichthyosaurs also resulted in the absence of a clearly preferred model, though to an even greater degree because of decreased power (Fig. S11C).

Filter-feeding has long been considered to be a vital precondition in cetaceans and other large marine vertebrates for the evolutionary acquisition and maintenance of giant body sizes (*136*, *137*), although there may be exceptions (*110*). Excluding filter-feeding cetaceans from the

analysis is somewhat problematic because we cannot reject the hypothesis that at least some of the Late Triassic giant ichthyosaurs were filter feeders as well (*45*, *138*). Nonetheless, absent clear affirmatory evidence for filter-feeding ichthyosaurs, we thought it was a necessary step to better understand the patterns in the data. Interestingly, excluding filter feeding cetaceans led to the EB and trend models being preferred over the others, but with a degree of support that was much less clear than in ichthyosaurs (Fig. S11E). Mean Akaike weight for EB is 0.40 (median=0.36), while the trend model receives a mean Akaike weight of 0.24 over 100 iterations (median= 0.23). The slopes of the trend model are negative with a few exceptions, therefore suggesting that (with filter-feeders excluded) cetaceans evolved with a slowing rate through time.

Excluding extant lineages also resulted in EB and trend models being preferred over the others, though again the support was not as strong as in ichthyosaurs (Fig. S11D). Mean Akaike weight for the EB model is 0.39 (median=0.36), while mean Akaike weight for the trend model is 0.22 (median=0.21). The trend model featured negative slopes, on average, and therefore the combined conditional probability for EB-like processes after extant species have been removed is 0.61. However, the same problem applies as to the previous analysis because we cannot reject the hypothesis that gigantism in Late Triassic ichthyosaurs was also caused by global oceanographic changes that allowed a filter-feeding lifestyle to evolve which in turn lifted the maximum size limit. We also explored the option of excluding both extant lineages and filter feeders (Fig. S11F) and of excluding extant lineages and filter feeders and down-sampling to the *N* of ichthyosaurs (Fig. S11G). Whereas the former option lends support to an EB model, this effect disappeared after down-sampling. When removing filter feeders and matching *N* of ichthyosaurs, a slight preference for an OU model emerged Fig. S11I), while removal of filter feeders and extant species while matching *N* of ichthyosaurs did not prefer a single model over others (Fig. S11I). Finally, excluding cetaceans that are not fully aquatic did not change the major pattern of the model fitting results (Fig. S11J), with emerging support for EB but not nearly as strong as seen in ichthyosaurs.

As a final step of our exploration of the pattern of body size evolution in ichthyosaurs, we intended to check whether the unique tree shape of ichthyosaurs allowed for reliable estimates of model adequacy. Ichthyosaurs diverge rapidly in the early phase of their evolution, and we discussed whether the early rapid divergence may render it improbable to detect the true

underlying model of trait evolution. To address this concern, we performed two simulation studies. Specifically, we used the BM and EB parameters estimated from the data to simulate traits for our ichthyosaur phylogeny, and then we tested whether or not we were able to identify the correct model with our chosen methodological approach. If our approach to model fitting worked reliably, one would expect the largest Akaike weight to be found for the model under which the traits were simulated. Our results (Fig. S11K, L), confirm that we were able to correctly select the BM and EB model for the simulated traits (BM and EB, respectively), suggesting that our results are not an artifact of the unusual shape of the ichthyosaur tree.

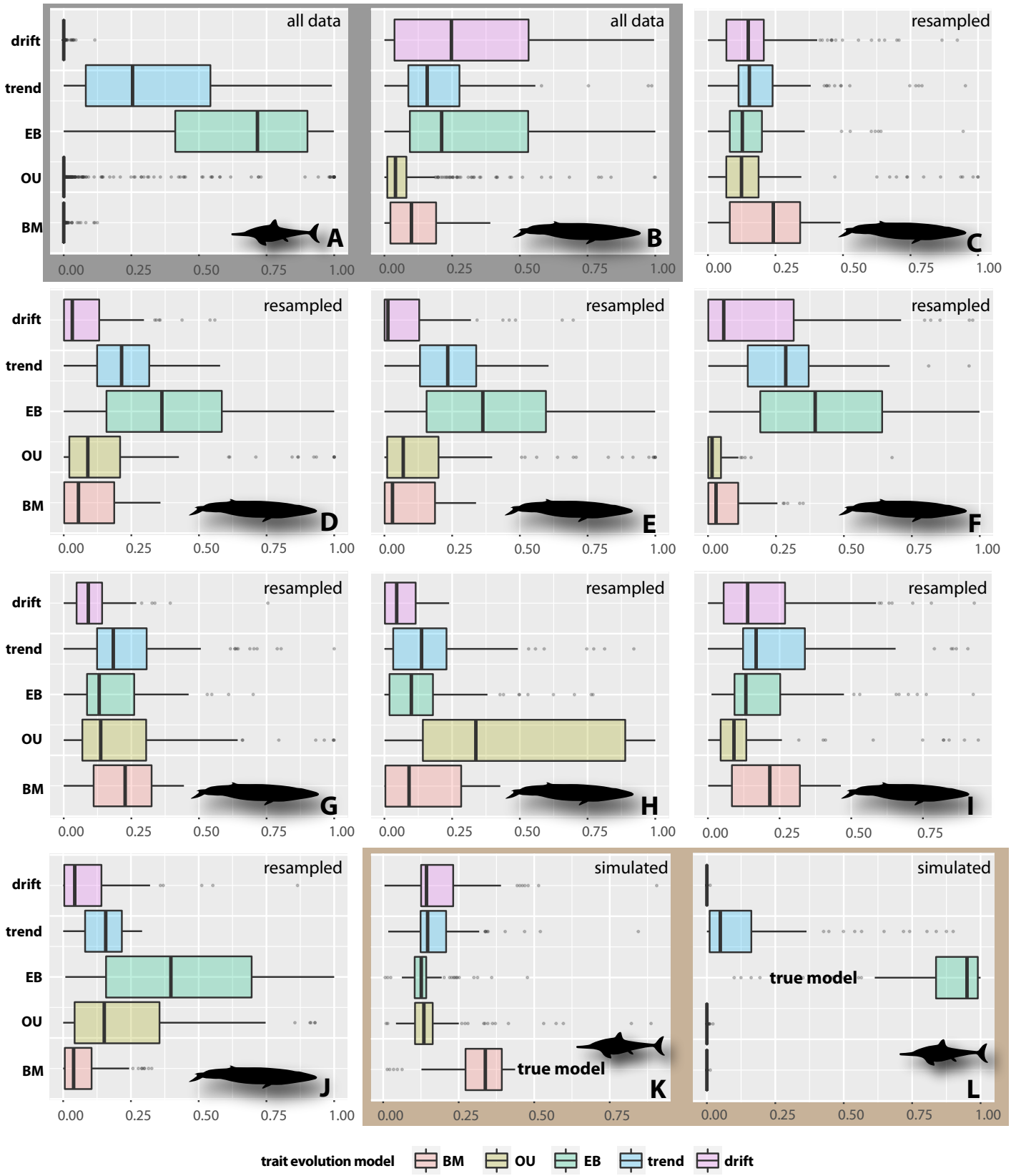
all data
resampled
simulated
drift
trend
EB
OU
BM
true model
A
B
C
D
E
F
G
H
I
J
K
L
0.00
0.25
0.50
0.75
1.00
trait evolution model
BM
OU
EB
trend
drift

Fig. S11. Body size evolution model evaluation and simulation in ichthyosaurs vs. cetaceans. (A) Model-fitting results for ichthyosaurs using Akaike weights for five different models. Note the very strong support for the EB model and the trend model compared to all others. **(B)** Model-fitting results for cetaceans using Akaike weights for five different models. Note the lack of a preferred model. **(C)** Model fitting for cetaceans downsampled to the N of ichthyosaurs. **(D)** Model fitting for cetaceans excluding extant lineages. **(E)** Model fitting for cetaceans excluding filter feeders. The best model is EB. **(F)** Model fitting for cetaceans excluding filter feeders and extant lineages. The best model is EB, but the support is much less than for ichthyosaurs. **(G)** Model fitting for cetaceans downsampled to the N of ichthyosaurs and excluding extant taxa. Note the lack of a preferred model. **(H)** Model fitting for cetaceans excluding filter feeders and randomly downsampled to the N of ichthyosaurs. **(I)** Model fitting for cetaceans excluding filter feeders and extant lineages and randomly downsampled to the N of ichthyosaurs. Note the lack of a preferred model. **(J)** Model fitting for cetaceans including only Pelagiceti. EB and OU models are best. **(K)** Model simulation of ichthyosaur data using a BM model. Note the week preference for the BM model. **(L)** Model simulation of ichthyosaur data using an EB model. Note the very strong support for the EB model. Abbreviations for models: BM, Brownian motion; OU, Ornstein-Uhlenbeck; EB, early burst.

Table S8. Settings of the bayOU prior functions.

Model parameter	**Distribution function**	**Parameter values of the prior function**
α	dhalfcauchy	scale=0.1
σ^2	dhalfcauchy	scale=0.1
k	cdpois	lambda=1, kmax=50
θ	dnorm	mean=mean(trait), sd=1.5*sd(trait)

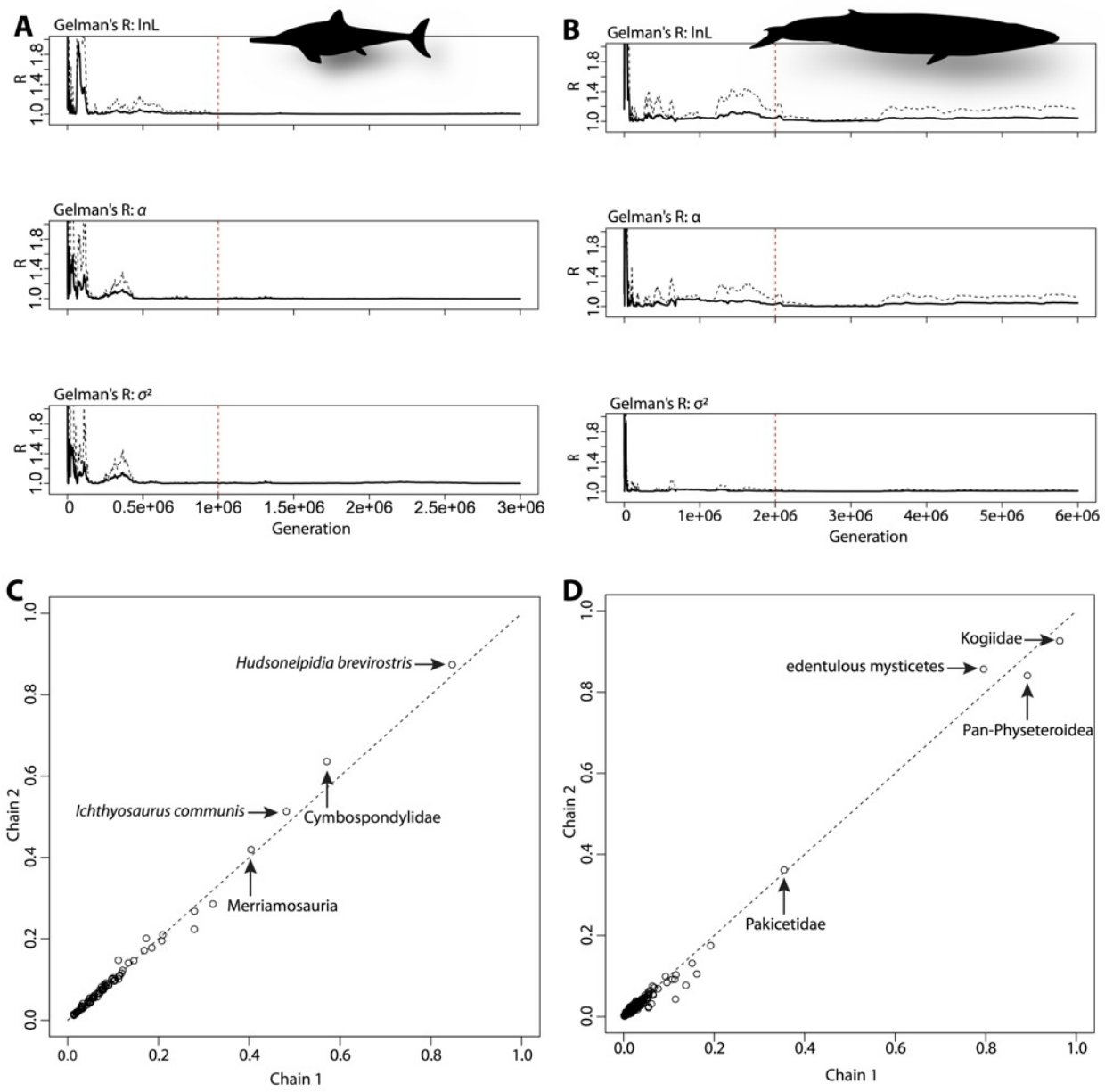

Fig. S12. Diagnostic plots for bayOU analyses. We checked whether independent Markov chains from both ichthyosaur (**A**) and cetacean (**C**) analyses had converged on similar regions in the parameter space by Gelman's R for log likelihood, σ2, and α. Convergence is also supported by the plots of the posterior probabilities for shifts along branches against each other, where posterior probabilities fall along a line with a slope of one for both ichthyosaur **(B)** and cetacean **(D)** data. The labeled posterior probabilities represent the adaptive shifts that we selected for detailed interpretations.

Table S9. Parameter estimates of bayOU, averaged from two Markov chains.

	regime	$\boldsymbol{\theta}$	**posterior probability**	**posterior/prior probability**
Ichthyosaurs	root	135 mm skull length	n/a	n/a
	Cymbospondylidae	1443 mm skull length	0.603292	56.7
	Merriamosauria	983 mm skull length	0.411529	38.7
	Hudsonelpidia brevirostris	124 mm skull length	0.860299	80.9
	Ichthyosaurus communis	228 mm skull length	0.497312	46.8
Cetaceans	root	222 mm skull width	n/a	n/a
	edentulous mysticetes	1224.6 mm skull width	0.825922	413
	Pan-Physeteroidea	1919.8 mm skull width	0.866299	433.2
	Kogiidae	121 mm skull width	0.944807	472.4

Ancestral state estimates. The ancestral skull width of cetaceans, inferred through fitContinuos (BM model) over 100 trees is estimated at 147.3 mm, while the ancestral skull length of ichthyosaurs, inferred through fitContinuous (EB model) is estimated at 111,1 cm. These ancestral state estimates are congruent with the estimated local optima (θ) at the root for both cetaceans (222 mm) as well as ichthyosaurs (135 mm) (table S9).

List of R packages used for computational trait evolution.

'ape' (*139*),

'bayOU' (*32*),

'dplyr' (used during initial analyses, *140*),

'geiger' (*129, 130*)

'googlesheets4' (used during initial analyses, *141*),

'ggplot2' (*142*),

'mvMORPH' (*143*),

'paleotree' (*144*),

'phytools' (*31*)

'picante' (*145*),

'reshape2' (*146*),

'strap' (*147*),

'tidyverse' (used during initial analyses, *142*).

The Fossil Hill Fauna: Collecting History and Geological Setting

The Fossil Fauna Fauna is hosted by the Fossil Hill Member, a formally named stratigraphic unit that is widespread in the outcrop area of the Star Peak Group (*35*). However, basin and range tectonics lead to a strong fragmentation of Star Peak outcrop (*35*). Note that because of this outcrop discontinuity, the Fossil Hill Member is part of different formations in different parts of the outcrop area (*35*, *148*). Thus, in the westerly outcrops of the Humboldt Range and West Humboldt Range, the Fossil Hill Member is part of the Prida Formation but in the central outcrops of the Augusta Mountains, it is part of the Favret Formation (*35*). The Favret Formation spans the middle to late Anisian (Middle Triassic), a period covering over two million years (*34*). The Fossil Hill Member itself is a black shale unit of variable thickness, representing deposition in anoxic bottom waters below storm wave base (*35*, *148*). Halobiid bivalve fossils also suggest anoxic or dysoxic bottom waters. However, the surface waters were well aerated and hosted a substantial diversity of life as indicated by the abundant ammonoids and the common marine reptile remains.

Vertebrate fossil collecting in the Fossil Hill Member started in the late 19th century in the West Humboldt Range near Lovelock, NV, and in the New Pass Range near Austin, NV (*38*). This material forms the basis of J.C. Merriam's classic work on Triassic ichthyosaurs (*38*) and is accessioned to collections of the Museum of Paleontology of the University of California at Berkeley (UCMP). Collecting activity in the Fossil Hill Member of the remote Augusta Mountains of southeastt Pershing County started in 1990 following an initial discovery by H. Bucher (*149*) and has been continued since, albeit intermittently. The finds have been partially described in a series of papers (*8*, *16*, *17*, *149 - 152*) (table S3).

Our fieldwork in the Augusta Mountains involved geological mapping (Fig. S13) and surveying of skeletons (table S10). Collecting is ongoing as well. The fossils from the Fossil Hill Member of the Augusta Mountains were collected with permits of the Bureau of Land Management. The specimens collected before 2011 were primarily deposited at the Field Museum of Natural History, Chicago (FMNH), with single specimens having been accessioned at the Cincinnati Museum of Natural History (CMC). Since 2011, the Natural History Museum of Los Angeles County (LACM) has been the Federal Repository for the finds from the Augusta Mountains. The census of the finds from the 1993 to 2018 (Data S7) form the basis for our energy flux modeling.

In the Augusta Mountains, the Fossil Hill Member reaches a thickness of up to 300 m, and several middle and late Anisian ammonoid zones occur in succession (*18*), representing a time span of perhaps two million years, from 244 to 242 million years ago, based on the latest geological time scales (*34*). Marine reptile finds are generally preserved as isolated complete skeletons, albeit often partially destroyed by weathering before their discovery (*8*, *16*, *17*, *149 - 152*).

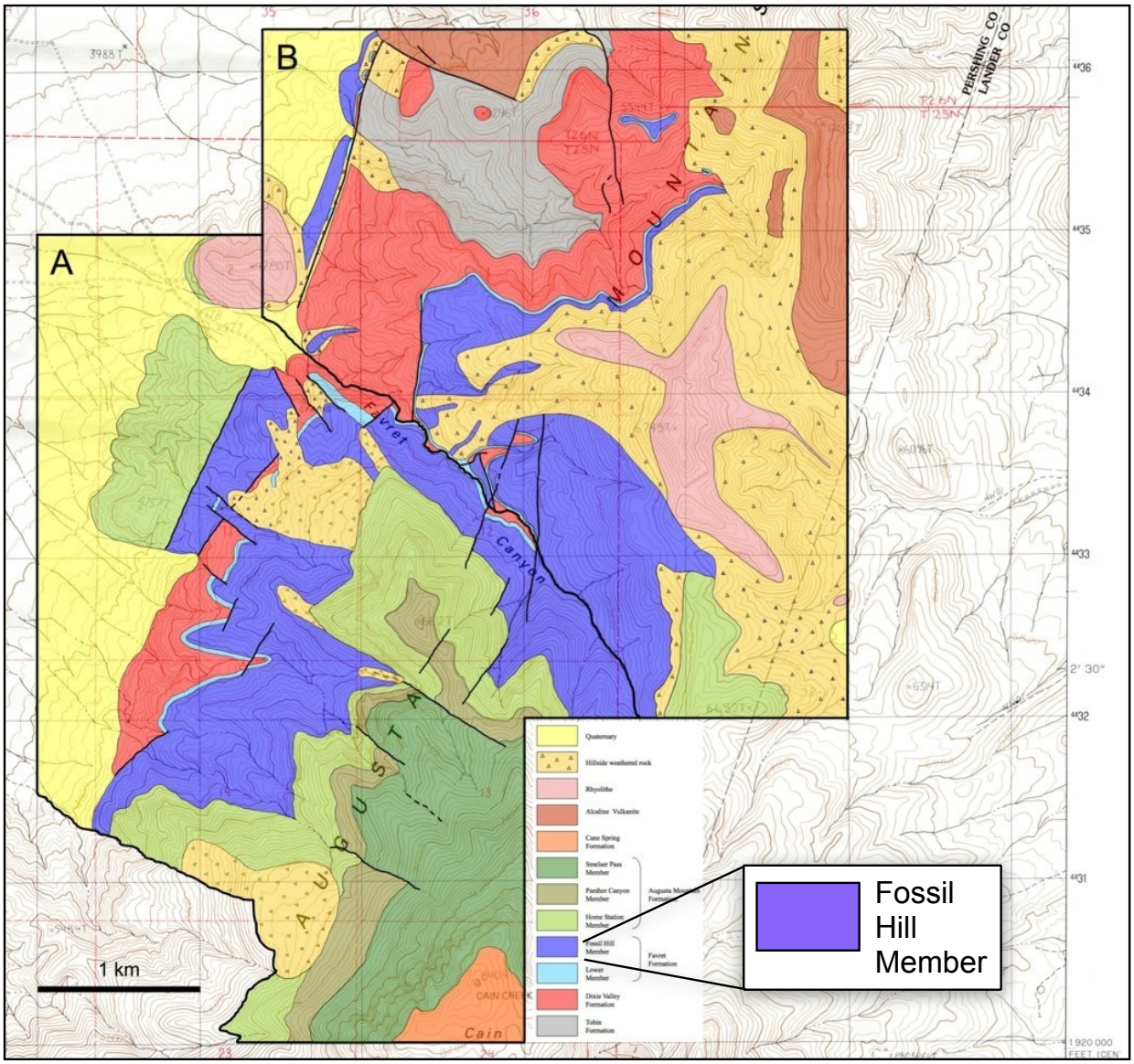

Fig. S13. Geologic map of the Augusta Mountains, Pershing County, Nevada, USA. Map base is USGS 7.5' Quadrangle 'Cain Mountain'. Geology is based on the unpublished maps by Katja Waskow and Janka Brinkkötter (University of Bonn, Germany).

Table S10. Vertebrate fauna of the Fossil Hill Member, Anisian, Middle Triassic, Nevada, USA. Based on published data, field survey data, and collections data from the CMC, FMNH, and LACM. Note that this single lithostratigraphic unit, the Fossil Hill Member, is part of two formations, the Prida Formation and the Favret Formation. The current taxonomic ichthyosaur tally stands at eight species (including *Omphalosaurus*). Collections abbreviations: CMC, Cincinnati Museum Center, Cincinnati, Ohio, USA; FMNH, Field Museum of Natural History, Chicago, Illinois, USA; LACM, Natural History Museum of Los Angeles County, Los Angeles, California, USA.

Taxon	Clade	Formation	Major references
Several	Chondrichthyes	Prida	*36*, *153*
Indet.	Actinopterygii	Favret	*151*
Saurichthys	Actinopterygii	Favret	*151*
Indet.	Coelacanthidae	Favret	CMC collections (Data S7)
Omphalosaurus nevadanus	Ichthyosauria	Prida & Favret	*40*, Data S7
Phalarodon fraasi	Ichthyosauria	Prida & Favret	*39*, *77*, *155*
P. callawayi	Ichthyosauria	Favret	*39*, *77*, *155*
Cymbospondylus petrinus	Ichthyosauria	Prida & Favret	*40*
C. nichollsi	Ichthyosauria	Favret	*16*
C. duelferi	Ichthyosauria	Favret	*17*
C. youngorum sp. nov.	Ichthyosauria	Favret	this study
Thalattoarchon saurophagis	Ichthyosauria	Favret	*8*
Augustasaurus hagdorni	Sauropterygia	Favret	*150*, *152*

Ecological and Evolutionary Stability of the Fossil Hill Member Food Web Tested by Energy Flux Modeling

Rationale. In this modeling study, we had two major aims: first, testing whether the fauna uncovered so far from the Fossil Hill Member outcrop in the Augusta Mountains constitutes a functional and stable marine pelagic food web (hypothesis 1), and second, testing whether any surplus energy could nourish an additional population of an extremely giant bulk feeder, as yet undiscovered (hereafter called 'super-giant', hypothesis 2). Such a super-giant bulk feeder would have been an ichthyosaur or possibly other marine reptile that captured multiple small invertebrates or fish at once, and this animal thus would have fed very low in the food web. Our reasoning was that compared to modern marine food webs, a striking difference is the Fossil Hill Fauna's lack of very large to extremely giant bulk feeders such as mysticetes and bulk-feeding sharks. Because we found support for hypothesis I, we tested whether the abundantly preserved ammonoids could have provided the energy calculated by the model needed for sustaining viable populations of the other consumers of the Fossil Hill food web. We found that the energy provided by the ammonites was a magnitude larger than that calculated by our model and thus set up the second modeling experiment in which we added a hypothetical blue whale-sized ichthyosaur to the Fossil Hill food web to evaluate whether this new web was again functional and stable.

To test our hypotheses, we used an ecological modeling framework designed for modern aquatic and terrestrial food webs (*41*) and accordingly assumed that the taxa of the Fossil Hill Fauna lived simultaneously and represented consumers in a pelagic food web. We thus treated the field data set of occurrences of fossil reptiles and other fossils from the Fossil Hill Member in the Augusta Mountains as if they all lived at the same time, thus time-averaging the data set in the process. We feel justified in this approach because we are interested in addressing the question of ecological and evolutionary stability (for our definitions, see below), and do not aim at precise quantitative predictions of characteristics of the Fossil Hill food web.

Background 1: The Fossil Hill Member ecosystem and field data from the Augusta Mountains. Input data for modeling come from the fossil record and outcrop of the Fossil Hill Member of the Augusta Mountains. In modeling the Fossil Hill food web, however, we do not deal with real populations but with faunal assemblages accumulated over geological time. The

data we obtain from our fieldwork are thus the relative abundance and body size of the taxa, which we combined in a hypothetical food web.

Fossils found throughout the 300 m-thick outcrop of the Fossil Hill Member, and environmental conditions remained stable during the time of deposition of this rock unit (*35*, *148*). Marine reptile fossils thus accumulated stochastically over time, and our census (Data S7) provides the time-averaged relative abundance of the taxa in the food web. Treating the fossils as contemporaneous also solves the problem of the low sample size for marine reptiles in the field data set. For example, the observation that *Phalarodon* spp. is twice as abundant as *Cymbospondylus nichollsi* (table S11, Data S7) would not statistically hold if it were not for the time averaging. This is because marine reptile fossils tend to occur in distinct zones, and each zone may have a somewhat different composition. We mention this as a possible caveat. Increasing sample size and stratigraphic resolution by further fieldwork and preparation obviously is not an option given the large to giant body size of most skeletons, such as *Cymbospondylus youngorum* sp. nov..

Background 2: Energy flux modeling approach. In our modeling study, we treated the fauna from the Fossil Hill Member of the Augusta Mountains as an extinct marine pelagic food web in terms of its ecological and evolutionary stability over time. We aimed at clarifying the functioning and stability of this food web. We thus define ecological stability over time in the sense that the energy provided by the primary producers to the food web and the energy fluxes between all of its consumers are sufficient to maintain viable populations of each consumer taxon over ecological time scales, thereby assuming the absence of any environmental fluctuations (*41*). All populations must get enough energy, and population sizes must be large enough so that each population can survive over many generations, i.e., the food web is functional and stable. We define evolutionary stability over time in the sense that no new taxon can become an additional member of this food web due to energetic limitations.

This raises the question of whether the documented ammonoids of the Fossil Hill Fauna might provide enough energy to additionally sustain a viable population of a hypothetical super-giant ammonoid feeder. Without an increase in the energy delivered by primary producers that would have covered its energetic demands, the population of this ichthyosaur would have had to survive at the expense of other consumers in the food web. These other consumer populations would shrink in the number of individuals and in total biomass because the hypothetical super-

giant's population would considerably increase interspecific competition for energy (i.e., prey animals). There are two possible outcomes of this increased interspecific competition: either, the hypothetical super-giant outcompetes one or several of the other Fossil Hill taxa, and their populations will go extinct. This will change the composition of the faunal assemblage. Alternatively, populations of the other taxa and the super-giant ichthyosaur will coexist for many generations without going extinct. From the perspective of our modeling approach, coexistence of all Fossil Hill taxa together with this super-giant would indicate that the Fossil Hill Fauna as recorded in the field is not complete yet and that the super-giant awaits discovery in the Fossil Hill Member of the Favret Formation in the Augusta Mountains or could be added to the Fossil Hill Fauna later by evolution. No support for coexistence of this hypothetical super-giant with the other Fossil Hill taxa known so far might suggest insufficient primary production in the Middle Triassic to sustain its population (*9*).

Hypotheses tested and their implications for the Fossil Hill Fauna. Hypothesis 1 (H1): The faunal assemblage of extinct invertebrate and vertebrate taxa as documented in the fossil record represents the consumers of an ecologically stable food web. Outgoing energy fluxes from all currently known or modelled taxa of the Fossil Hill Fauna are high enough to sustain viable populations of each over ecological time scales.

A rejection of H1 indicates that the Fossil Hill Fauna as currently seen in the fossil record was not functional. For example, some taxa could still be missing, incorrectly identified, or their abundances in the community could be wrong. A rejection of H1 would also be consistent with *C. youngorum* sp. nov. being a spurious migrant or drifted in as a carcass. On the contrary, support of H1 suggests that this food web was indeed functional and stable, i.e., populations of all taxa of the Fossil Hill Fauna obtained sufficient energy to persist and could have coexisted. Support of H1 also makes it plausible that gigantism in ichthyosaurs (as documented by *C. youngorum* sp. nov.) evolved rapidly in the first two million years of their known history.

Hypothesis 2 (H2): The Fossil Hill assemblage of extinct invertebrate and vertebrate taxa comprises the consumers of an ecologically but not evolutionarily stable food web. A super-giant bulk feeder can be added to the Fossil Hill food web and coexist with all other taxa over ecological time scales. With respect to the energy flux in this food web, this means that outgoing energy from low trophic levels (e.g., from ammonoids) is sufficient to support a viable

population of this super-giant together with populations of all other taxa known so far. This super-giant could indeed have coexisted with the other taxa from the Fossil Hill Fauna but has not been discovered yet or it could be added later by evolution. Support for H2 would indicate that *C. youngorum* sp. nov. does not represent the potential maximum ichthyosaur body size in the early Middle Triassic.

Rejection of H2, on the other hand, suggests that the Fossil Hill food web indeed differs from modern ones, i.e., it did lack such a super-giant marine amniote. Rejection of H2 further would be consistent with a current hypothesis on maximum body size evolution in marine vertebrates and findings on lower limits of maximum body size in Mesozoic food webs (*6, 9*).

Food web members modeled. Our model of the Fossil Hill food web has eleven members. Nine of these are specific marine vertebrate taxa (table S10) but the two members lowest in the food web pool different kinds of animal taxa. The member 'shelled invertebrates' ('invertebrates' for short) comprises primarily ammonoids, but also halobiid bivalves and crustaceans. The ammonoids could potentially pool different species that even may have preyed among each other, but this cannot be detected from the fossil record; crustaceans are not preserved as fossils, however. The member 'pooled non-shelled invertebrates and fish' ('fish' for short) comprises coleoid cephalopods such as squid and small to medium-sized fish. We combined small to medium-sized fish and small to medium-sized coleoids in the member 'fish' based on the rationale that the same kind of predator is adapted to feeding on these groups among modern ocean predators. Coleoids are not represented in the Fossil Hill Fauna as fossils, but they are well known from the Triassic, and their horny hooklets are commonly found in stomach contents of contemporaneous ichthyosaur finds (e.g., *15*). Finds of small to medium-sized fish are also rare in the Fossil Hill Member (*8*) but we must assume the presence of abundant fish in the Fossil Hill sea (see above). We also pooled fish and non-shelled invertebrates into a single member in order to keep the model's complexity as low as possible.

The nine marine vertebrate taxa are coelacanth fish, *Augustasaurus, Phalarodon* spp. (the two species of this genus), *Omphalosaurus nevadanus, Cymbospondylus duelferi*, *C. nichollsi*, *C. petrinus*, *C. youngorum* sp. nov., and *Thalattoarchon saurophagis* (table S10). We separated out the coelacanths from the other fish because of their much larger size, documented by an undescribed find 1.6 m in length (CMC GWS-96-17, Data S7). The mixosaurian ichthyosaurs

Phalarodon callwayi and *P. fraasi* of the Fossil Hill Fauna (*39*, *149*, *151*, Data S7) were pooled as *Phalarodon* spp. in our model because they are similar-sized, both taxa are morphologically difficult to distinguish based on incomplete skeletons, and their feeding strategies are difficult to distinguish from each other as well.

In our modeled food web, shelled invertebrates ('invertebrates') and pooled non-shelled invertebrates and fish ('fish', they feed on 'invertebrates') provide the energy available to the other, trophically higher and substantially larger-bodied, Fossil Hill vertebrate consumer taxa. We chose this approach to taxon delimitation in the model because primary producers (all marine photoautotrophic and chemoautotrophic organisms) and many primary and secondary consumers (e.g., bacteria, fungi, zooplankton, polychaetes, jellyfish, squid) are not preserved in the fossil record, and reliable estimates of their species richness, individual numbers, and body masses required for modeling the food web do not exist. Nevertheless, both members include taxa from the trophically lowest level being preserved. We note that the omission of trophically even lower taxa is possible because of the top-down approach of our energy flux model.

Trophic interactions modeled between food web members. The main lines of evidence we used for inferring predator diet were skull morphology, nature of the dentition, and absolute and relative body shape and body size. We allowed each taxon of generalist and macropredatory ichthyosaurs to feed on prey up to half its mass. This upper boundary is consistent with predator-prey size relationships of extant marine elasmobranchs and mammals (*156*) and with the new discovery from the Middle Triassic of China of a thalattosaur of ~ 4 m in total length preserved as stomach content of a specimen of the ichthyosaur *Guizhouichthyosaurus* of ~ 5 m in total length (*157*). We also used published insights into diet, such as fossilized stomach contents, where available.

In general, most of the ichthyosaurs and *Augustasaurus* must have fed on fish and squid (coleoid cephalopods), and large ichthyosaurs must have additionally preyed on smaller-sized marine reptiles, both mature individuals of smaller species (Fig. S14) as well as juveniles of larger species. Note, however, for trophic interactions between taxa, we only considered adults for the sake of minimizing the energy flux model's complexity and assumptions required. In the following, we review the fauna taxon-by-taxon, providing the justification for the trophic interactions used in our model (Fig. S14). The large coelacanth fish (table S11) would have fed

on small to medium-sized fish and squid (the member 'fish', Fig. S14), but not on any other of the marine reptiles. Clearly, because of their size, coelacanth fish also did not feed on invertebrates, either. *Phalarodon callwayi* and *P. fraasi* (*39*, Data S7) are the small-sized mixosaurian ichthyosaurs of the Fossil Hill Fauna (1.5 and 2.8 m body length, respectively; average body length = 2.15 m) (*39*) (table S11). These two species are characterized by a distinctly heterodont dentition in a slender snout. They used their posterior globular teeth for crushing shelled invertebrates, whereas the anterior conical teeth were used for snapping (for feeding terminology, see *158*) for fish and squid.

Next in body mass is *Augustasaurus* (table S11). *Augustasaurus* presumably was a fish and squid specialist given its very long neck, small head, and fang-like teeth, the same diet as inferred for other pistosauroids including long-necked plesiosaurs (*150*, *152*, *159*). *Omphalosaurus* and *Cymbospondylus duelferi* (*17*) are the medium-sized ichthyosaurs of the Fossil Hill assemblage (3-5 m; table S11). The latter probably fed on fish and squid, as indicated by its elongated snout and conical teeth, but not on the small invertebrates, i.e., the ammonoids. However, *C. duelferi* may have taken large prey for its size such as *Phalarodon* spp. and coelacanths because of its relatively large and widely spaced teeth, but not *Augustasaurus* and *Omphalosaurus*, both of which were too large. *Omphalosaurus* probably was a bulk feeder specialized in grinding up ammonoids (*40*, *160*, Data S7).

The ichthyosaurs *C. petrinus* (*38*) and *C. nichollsi* (*16*) are the large-sized members of the Fossil Hill Fauna (7-11 m; table S11) and conform to the generalized piscivore (fish and squid) pattern. Occasionally encountered stomach contents for this ecomorphotype tend to be dominated by coleoid squid hooklets, e.g., in the Alpine *C. buchseri* (*15*). However, as opportunistic feeders, these two species would have fed on anything smaller than themselves (but not on small invertebrates such as ammonoids). Given the similarity in size between the two species, *C. petrinus* did not feed on *C. nichollsi*, however. *Cymbospondylus youngorum* sp. nov., the new giant ichthyosaur taxon described in this paper, must have been a generalist feeder. It must have taken fish as well as squid based on its numerous and densely spaced teeth. As is the case for the other two large generalist feeders, *C. nichollsi* and *C. petrinus*, *C. youngorum* sp. nov. could have fed on anything smaller than itself (i.e., half of its own body mass in our model) (*157*, *158*), with the probable exception of the macropredatory *Thalattoarchon* (Fig. S14). *Thalattoarchon saurophagis* (>> 8.6 m body length) is the apex predator of the Fossil Hill assemblage as evidenced by its large slicing teeth and large size (*8*). However, *Thalattoarchon*

did not feed on *C. youngorum* sp. nov. because of the much larger size of the latter, which would have required a pack hunting strategy of the former. We have no evidence for such behavior on the part of *Thalattoarchon*, however. We also assumed that *Thalattoarchon* did not feed on ammonoids and fish (including squid) because of its macropredatory adaptations. Predator-prey relationships used for food web modeling are shown in Fig. S14.

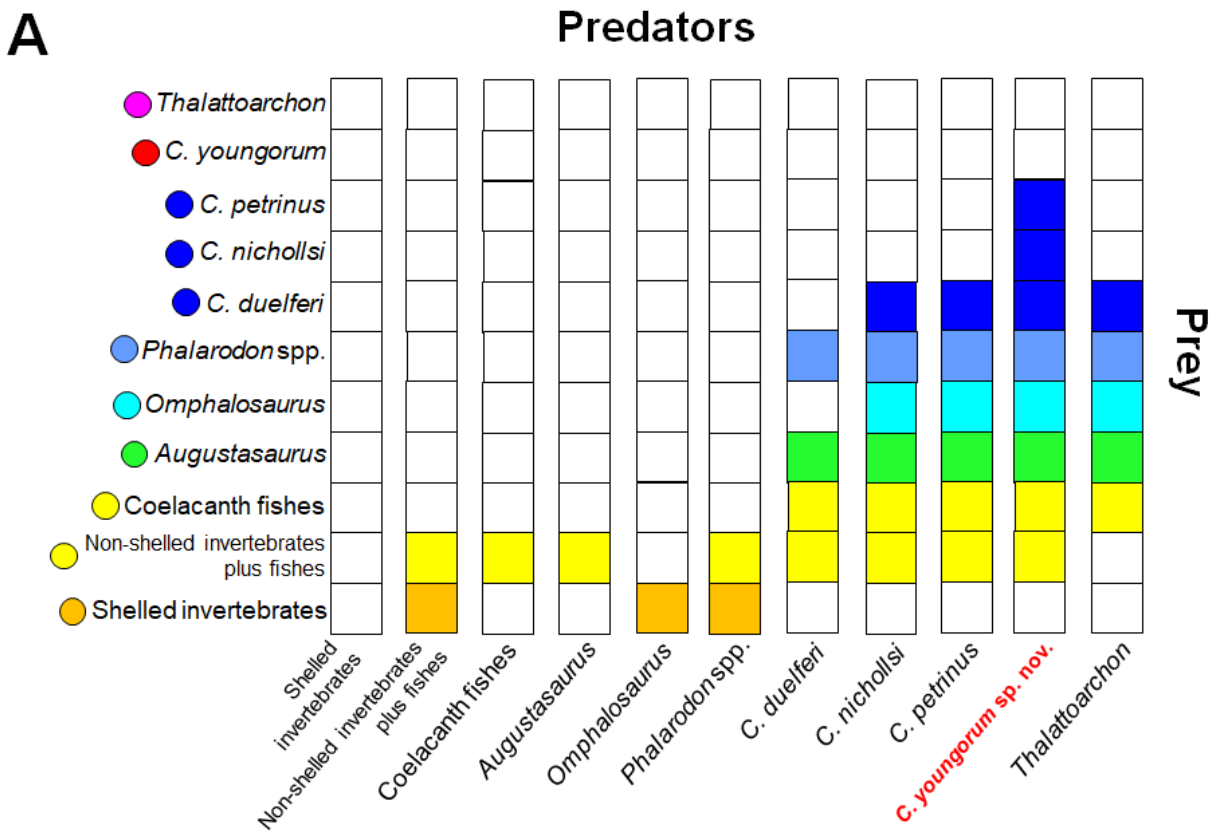
A
Predators
Prey
Thalattoarchon
C. youngorum
C. petrinus
C. nichollsi
C. duelferi
Phalarodon spp.
Omphalosaurus
Augustasaurus
Coelacanth fishes
Non-shelled invertebrates plus fishes
Shelled invertebrates
Shelled invertebrates
Non-shelled invertebrates plus fishes
Coelacanth fishes
Augustasaurus
Omphalosaurus
Phalarodon spp.
C. duelferi
C. nichollsi
C. petrinus
C. youngorum sp. nov.
Thalattoarchon

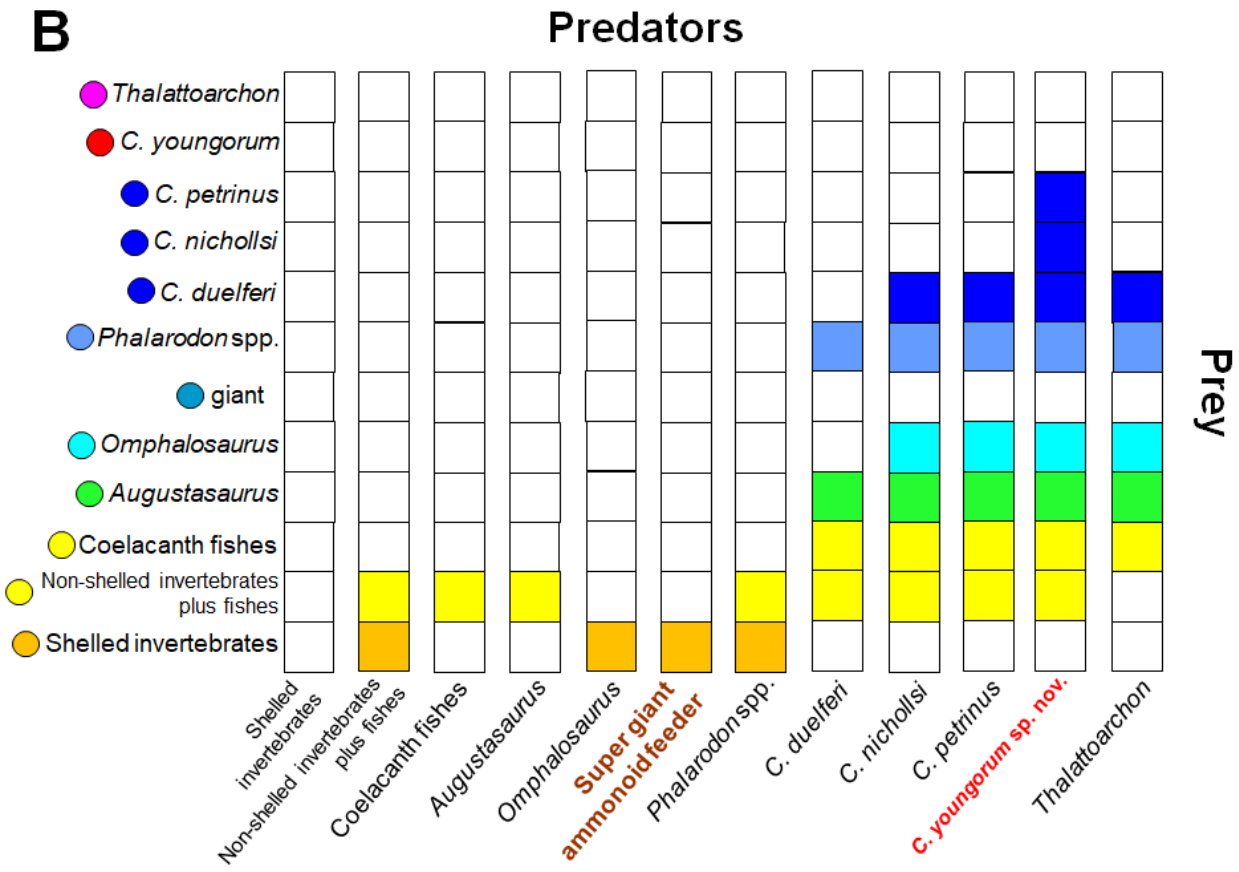
B
Predators
Prey
Thalattoarchon
C. youngorum
C. petrinus
C. nichollsi
C. duelferi
Phalarodon spp.
giant
Omphalosaurus
Augustasaurus
Coelacanth fishes
Non-shelled invertebrates plus fishes
Shelled invertebrates
Shelled invertebrates
Non-shelled invertebrates plus fishes
Coelacanth fishes
Augustasaurus
Omphalosaurus
Super giant ammonoid feeder
Phalarodon spp.
C. duelferi
C. nichollsi
C. petrinus
C. youngorum sp. nov.
Thalattoarchon

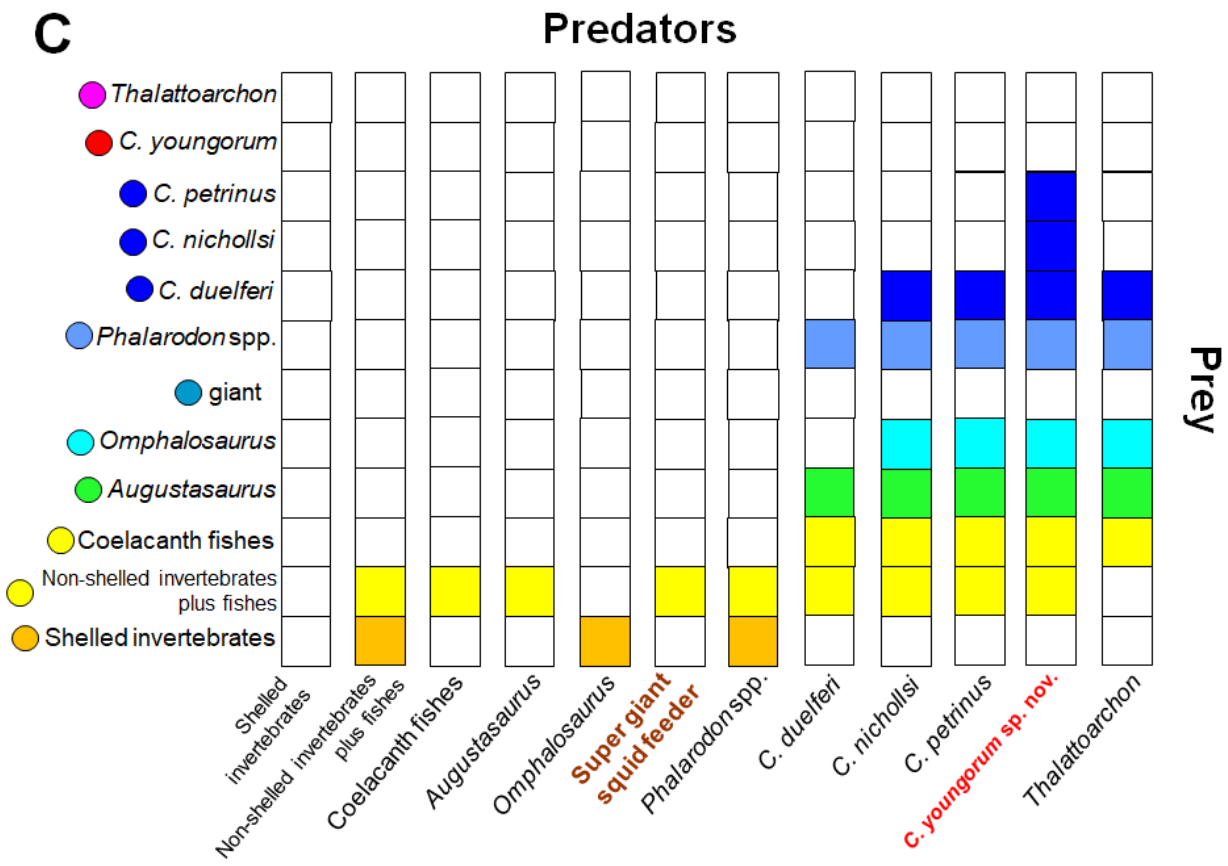

Fig. S14. Trophic interaction matrix implemented in the two different model scenarios (H1 and H2). (A) Standard scenario reflecting all vertebrate taxa in the fossil record (H1). **(B)** H2.1 scenario in which a 'super-giant ammonoid feeder' (200 tons, ca. 30 m long) feeding exclusively on 'shelled invertebrates' (primarily ammonoids) is added to the standard scenario. **(C)** H2.2 scenario in which a 'super-giant squid feeder' (200 tons, ca. 30 m long) feeding exclusively on 'non-shelled invertebrates (primarily squid) and fish' is added to the standard scenario. Stacked boxes represent the diet of predatory taxa. Filled boxes indicate that a taxon is taken by the predator, whereas white indicates that it is not. *C.* = *Cymbospondylus*.

Setting up the food web model. We employed the recently published R package *fluxweb* (*41*) in R version 3.5.2 (Data S8). Visualization of results was done in TIBCO Statistica 13.3. *Fluxweb* provides a modeling framework for estimating energy fluxes in a food web of a user-defined number of taxa (nodes). It calculates energy fluxes in a top-down manner (from higher trophic levels down to the primary producers). Energy loss at each node (taxon) then balances its consumptive gains. The primary output of *fluxweb* modeling is a matrix of energy fluxes (F_{ij}) among the nodes of the food web, describing the energy flux from each node of the web to each of the other nodes. The *fluxweb* model also derives a stability value for the food web by applying an ordinary differential equation approach (Lotka-Volterra equations for multiple species with F_{ij} giving the energy flux between 'species') to total biomasses of food web members and searching for equilibrium total biomasses of members. The stability value of a modeled food web reflects the smallest total biomass under equilibrium and in the absence of environmental perturbations.

The *fluxweb* model considers a given number of taxa (n). It is parametrized by only a few values needed for each taxon (node, $i \leq n$) of the food web: body mass of the individuals of the population (BM_i), total biomass of the population (TB_i), assimilation efficiency (e_i) and physiological loss (X_i). It is further parametrized by the trophic interaction matrix (W_{ij}), containing for each taxon the information on which taxa i the taxon j feeds ($1 \leq i, j \leq n$). Unlike other tools developed for modern marine and terrestrial food webs (e.g., *161 - 164*), the very limited number and type of model parameters required by *fluxweb* (*41*) allows modeling of energy flux in extinct food webs. *Fluxweb* can work with this low number of parameters because it is based on the allometric trophic network theory (for a recent review refer to *42*).

Model parameter n*: Taxa considered*. We entered the eleven taxa described before into the *fluxweb* model (table S11). Out of these the 'invertebrates' are basal to all other taxa in our modeled food web, i.e., the energy flux outgoing from 'invertebrates' provides and finally limits the energy available to any other taxon in this web. The total biomass of 'invertebrates' reflects the total energy that any primary producer and consumer of the Fossil Hill Fauna had passed on to them, irrespective of whether these taxa are preserved in the fossil record or not. We thus only modeled the trophically higher part of the food web of the Fossil Hill Fauna. We thereby ignored any potential trophic interaction of taxa within the 'invertebrates' because we only modeled how much energy is going out from 'invertebrates'.

For the unknown lower trophic part, there are two alternative interpretations regarding the total biomass of the basal 'invertebrates'. For any given amount of primary production, a short food chain with few energy transfers results in a larger total biomass of 'invertebrates' than a longer food chain with more energy transfers. Given a fixed length of the food chain, i.e., a fixed number of energy transfers between the primary producers and the trophically higher 'invertebrates', the total biomasses of the latter will increase with an increasing amount of primary production. The detrital food chain of ecosystems in which the source of energy is dead organic matter or detritus, had to be ignored in our model due to lack of information on taxa involved. Thus, modeled consumers of the food chain have access to 100% of the total biomass of their prey populations; no portion of this biomass (e.g., dead individuals) enters the detrital food chain. We consider the latter as unproblematic, as the giant *C. youngorum* sp. nov. together with the apex predator *Thalattoarchon saurophagis* most probably fed on all smaller-sized taxa, the latter irrespective of whether individuals were alive or dead (*8*). The extant great white shark has a feeding strategy (*46*) similar to that that we assumed for *Thalattoarchon saurophagis*.

Model parameter BM_i, $i \leq n$*: Body masses*. For all modeled taxa, body masses were either calculated from their total body length (only ichthyosaurs) or estimated based on their body size and shape (all others, table S11). Only for *C. youngourum*, we first calculated total body length from the humerus length of LACM DI 157871 (Fig. S7A, table S2), whereas for all other ichthyosaurs total body lengths were retrieved from the literature. Ichthyosaur body masses were inferred from our regression on body mass against total body length (Fig. S7B). For all ichthyosaur taxa, except for *C. youngourum*, we also evaluated the regression's 95% prediction interval at their total body length to capture uncertainties in body masses (table S11). For *C. youngourum* sp. nov., we took into account error propagation by evaluating the 95% prediction interval of the regression of total body length on humerus length (Fig. S7A) and that of body mass on total body length (Fig. S7B). The body mass of 'invertebrates' was inferred as average body mass from an ammonite field sample (table S12). In addition, we conducted a sensitivity analysis for invertebrate body mass and showed that our modeling results are highly robust against large errors in their body masses (Fig. S15). The body mass range considered in the sensitivity analysis of invertebrates was 0.02 g to 1675 g. For 'fish', coelacanth fish, and the sauropterygian *Augustasaurus*, we *a priori* assumed fixed body masses (table S11). We provide

arguments in the Methods section of the main text that our modeling results also must be robust in terms of errors in body estimates on these three members of the food web.

Table S11. Energy flux model parameters and values of the Fossil Hill taxa for the standard (H1) and the H2 scenario. Total biomass (TB_i) is the number of individuals documented in the Fossil Hill Member of the Augusta Mountains times the body mass assumed or estimated for this taxon (BM_i). For assimilation efficiencies (e_i), we used the extant animal model (*41*). For ichthyosaurs, BM_i was calculated from published total body lengths, except for *C. youngorum* sp. nov., for which we first estimated total body length from the humerus length of LACM DI 157871 (Fig. S8). BM_i and TB_i are given with 95% prediction intervals for all ichthyosaurs, except for *C. youngorum* sp. nov.. For the latter, the lower mass is the lower limit of the 95% prediction interval of body mass predicted for a total body length of 12.479 m (Fig. S8A), which is the lower limit of the 95% prediction interval of total length predicted from humerus length (Fig. S8B). The upper mass is the upper limit of the 95% prediction interval of body mass predicted for a total body length of 24.958 m (Fig. S8B), which is the limit of the 95% prediction interval of total length predicted from humerus length (Fig. S8B). The metabolic type and the scaling equation (normalization constant, exponent) define the physiological losses (X_i) for each of the modeled taxa (i). Losses are modeled in *fluxweb* via mass-specific metabolic rates and thus depend on BM_i. Scaling regressions on the metabolic rate of invertebrates, ectothermic vertebrates, and endothermic vertebrates are from Brown et al. (*44*), data from extant species, BM_i in grams. *C.* = *Cymbospondylus*. Sources of ichthyosaur total body lengths: [1)] Sander and Faber 2003 (*160*); [2)] average length of *Phalarodon callwayi* (1.5 m) and *P. fraasi* (2.8 m), Schmitz et al. 2004 (*39*); [3)] Klein et al. 2020 (*17*); [4)] Fröbisch et al. 2006 (*16*); [5)] Merriam 1908 (*40*); [6)] Fröbisch et al. 2013 (*8*). Note that we assumed physiological losses as seen in modern endothermic vertebrates for all ichthyosaurs.

Taxon	Number of individuals	Total body length (m)	Body mass (BM_i, kg)	Total biomass (TB_i, kg)	Assimilation efficiency (e_i)	Metabolic rate (Watts per gram)	Scaling normalization constant	Scaling exponent
Shelled invertebrates	unknown		0.01	unknown	0.906	(ectothermic) invertebrate	17.17	-0.29
Non-shelled invertebrates plus fish	unknown		1.00	unknown	0.906	ectothermic vertebrate	18.18	-0.29
Coelacanth fish	1		50.00	50.00	0.906	ectothermic vertebrate	18.18	-0.29
Augustasaurus hagdorni	3		100.00	300.00	0.906	ectothermic vertebrate	18.18	-0.29
Omphalosaurus nevadanus	1	5[1)]	783.56 (442.18, 1388.48)	783.56 (442.18, 1388.48)	0.906	endothermic vertebrate	19.50	-0.29
Phalarodon spp.	19	2.15[2)]	52.34 (29.89, 91.64)	994.46 (567.91, 1741.16)	0.906	endothermic vertebrate	19.50	-0.29
C. duelferi	1	4.4[3)]	520.07 (294.35, 918.88)	520.07 (294.35, 918.88)	0.906	endothermic vertebrate	19.50	-0.29

Model parameter TB_i*: Total biomasses of member populations*. Except for 'invertebrates' and 'fish' members, we calculated total biomasses for each member as the product of their body mass (BM_i) and field data, i.e., the number of individuals recorded from the Fossil Hill Member of the Favret Formation (i.e., 3.6 km^2; table S11, Data S7) in the Augusta Mountains.

For the members 'invertebrates' as well as for 'fish', we evaluated the model assuming different total biomasses for each member. With this, we aimed at the information on invertebrates and fish of the FHF being precarious or even absent from the fossil record. Our standard set on total biomasses (in kg) used for 'invertebrates' was {1,000; 10,000; 100,000} and that for 'fish' was {1; 10; 100; 1,000; 10,000; 100,000}. It revealed 15 combinations of total biomasses of groups that we considered in each evaluation of the model. Because fish feed among others on invertebrates (regardless of whether they are shelled or not), and their generation time is usually longer than that of these smaller invertebrates, the total biomass of fish and thus of the member 'fish' cannot exceed that of the trophically lower member 'invertebrates'.

Model parameter e_i : *Assimilation efficiencies*. The assimilation efficiency is a measure of how much energy a consumer extracts from its food. It measures the proportion of ingested energy that an individual assimilates for respiration and uses for biomass production (growth plus reproduction). Species differ in their efficiency of digesting food. For example, many animals assimilate only a fraction of the food across the gut wall, and the remainder is expelled from the body as waste products (feces, which most likely contribute to the detrital chain of a food web). *Fluxweb* has three options for implementing assimilation efficiencies based on extant animals, plants, and detritus (*41*). We chose the animal model for all our animal taxa (table S11).

Model parameter X_i*: Physiological losses*. Physiological losses relate to the production efficiency of taxa. Of the energy that is finally assimilated by an individual (i.e., the proportion ($1-e_i$) of the energy ingested), some is used for respiration (e.g., metabolism, movement), whereas the remainder goes to production, the latter including both production of new tissues (e.g., individual growth) and reproduction (e.g., eggs). The production efficiency then rates how much of the assimilated energy an individual finally stores as biomass (i.e., that is allocated to growth and reproduction). In extant species, production efficiencies and thus physiological losses vary across taxonomic groups, with invertebrates storing the largest fraction of the assimilated

energy as production (having the lowest physiological losses), ectothermic vertebrates storing an intermediate fraction (having intermediate losses), and endothermic vertebrates storing the smallest fraction (having the highest physiological losses) (*165*). *Fluxweb* provides the option of assessing physiological losses of taxa from estimating losses from mass-specific metabolic rates (*44*), which makes it applicable to extinct taxa. The (mass-specific) metabolic rate of a taxon (X_i) is derived from an allometric equation ($X_i = x_0 BM_i^b$), where x_0 and b are constants that depend on the metabolic type of the taxon. Metabolic types implemented in the *fluxweb* package (Data S8) are modern (ectothermic) invertebrates, ectothermic vertebrates, and endothermic vertebrates, ordered by their energetic demands (*44*). Metabolic types and allometric equations used to model physiological losses from body masses of taxa are listed in table S11 and plotted in Fig. S15.

In our model, we assumed physiological losses (X_i) as seen in modern endothermic vertebrates for all ichthyosaur taxa. Several lines of evidence for endothermy in ichthyosaurs support this assumption, i.e., that they had a high basal metabolic rate and actively regulated their body temperature. These include: (1) Bone histology, because ichthyosaurs generally show fibrolamellar bone which indicates fast growth (e.g., *166 - 168*). (2) Ichthyosaurian skeletal and soft part anatomy, indicating adaptation to continuous cruising, as seen in cetaceans (*27*, *169 - 171*). Similarly, large fish of the same lifestyle, i.e., tunas, swordfish, and lamnid sharks, also evolved regional endothermy. However, the latter are sometimes considered mesothermic (*75*). These fish species recycle metabolic heat produced by their muscles to become somewhat warmer than the environment, but they cannot defend their body temperature against the environment as modern endotherms do. (3) An extensive blubber layer (*172*) as in extant mammalian marine endotherms. Blubber is only of use in animals that generate body heat metabolically and defend their body temperature against the colder water. (4) Direct isotopic estimates of body temperature in ichthyosaurs (and plesiosaurs) show values as in modern endotherms and are different from that of extinct ectotherms in the same habitat (*173*). However, such high body temperatures can temporarily be found in mesotherms, too. (5) Finally, the exceptional body size of the largest ichthyosaurs, such as *C. youngorum* sp. nov., which surpasses any extant or fossil non-cetacean marine vertebrate, i.e., any bony fish or chondrichthyan. There are good reasons to assume that giant size is not possible in ectothermic animals, on land or in the sea (*174*) because only endotherms with permanent high metabolic rates can grow sufficiently quickly to reach such large size (*175*). However, the Fossil Hill food web's stability (H1) does not depend on the assumption of high mass-specific metabolic rates in

ichthyosaurs (i.e., the metabolic type used to implement physiological losses in ichthyosaurs) (Fig. S15, S18).

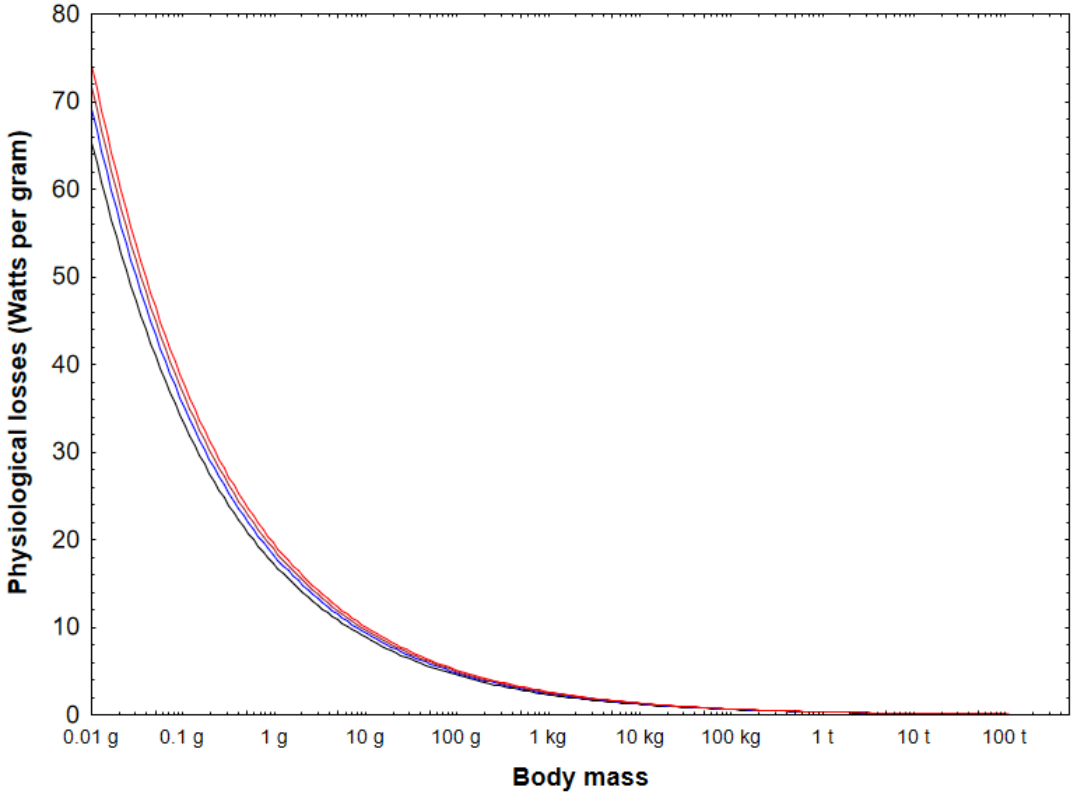

Fig: S17. Physiological losses (X_i) plotted against body mass (BM_i). Losses are modeled in *fluxweb* via mass-specific metabolic rates and thus are set by the body mass of the food web member (table S11). Scaling equations on the mass-specific metabolic rate of invertebrates (black), ectothermic vertebrates (blue), and endothermic vertebrates (red) are from Brown et al. (*44*) and listed in table S11. The mesothermic vertebrate model (brown) was established in this study (see section Methods of the main text). All equations use grams as unit of mass. The body masses plotted span ten orders of magnitude and cover the mass of the smallest ammonite size class (0.02 g, size class V) and the upper body mass limit of *Cymbospondylus youngorum* (135.81 t). Notably, the variation in X_i is smaller than one magnitude across this huge body mass range. This explains (1) that stability values and energy fluxes calculated for the standard scenario using a body mass for 'invertebrates' of 0.02 (size class V) or of 1675 g (size class I) were nearly identical to those obtained for 10 g (standard mass, table S11), given that we fixed their total biomass in our model to 1,000 kg, 10,000 kg or 100,000 kg. It further explains (2) that we found small changes in stability values and energy fluxes for ectothermic and mesothermic ichthyosaurs compared to endothermic ichthyosaurs (fig. S18).

Model parameter W_{ij}*: Trophic interaction matrix*. This matrix informs on trophic relationships, i.e., which taxa a given taxon feeds on. Matrix entries are ones and zeros, with unity coding that taxon j feeds on taxon i, and zero that it does not feed on taxon i. Thus, in principle, cannibalism (i = j) is possible in our *fluxweb* model, but we did not consider cannibalistic loops for any member, except for 'fish'. Note that for basal taxa (the member 'invertebrates'), an implementation of cannibalistic loops is not possible in *fluxweb* and thus no modeling of potential within-member trophic interactions. The body masses assumed for the food web's members most probably reflect fully-grown individuals. A cannibalistic loop would then imply that fully-grown individuals feed on similar-sized individuals from their own population, but preying upon younger/smaller individuals in their own population is more realistic. For the member 'fish', this cannibalistic interaction implements that, e.g., fish species prey on non-shelled invertebrates and other smaller fish species. Modeling cannibalism (i.e., preying on the own population) generally reduces the energy that other taxa can consume from this population. We erected the trophic interaction matrix W_{ij} from the trophic interactions justified above (Fig. S14).

Running the model. After parametrization of the model based on the Fossil Hill Fauna, we calculated the energy flux matrix F_{ij} by applying the *fluxing* function from *fluxweb*. As noted, input parameters of this function are the trophic interaction matrix (W_{ij}), a vector with the total biomass of all taxa (TB_i), a vector with the assimilation efficiencies of all taxa (e_i), and a vector with the physiological losses of all taxa (X_i). All of these parameters were chosen as described earlier (Fig. S14, table S11).

We applied the *stability.value* function from *fluxweb* to test whether the modeled food web is stable. The input parameters of this function are the energy flux matrix F_{ij} estimated by the *fluxing* function, a vector with the total biomass of taxa (TB_i), a vector with the assimilation efficiencies of taxa (e_i), and a vector with the physiological losses of taxa (X_i). For basal taxa that do not consume other taxa, the *stability.value* function requires values on annual growth rates of their total biomass. We thus assumed a growth rate of 0.5 for the basal 'invertebrates' that Gauzens et al. (*41*) also chose for modern basal aquatic taxa. The *stability.value* function computes the resilience of the community (the modeled faunal assemblage) comprising the food web under equilibrium conditions. The function returns the maximum eigenvalue of the Jacobian matrix of the applied Lotka-Volterra-like system of ordinary differential equations (multispecies

approach). The food web is stable when all eigenvalues of this matrix are negative, or if the largest of these is negative, respectively. The equations model the dynamics of the population's total biomass over time for each taxon in the food web in the absence of environmental perturbations. The change in the total biomass of each taxon results from biomass production (incoming energy from populations on which a taxon preys upon, which depends on the total biomass of taxa preyed on) and consumption (depends on assimilation efficiencies and physiological losses of taxa involved). The initial total biomass of each population in the Lotka-Volterra-like system equals that passed on to the function (TB_i), i.e., the biomass we estimated from the number of individuals and their body mass in the FHF sample (except for 'invertebrates' and 'fish' for which we considered a total of 15 combinations of their total biomasses, table S11). Note that equilibrium total biomasses calculated from the ordinary linear equations must not equal the initial total biomasses (TB_i) of taxa that were passed to the *stability.value* function. Equilibrium total biomasses of taxa are not an output parameter of this function. However, the larger the smallest equilibrium total biomass across taxa, the more negative is the stability value and thus the more stable is the food web.

Testing H1 and H2. To test the two hypotheses H1 and H2, we established two different modeling scenarios for the Fossil Hill food web. For each scenario, we aimed at finding out whether the food web is functional (i.e., an energy flux matrix F_{ij} was returned by the *fluxing* function and this matrix is realistic from a modern ecological perspective) and stable (i.e., all total biomasses are larger than zero under equilibrium conditions and thus the largest eigenvalue is negative). For each scenario, we therefore first generated the respective food web's energy flux matrix with the *fluxing* function and then calculated the maximum eigenvalue of the Jacobian matrix with the *stability.value* function (*41*).

Our standard scenario addresses H1. Model parameter values are listed in table S11 and the trophic interaction matrix W_{ij} is shown in Fig. S14A. As noted, this scenario models an area of 3.6 km^2 of the sampled extinct marine ecosystem. Total biomasses of marine reptile taxa needed for modeling (TB_i) were estimated from our field sampling of the Fossil Hill Fauna (table S11).

To test H2 (H2 scenario), we added one individual of a super-giant bulk-feeding ichthyosaur to the standard scenario while keeping anything else as in the standard scenario. This

super-giant bulk feeder either feeds exclusively on 'invertebrates' (H2.1, e.g., a super-giant ammonoid-feeding ichthyosaur) or it feeds exclusively on 'fish' (H2.2, e.g., a super-giant ichthyosaur taking the small prey items covered in this group in bulk, i.e., a squid and fish feeder). The body mass of this individual was set at 200 tons, i.e., the mass of the largest blue whale measured so far (*64*). The total length of this super-giant is about 30 m as calculated from the total length vs. body mass regression function (Fig. S8B). For this ichthyosaur, we assumed the metabolic type 'endothermic vertebrate' and an assimilation efficiency of 0.906. The trophic interaction matrices used for the H2 scenarios are provided in Fig. S14B, C.

Calculating characteristics of modeled food web. We calculated three characteristics of the food web in order to evaluate its functioning for the H1 and H2 scenarios from the energy flux matrix that we estimated with the *fluxweb* model (F_{ij}) for each of the 15 combinations of total biomass of 'invertebrates' and 'fish'. The first characteristic is the total energy flux going out from the basal 'invertebrates' ($EF_{s\_invertebrates}$). It provides information on how much energy from the member 'invertebrates' is available to all trophically higher consumers of the food web. The second is $EF_{all\ other\ taxa}$, which we defined as the sum of energy flux going out from the members 'invertebrates' and 'fish' that goes to *C. youngorum* sp. nov. and *Thalattoarchon*. *Cymbospondylus youngorum* sp. nov. and *Thalattoarchon* are at the top of the modeled Fossil Hill food web (they are not consumed by any other member), whereas 'invertebrates' and 'fish' are at its bottom. All other taxa from the food web are trophically in between the members 'invertebrates' and 'fish' and the two top consumers *C. youngorum* sp. nov. and *Thalattoarchon*. They directly or indirectly (via feeding on taxa that fed on 'invertebrates' or 'fish') make use of the energy going out from 'invertebrates' and 'fish' that is not used by *C. youngorum* sp. nov. and *Thalattoarchon*. We next calculated the ratio of $EF_{all\ other\ taxa}$ and $EF_{s\_invertebrates}$ ($EFR_{all\ other\ taxa\ to\ s\_invertebrates}$) to understand how much energy is lost between trophic levels. Because energy is always lost between trophic levels (e.g., through feces and metabolism), we expected this ratio to be considerably smaller than unity. In modern marine ecosystems, only about 10 % of the energy available at one trophic level is available at the next higher level (*165*), e.g., from primary consumers to secondary consumers or from secondary to tertiary consumers, and so on. Our trophic interaction matrices (Fig. S14) produce five consumer levels (bottom, level 1: 'invertebrates' and 'fish'; level 2: coelacanth fish, *Augustasaurus* and *Phalarodon* spp.; level 3: *C. duelferi*; level 4: *C. nichollsi* and *C. petrinus*; top, level 5: *C. youngorum* sp. nov. and

Thalattoarchon). This suggests that the about 90 % energy loss between trophic levels seen in extant ecosystems would be consistent with $EFR_{\text{all other taxa to s\_invertebrates}}$ being around 0.1^4. For model evaluation, we made the interpretation of $EFR_{\text{all other taxa to s\_invertebrates}}$ more convenient by taking the fourth root of the raw value (= average across four consumer levels). Finally, to assess the stability of the food web, we checked whether the maximum eigenvalue of the Jacobian matrix returned by the *stability.value* function was negative. Note that a food web is the more stable, the more negative this stability value is and that stability values of extant food webs range between -10 and 0 (*41*).

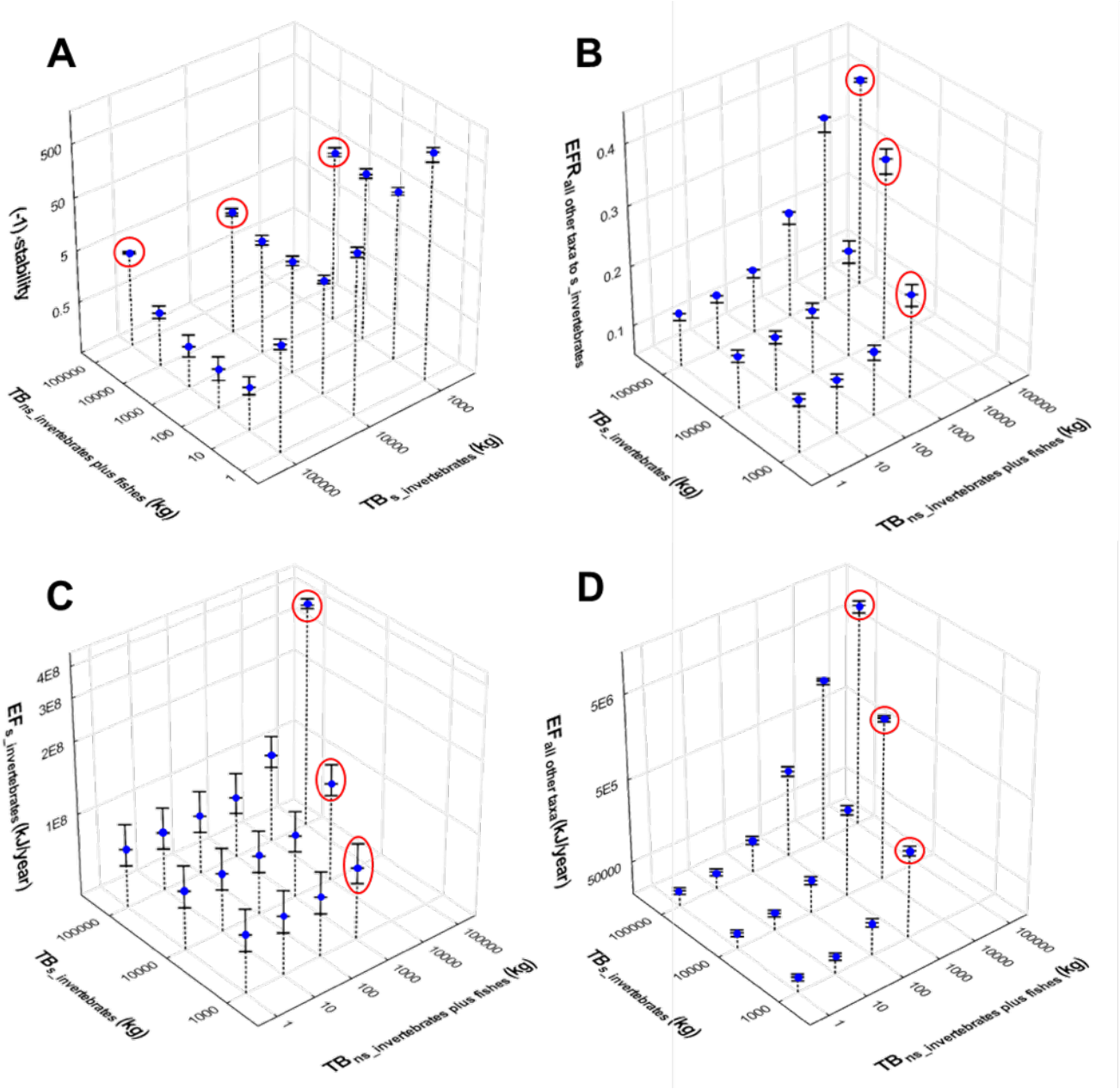

Fig. S16. Results obtained for the standard scenario (H1). The standard scenario (Fig. S14A, table S11) tests H1 for different combinations of total biomass of 'invertebrates' and 'fish'. The standard scenario was also evaluated for three situations of body masses assumed for ichthyosaurs (table S11). Blue circles refer to values obtained when using the standard body mass for all ichthyosaurs. Whiskers refer to the situation that all ichthyosaurs were lighter than the standard and heavier than the standard, respectively (table S11, body masses inferred from 95% prediction intervals, Fig. S7). **(A)** The stability values estimated by the model. **(B)** The ratio of the sum of fluxes going out from 'invertebrates' and 'fish' to *C. youngorum* sp. nov. and *Thalattoarchon* and of the total flux going out from 'invertebrates' ($EFR_{\text{all other taxa to s\_invertebrates}}$). **(C)** The total outgoing energy from 'invertebrates' ($EF_{\text{s\_invertebrates}}$), and **(D)** the sum of outgoing fluxes from 'invertebrates' and 'fish' to *C. youngorum* sp. nov. and *Thalattoarchon* ($EF_{\text{all other taxa}}$).

These four characteristics of the food web are shown for all 15 different combinations of total biomass of 'invertebrates' and 'fish' studied. In (A) and (B), the upper whiskers refer to the situation that all ichthyosaurs were lighter, whereas in (C) and (D) they refer to that all ichthyosaurs were heavier than the standard (table S11). All stability values calculated by the *fluxweb* model are negative (A) indicating a stable food web, and energy flux ratios (B) correctly predict a clear loss of energy between trophic levels, except for the combinations in which total biomass of 'invertebrates' and 'fish' are identical (red circles and ovals) and ratios are unrealistically large (around 40 %) from a modern perspective. Note that we multiplied stability values by -1. TB = total biomass (kg), EF = outgoing energy flux (kJ/year), EFR = outgoing energy flux ratio. The total energy flux of the food web is shown in Fig. S17.

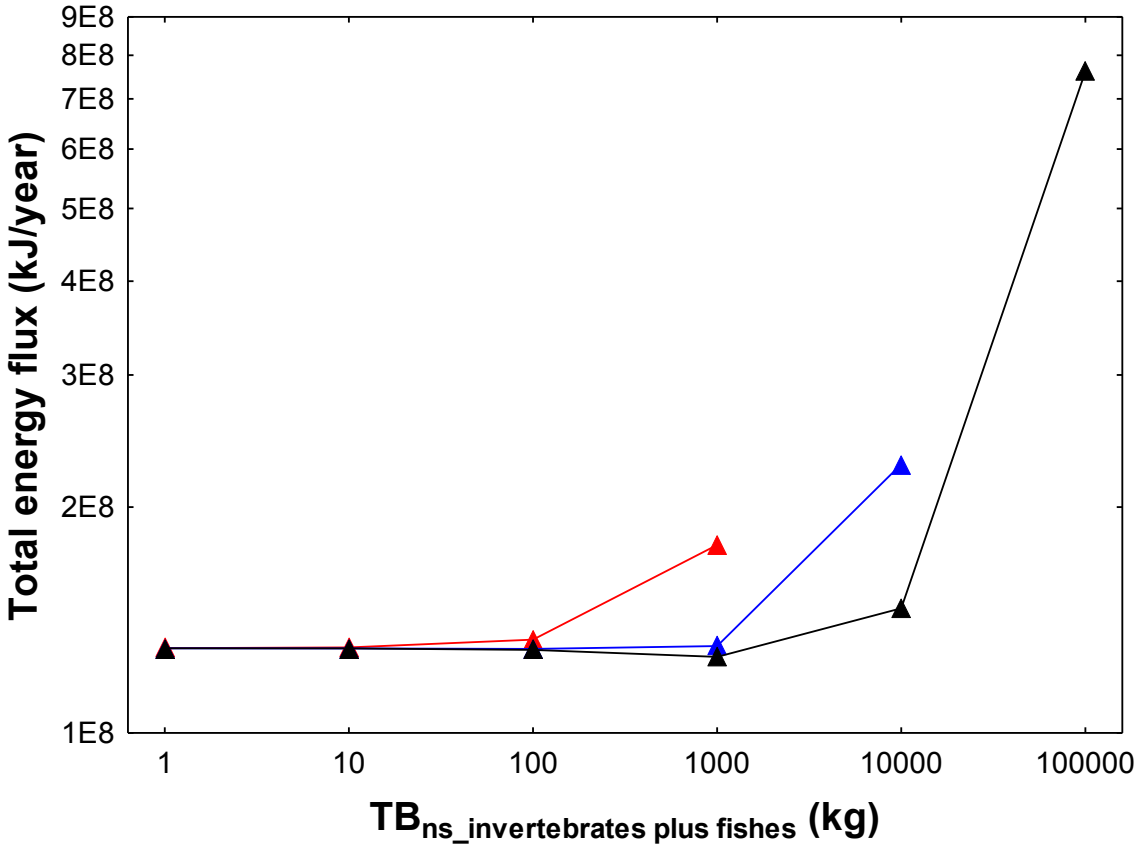

Fig. S17. The total energy flux in the Fossil Hill food web for each of the 15 different combinations of total biomass of 'invertebrates' and 'fish' and the standard scenario H1. The total energy flux was calculated from the respective energy flux matrix (F_{ij}) by summing up all its entries. Red = 1,000 kg of 'invertebrates', blue = 10,000 kg of 'invertebrates', and black = 100,000 kg of 'invertebrates'. Note that for all combinations in which the total biomass of 'invertebrates' exceeds that of 'fish', total energy fluxes are rather similar, and the average flux is $1.3*10^8$ kJ/year.

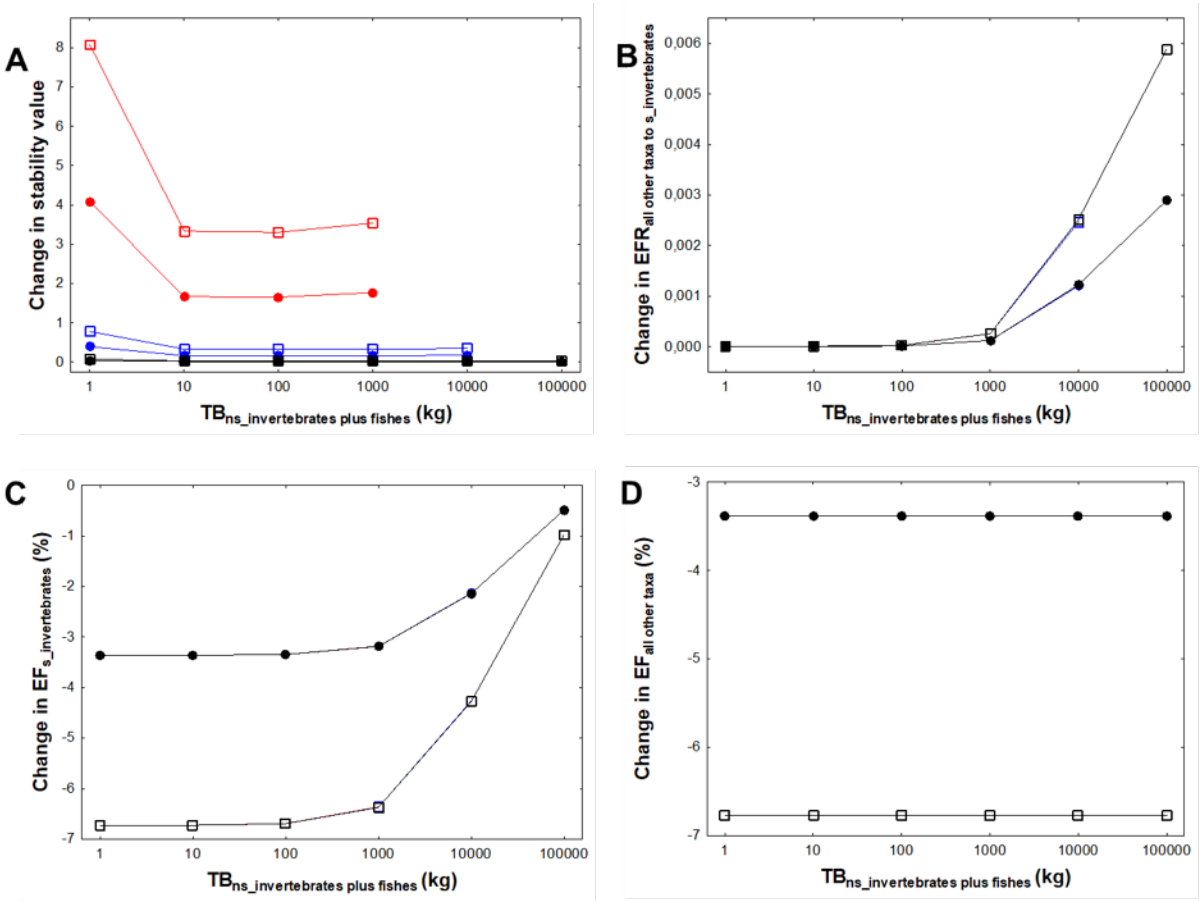

Fig. S18. Sensitivity analysis of the four characteristics of the FHF energy flux model to different assumptions on physiological losses (X_i) in ichthyosaurs (endothermic / mesothermic / ectothermic). Results are expressed as differences to the endothermic metabolic type (Fig. S16). Open squares, ectothermic vertebrate metabolic type; dots, mesothermic metabolic type. Colors distinguish different total biomasses assumed for 'invertebrates' (red = 1,000 kg, blue = 10,000 kg, black = 100,000 kg). **(A)** Differences in stability values between different X_i metabolic types. **(B)** Differences in $EFR_{\text{all other taxa to s\_invertebrates}}$ between different X_i metabolic types. **(C)** Relative differences in $EF_{\text{s\_invertebrates}}$ between different X_i metabolic types. **(D)** Relative differences in $EF_{\text{all other taxa}}$ between different X_i metabolic types. Note that stability values (A), relative differences in $EF_{\text{s\_invertebrates}}$ (C), and relative differences in $EF_{\text{all other taxa}}$ (D) are largest in the endothermic vertebrate metabolic type, intermediate in the mesothermic metabolic type, and smallest in the ectothermic metabolic type, whereas $EFR_{\text{all other taxa to s\_invertebrates}}$ (B) are highest in the ectothermic metabolic type, intermediate in the mesothermic metabolic type, and lowest in the endothermic metabolic type. All stability values obtained for non-endothermic X_i are negative and indicate a functional and stable food web. Due to the top down approach of *fluxweb*, $EF_{\text{s\_invertebrates}}$, the energy that is available to all trophically higher consumer taxa, was smallest for ectothermic ichthyosaurs, intermediate for mesothermic ichthyosaurs and highest for endothermic ichthyosaurs. This is because the lower energy demands of non-endothermic ichthyosaurs produce smaller $EF_{\text{all other taxa}}$ values than for endothermic ichthyosaurs. The resulting overall reduction in energy flux implies smaller total biomasses of taxa under equilibrium and thus larger stability values (more positive values) and a less stable food web.

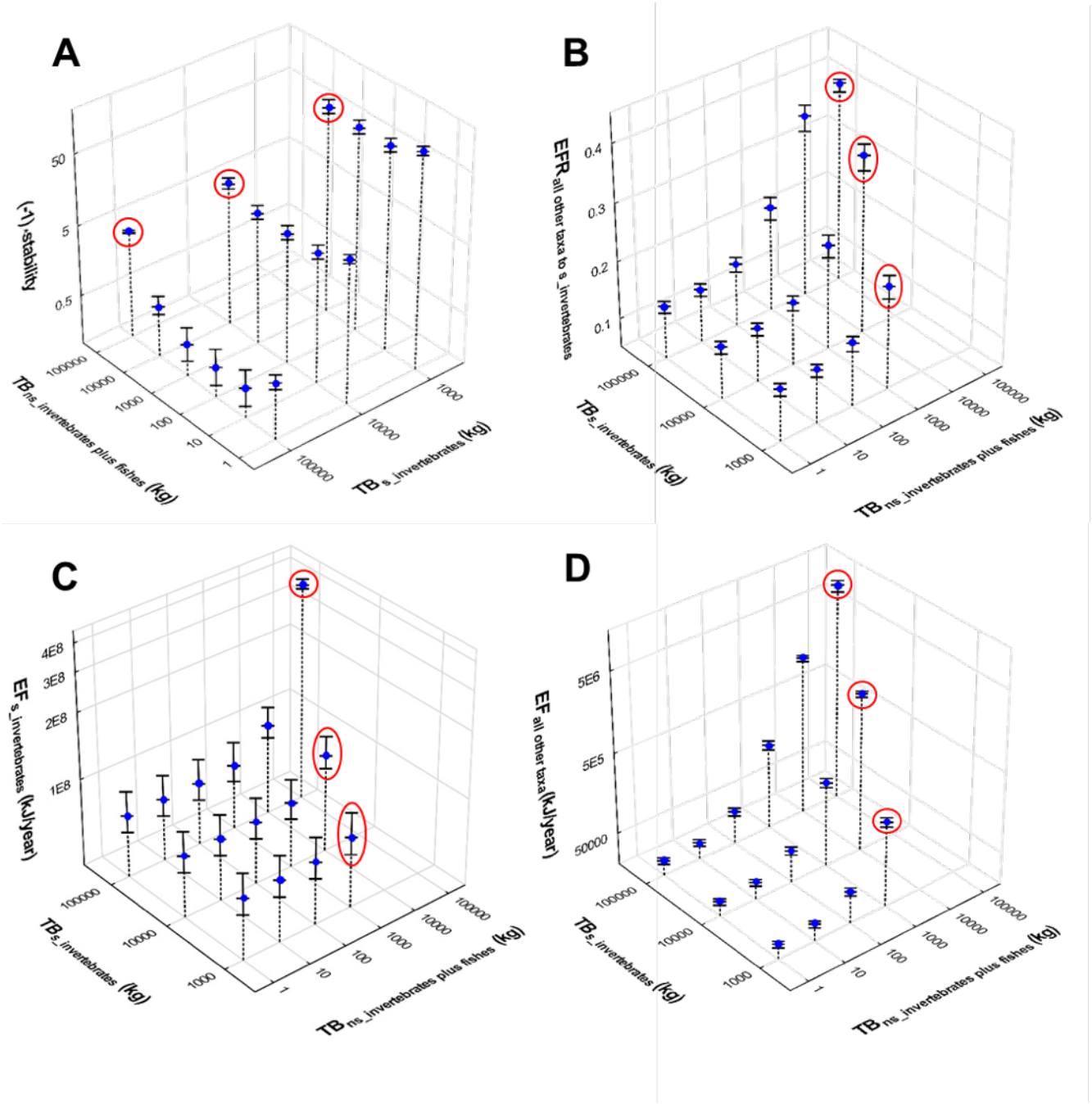
A
(-1)-stability
50
5
0.5
TB ns_invertebrates plus fishes (kg)
100000
10000
1000
100
10
1
TB s_invertebrates (kg)
1000
10000
100000
B
EFR all other taxa to s_invertebrates
0.4
0.3
0.2
0.1
TB s_invertebrates (kg)
100000
10000
1000
TB ns_invertebrates plus fishes (kg)
1
10
100
1000
10000
100000
C
EF s_invertebrates (kJ/year)
4E8
3E8
2E8
1E8
TB s_invertebrates (kg)
100000
10000
1000
TB ns_invertebrates plus fishes (kg)
1
10
100
1000
10000
100000
D
EF all other taxa (kJ/year)
5E6
5E5
50000
TB s_invertebrates (kg)
100000
10000
1000
TB ns_invertebrates plus fishes (kg)
1
10
100
1000
10000
100000

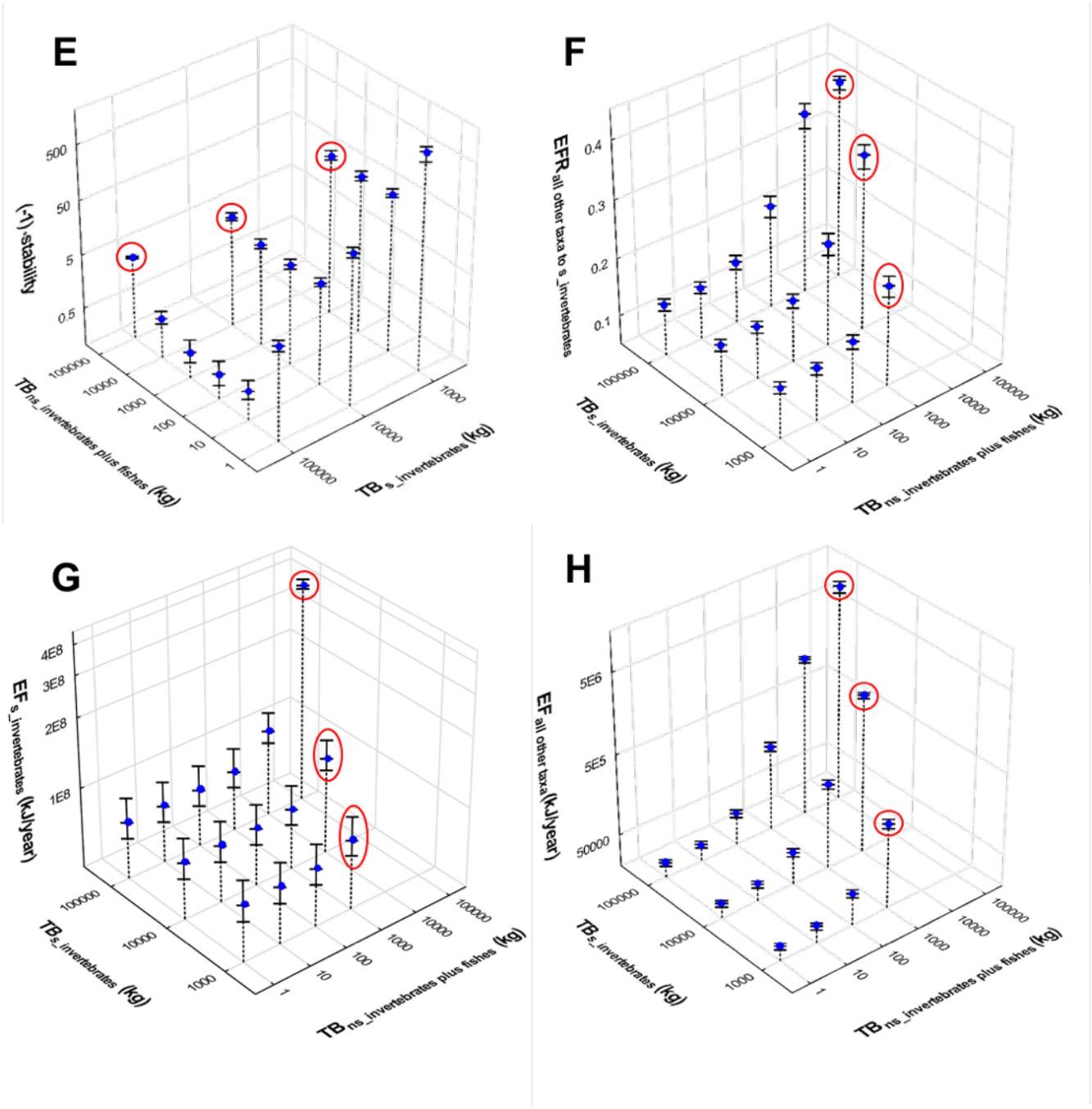

Fig. S19. Results obtained for the H2 scenario for different combinations of total biomass of 'invertebrates' and 'fish'. (A, E) The stability values estimated by the model. **(B, F)** Ratios of the sum of fluxes going out from 'invertebrates' and 'fish' to *C. youngorum* sp. nov. and *Thalattoarchon* and of the total flux going out from 'invertebrates' ($EFR_{\text{all other taxa to s\_invertebrates}}$). **(C, G)** Outgoing fluxes from 'invertebrates' ($EF_{\text{s\_invertebrates}}$), and **(D, H)**, outgoing fluxes from 'invertebrates' and 'fish' to *C. youngorum* sp. nov. and *Thalattoarchon* ($EF_{\text{all other taxa}}$). In (A, B, E, F), the upper whiskers refer to the situation that all ichthyosaurs are lighter than the standard. In (C, D, G, H), the whiskers refer to that all ichthyosaurs are heavier than their standard. Note that all stability values are negative, but for convenience, absolute values are depicted. Results suggest that for each of the 15 combinations of total biomasses, the modeled food web is stable and ecologically reasonable when the total biomass of 'fish' is smaller than that of the

'invertebrates'. All stability values are negative (A, E), and the energy flux ratios (B, F) correctly predict a clear loss of energy between trophic levels, except for the combinations in which total biomass of 'invertebrates' and 'fish' are identical (red circles and ovals) and ratios are unrealistically large (around 40 %) from a modern perspective. TB = total biomass (kg), EF = outgoing energy flux (kJ/year), EFR = outgoing energy flux ratio, red circles and ovals = the total biomass of 'fish' equals that of 'invertebrates'. Due to the top down approach used by *fluxweb* and because of the super-giant ichthyosaur feeding exclusively on members of the lowest trophic level of the FHF food web, only the outgoing energy flux from 'invertebrates' and 'fish' increased in H2, whereas the incoming energy flux of all other taxa did not differ between H1 and H2 (Fig. S20). When compared to the standard scenario (H1) overall changes in stability values, $EF_{s\_invertebrates}$, $EF_{all\ other\ taxa}$ and $EFR_{all\ other\ taxa\ to\ s\_invertebrates}$ are small for H2 (Fig. S19).

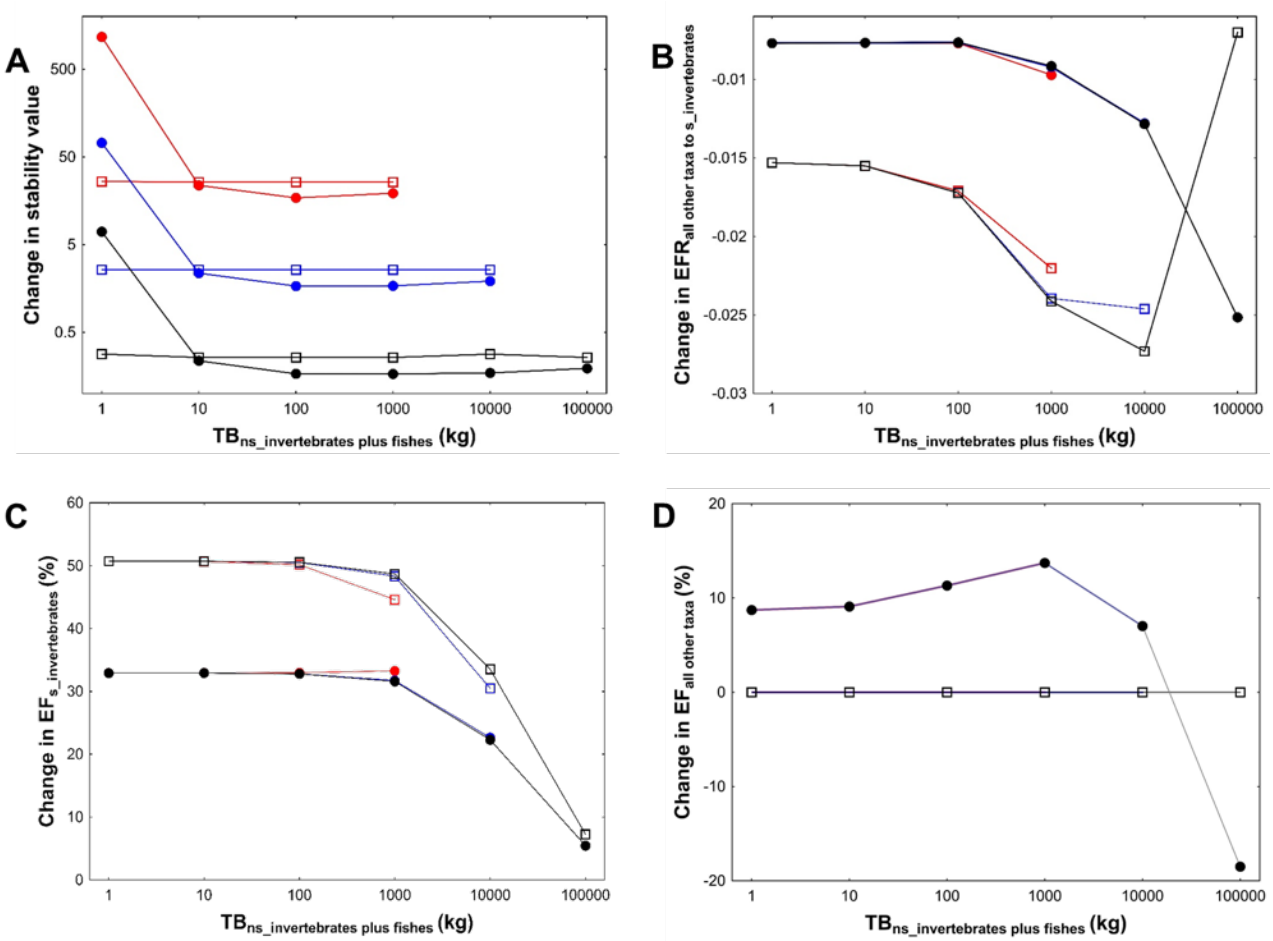

Fig. S20. Changes in the four characteristics of the food webs in scenario H2 assuming different total biomasses of 'invertebrates' and 'fish' compared to the same combinations in the standard scenario H1. For testing H2, we added one individual of a super-giant ichthyosaur to the H1 scenario and kept anything else the same. This ichthyosaur takes either exclusively 'invertebrates' (H2.1, squares) or 'fish' (H2.2, dots). Colors distinguish different total biomasses assumed for 'invertebrates' (red = 1,000 kg, blue = 10,000 kg, black = 100,000 kg). **(A)** Differences in the stability values between H1 and H2. Note that the food web is always somewhat more stable in the H2 than in the H1 scenario. **(B)** Differences in $EFR_{\text{all other taxa to s\_invertebrates}}$ between H1 and H2; ratios are always smaller for H2 than for H1. **(C)** Relative differences in $EF_{\text{s\_invertebrates}}$ between H1 and H2; $EF_{\text{s\_invertebrates}}$ is always higher for H2 than for H1. **(D)** Relative differences in $EF_{\text{all other taxa}}$ between H1 and H2; $EF_{\text{all other taxa}}$ is always higher for H2 than for H1.

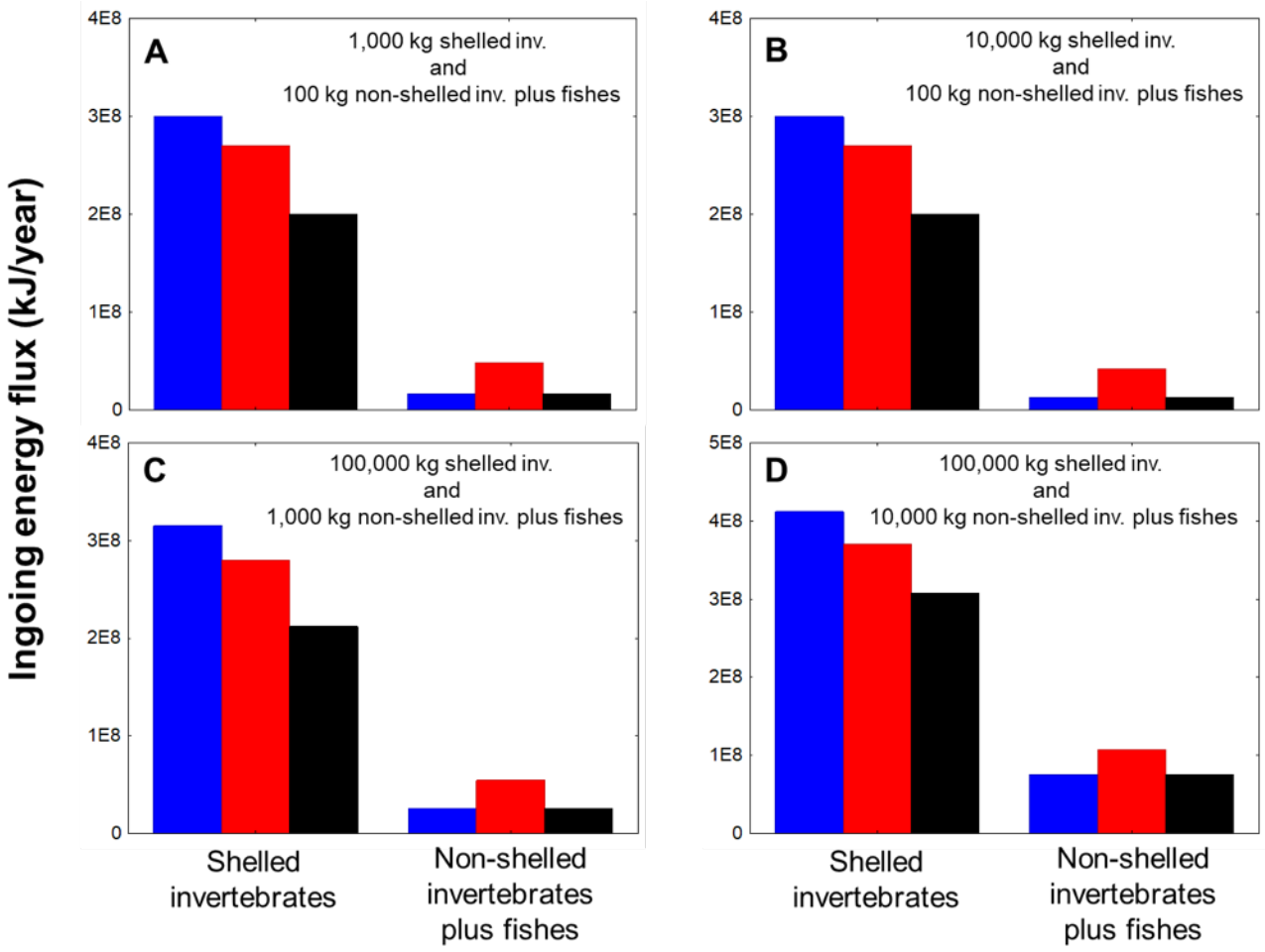

Fig. S21. Incoming energy flux to the two trophically lowest taxa for four different combinations of total biomass of 'invertebrates' and 'fish'. Fluxes were calculated for the standard scenario (H1) and for H2. Black = standard scenario, blue = H2.1 scenario, including a super-giant ichthyosaur feeding exclusively on 'invertebrates', red = H2.2 scenario, including a super-giant ichthyosaur feeding exclusively on 'fish'. **(A)** 1,000 kg of 'invertebrates' combined with 100 kg of 'fish'. **(B)** 10,000 kg of 'invertebrates' combined with 100 kg of 'fish'. **(C)** 100,000 kg of 'invertebrates' combined with 1,000 kg of 'fish'. **(D)** 100,000 kg of 'invertebrates' combined with 10,000 kg of 'fish'. The total sum of incoming energy for a taxon is a proxy of its total biomass under equilibrium conditions. We assumed for the basal 'invertebrates' that the sum of the ingoing energy flux is about four times higher than the outgoing energy flux (*164*). When compared to H1 and averaged across all combinations in which the total biomass of 'invertebrates' is larger than that of 'fish', the super-giant feeding exclusively on 'invertebrates' consumes an increase in $EF_{s\_invertebrates}$ of $2.6*10^{-7}$ kJ/year. If the modeled super-giant exclusively feeds on 'fish', the average energy taken up from 'invertebrates' is $1.7*10^{7}$ kJ/year and that from 'fish' is $0.9*10^{7}$ kJ/year.

Table S12. Estimation of the total production rate of ammonoids preserved in the Fossil Hill Member in the Augusta Mountains. Production rate is the energy stored by an individual in its body plus the energy that it allocates to reproduction. Production rate is an upper limit to the energy flux from an individual of the population going to individuals of other taxa. Our field sampling revealed three different total biomasses of ammonoids (TB) based on the coverage of one square meter by ammonoid fossils. Estimated body masses (BM) of ammonoids ranged between 0.02 and 1675 grams. We assumed 10 g (the rounded average across sized individuals from our random sample, see Methods in the main text) as body mass for the food web member 'invertebrates' (table S11). #individuals = number of individuals, as derived from TB and BM. MR = metabolic rate, MR = 365*1.43*$BM^{0.71}$ (kJ/year, *44*), PR = production rate, PR = 0.25*MR (*176*). TPR = total production rate, TPR = #individuals*PR. For a comparison of ammonoid production rates to modeled rates of 'invertebrates' and to rates in modern marine ecosystems, refer to table S13.

TB (kg)	Coverage (%)	BM (g)	#individuals	MR (kJ/year)	PR (kJ/year)	TPR (kJ/year)
1458	15	0.02	72,900,000	32.5	8.1	5.9*10
1458	15	1675.00	870	101,549.9	25,387.4	2.2*10
2430	25	0.02	121,500,000	32.5	8.1	9.8*10
2430	25	1675.00	1,451	101,549.9	25,387.4	3.7*10
2916	30	0.02	145,800,000	32.5	8.1	1.2*10
2916	30	1675.00	1,740	101,549.9	25,387.4	4.4*10
Mean						4.8*10

Table S13. Comparison of production rates of the Fossil Hill food web to that of extant marine food webs. Modeled production rates of Fossil Hill members are averages across the twelve combinations of total biomasses of 'invertebrates' and 'fish' in which the former was larger than the latter. Rates were inferred from energy flux matrices and equal the sum of energy flux going out from the respective Fossil Hill Fauna members. Cusson and Bourget (*177*) conducted a meta-analysis on the mean production rate (in kJ per m^2*year) of different taxonomic groups in extant marine ecosystems based on 147 studies. Gaichas et al. (*178*) established production rates (in metric tons per m^2 * year) for different organism groups based on the average of five extant marine ecosystems. For comparison, we converted the rates given in the latter study by assuming that 1 kg biomass is 1,000 kJ, and we also scaled rates of extant marine ecosystems to the area of 3.6 km^2 being covered by the Augusta Mountains census of the Fossil Hill Fauna (table S11). The estimated production rate of the Fossil Hill ammonoids matches well rates recorded for invertebrates of extant marine ecosystems, whereas those predicted for H1 and H2 are almost one magnitude smaller. The total production rate of members 'fish' and 'coelancanth fish' of the Fossil Hill Fauna is about six times smaller (three magnitudes smaller) than that of fish in extant ecosystems. The production rate of all marine reptiles of the Fossil Hill Fauna is more than three magnitudes larger than that of modern amniotic vertebrates. Production rates of all extant vertebrates are twice that of all Fossil Hill Fauna vertebrates.

Ecosystem	Groups and members	Production rate (kJ/year)	Source
FHF	Ammonites (field sample)	4.8*10	Table S12
FHF	‚invertebrates'	5.3*10 7.9*10 8.2*10	Modeled
Modern	Benthic invertebrates (Mollusca+Annelida+Arthropoda+Echinodermata)	5.6*10	*(179)*
Modern	Invertebrates (without zooplankton)	6.4*10	*(180)*
FHF	Non-amniotic vertebrates (coelancanth fish)	2.5*10	Modeled
FHF	Non-amniotic vertebrates (‚fish'+coelancanth fish)	1.3*10	Modeled
Modern	Non-amniotic vertebrates (fish)	8.0*10	*(180)*
FHF	Amniotic vertebrates (marine reptiles)	2.5*10	Modeled
Modern	Amniotic vertebrates (whales+pinnipeds+birds)	8.1*10	*(180)*
FHF	Vertebrates (‚fish'+coelancanth fish+marine reptiles)	3.8*10	Modeled
Modern	Vertebrates (fish+whales+pinnipeds+birds)	8.1*10	*(180)*

Table S14. Estimated total basal metabolic rates of Fossil Hill marine reptile populations. Total basal metabolic rates (TBMR) of taxa are the basal metabolic rate of one individual (BMR) times the abundance of this taxon in the Fossil Hill Fauna (table S11, Data S7). BMR is calculated from the taxon's body mass (BM, table S11). For endothermic vertebrates, BMR is $365*1.625*BM^{0.71}$ (kJ/year, *44*) and for ectothermic vertebrates, BMR is $365*1.515*BM^{0.71}$ (kJ/year, *44*). When averaged across the twelve combinations with total biomasses of 'invertebrates' larger than that of 'fish', the modeled total energy flux in the Fossil Hill food web is $1.3*10^8$ kJ/year for the standard scenario (Fig. S16 and increases by $2.6*10^7$ kJ/year when a hypothetical super-giant bulk feeder is added to the food web (Fig. S20). A comparison of TBMR values of taxa with these average total energy fluxes indicates that abundances of at least *C. nichollsi*, *C. petrinus*, *C. youngorum* sp. nov., and of the hypothetical super-giant bulk feeder must have been substantially smaller than indicated by the fossil record. This is because their populations' BMR is not substantially smaller than the modeled total energy flux in the Fossil Hill food web. Low abundances of large to giant ichthyosaurs are consistent with the low abundances seen in whales and other large extant marine predators in today's oceans.

Taxon	BM (kg)	BMR (kJ per year)	Abundance	TBMR (kJ per year)
Augustasaurus hagdorni	100.00	1.5*10	3	4.5*10
Omphalosaurus nevadanus	783.56	6.7*10	1	6.7*10
Phalarodon spp.	52.34	1.0*10	19	1.9*10
C. duelferi	520.07	5.0*10	1	5.0*10
C. nichollsi	3000.08	1.7*10	10	1.7*10
C. petrinus	5731.06	2.8*10	10	2.7*10
C. youngorum sp. nov.	44698.63	1.2*10	3	3.6*10
Thalattoarchon saurophagis	4295.17	2.3*10	1	2.3*10
Hypothetical super-giant bulk feeder	200000.00	3.4*10	1	3.4*10

References and Notes

1. G. J. Vermeij, Gigantism and its implications for the history of life. *PLOS ONE* **11**, e0146092 (2016). doi:10.1371/journal.pone.0146092 Medline

2. N. P. Kelley, N. D. Pyenson, Vertebrate evolution. Evolutionary innovation and ecology in marine tetrapods from the Triassic to the Anthropocene. *Science* **348**, aaa3716 (2015). doi:10.1126/science.aaa3716 Medline

3. A. H. Knoll, M. J. Follows, A bottom-up perspective on ecosystem change in Mesozoic oceans. *Proc. Biol. Sci.* **283**, 20161755 (2016). doi:10.1098/rspb.2016.1755 Medline

4. J. A. Goldbogen, D. E. Cade, D. M. Wisniewska, J. Potvin, P. S. Segre, M. S. Savoca, E. L. Hazen, M. F. Czapanskiy, S. R. Kahane-Rapport, S. L. DeRuiter, S. Gero, P. Tønnesen, W. T. Gough, M. B. Hanson, M. M. Holt, F. H. Jensen, M. Simon, A. K. Stimpert, P. Arranz, D. W. Johnston, D. P. Nowacek, S. E. Parks, F. Visser, A. S. Friedlaender, P. L. Tyack, P. T. Madsen, N. D. Pyenson, Why whales are big but not bigger: Physiological drivers and ecological limits in the age of ocean giants. *Science* **366**, 1367–1372 (2019). doi:10.1126/science.aax9044 Medline

5. W. Gearty, C. R. McClain, J. L. Payne, Energetic tradeoffs control the size distribution of aquatic mammals. *Proc. Natl. Acad. Sci. U.S.A.* **115**, 4194–4199 (2018). doi:10.1073/pnas.1712629115 Medline

6. G. J. Slater, J. A. Goldbogen, N. D. Pyenson, Independent evolution of baleen whale gigantism linked to Plio-Pleistocene ocean dynamics. *Proc. Biol. Sci.* **284**, 20170546 (2017). doi:10.1098/rspb.2017.0546 Medline

7. B. C. Moon, T. L. Stubbs, Early high rates and disparity in the evolution of ichthyosaurs. *Commun. Biol.* **3**, 68 (2020). doi:10.1038/s42003-020-0779-6 Medline

8. N. B. Fröbisch, J. Fröbisch, P. M. Sander, L. Schmitz, O. Rieppel, Macropredatory ichthyosaur from the Middle Triassic and the origin of modern trophic networks. *Proc. Natl. Acad. Sci. U.S.A.* **110**, 1393–1397 (2013). doi:10.1073/pnas.1216750110 Medline

9. P. M. Hull, Emergence of modern marine ecosystems. *Curr. Biol.* **27**, R466–R469 (2017). doi:10.1016/j.cub.2017.04.041 Medline

10. See supplementary materials.

11. C. v. Linnaeus, *Systema Naturae. Regnum Animale* (L. Salvius, Stockholm, ed. 10, 1758).

12. H. F. Osborn, The reptilian subclasses Diapsida and Synapsida and the early history of the Diaptosauria. *Mem. Am. Mus. Nat. Hist.* **1**, 449–507 (1903).

13. H. M. D. de Blainville, Systéme de'Herpetologie. *Nouv. Ann. Mus. Hist. Nat. Paris* **4**, 233–296 (1835).

14. J. Leidy, Notice of some reptilian remains from Nevada. *Proc. Acad. Nat. Sci. Philadelphia* **20**, 177–178 (1868).

15. P. M. Sander, The large ichthyosaur *Cymbospondylus buchseri*, sp. nov., from the Middle Triassic of Monte San Giorgio (Switzerland), with a survey of the genus in Europe. *J. Vertebr. Paleontol.* **9**, 163–173 (1989). doi:10.1080/02724634.1989.10011750

16. N. Fröbisch, P. M. Sander, O. Rieppel, A new species of *Cymbospondylus* (Diapsida, Ichthyosauria) from the Middle Triassic of Nevada and re-evaluation of the skull osteology

of the genus. *Zool. J. Linn. Soc.* **147**, 515–538 (2006). doi:10.1111/j.1096-3642.2006.00225.x

17. N. Klein, L. Schmitz, T. Wintrich, P. M. Sander, A new cymbospondylid ichthyosaur (Ichthyosauria) from the Middle Triassic (Anisian) of the Augusta Mountains, Nevada, USA. *J. Syst. Palaeontology* **18**, 1167–1191 (2020). doi:10.1080/14772019.2020.1748132

18. C. Monnet, H. Bucher, New middle and late Anisian (Middle Triassic) ammonoid faunas from Northwestern Nevada (USA): Taxonomy and biochronology. *Foss. Strat.* **52**, 1–121 (2005).

19. B. Moon, A new phylogeny of ichthyosaurs (Reptilia: Diapsida). *J. Syst. Palaeontology* **17**, 129–155 (2019). doi:10.1080/14772019.2017.1394922

20. J. A. Massare, Tooth morphology and prey preference of Mesozoic marine reptiles. *J. Vertebr. Paleontol.* **7**, 121–137 (1987). doi:10.1080/02724634.1987.10011647

21. R. Motani, Evolution of fish-shaped reptiles (Reptilia: Ichthyopterygia) in their physical environments and constraints. *Annu. Rev. Earth Planet. Sci.* **33**, 12.11–12.26 (2005).

22. C. McGowan, Giant ichthyosaurs of the Early Jurassic. *Can. J. Earth Sci.* **33**, 1011–1021 (1996). doi:10.1139/e96-077

23. T. M. Scheyer, C. Romano, J. Jenks, H. Bucher, Early Triassic marine biotic recovery: The predators' perspective. *PLOS ONE* **9**, e88987 (2014). doi:10.1371/journal.pone.0088987 Medline

24. S. Gutarra, B. C. Moon, I. A. Rahman, C. Palmer, S. Lautenschlager, A. J. Brimacombe, M. J. Benton, Effects of body plan evolution on the hydrodynamic drag and energy requirements of swimming in ichthyosaurs. *Proc. Biol. Sci.* **286**, 20182786 (2019). doi:10.1098/rspb.2018.2786 Medline

25. R. Motani, D.-Y. Jiang, G.-B. Chen, A. Tintori, O. Rieppel, C. Ji, J.-D. Huang, A basal ichthyosauriform with a short snout from the Lower Triassic of China. *Nature* **517**, 485–488 (2015). doi:10.1038/nature13866 Medline

26. S. Nummela, T. Hussain, J. G. M. Thewissen, Cranial anatomy of Pakicetidae (Cetacea, Mammalia). *J. Vertebr. Paleontol.* **26**, 746–759 (2006). doi:10.1671/0272-4634(2006)26[746:CAOPCM]2.0.CO;2

27. J. G. M. Thewissen, J. D. Sensor, M. T. Clementz, S. Bajpai, Evolution of dental wear and diet during the origin of whales. *Paleobiology* **37**, 655–669 (2011). doi:10.1666/10038.1

28. M. A. MacIver, L. Schmitz, U. Mugan, T. D. Murphey, C. D. Mobley, Massive increase in visual range preceded the origin of terrestrial vertebrates. *Proc. Natl. Acad. Sci. U.S.A.* **114**, E2375–E2384 (2017). doi:10.1073/pnas.1615563114 Medline

29. J. M. Fahlke, K. A. Bastl, G. M. Semprebon, P. D. Gingerich, Paleoecology of archaeocete whales throughout the Eocene: Dietary adaptations revealed by microwear analysis. *Palaeogeogr. Palaeoclimatol. Palaeoecol.* **386**, 690–701 (2013). doi:10.1016/j.palaeo.2013.06.032

30. L. N. Cooper, M. T. Clementz, S. Usip, S. Bajpai, S. T. Hussain, T. L. Hieronymus, Aquatic habits of cetacean ancestors: Integrating bone microanatomy and stable isotopes. *Integr. Comp. Biol.* **56**, 1370–1384 (2016). doi:10.1093/icb/icw119 Medline

31. L. J. Revell, Phytools: An R package for phylogenetic comparative biology (and other things). *Methods Ecol. Evol.* **3**, 217–223 (2012). doi:10.1111/j.2041-210X.2011.00169.x

32. J. C. Uyeda, L. J. Harmon, A novel Bayesian method for inferring and interpreting the dynamics of adaptive landscapes from phylogenetic comparative data. *Syst. Biol.* **63**, 902–918 (2014). doi:10.1093/sysbio/syu057 Medline

33. C. M. Peredo, N. D. Pyenson, C. D. Marshall, M. D. Uhen, Tooth loss precedes the origin of baleen in whales. *Curr. Biol.* **28**, 3992–4000.e2 (2018). doi:10.1016/j.cub.2018.10.047 Medline

34. J. D. Walker, J. W. Geissman, S. A. Bowring, L. E. Babcock, "Geologic time scale v. 5.0" (Geological Society of America, 2018).

35. K. M. Nichols, N. J. Silberling, Stratigraphy and depositional history of the Star Peak Group (Triassic), northwestern Nevada. *Spec. Pap. Geol. Soc. Am.* **178**, 1–73 (1977).

36. G. Cuny, O. Rieppel, P. M. Sander, The shark fauna from the Middle Triassic (Anisian) of North-Western Nevada. *Zool. J. Linn. Soc.* **133**, 285–301 (2001). doi:10.1111/j.1096-3642.2001.tb00627.x

37. O. Rieppel, *Handbook of Paleoherpetology / Sauropterygia I.: Placodontia, Pachypleurosauria, Nothosauroidea, Pistosauroidea* (Friedrich Pfeil, 2000).

38. J. C. Merriam, *Triassic Ichthyosauria, with Special Reference to the American Forms* (Memoirs of the University of California, The University Press, 1908).

39. L. Schmitz, P. M. Sander, G. W. Storrs, O. Rieppel, New Mixosauridae (Ichthyosauria) from the Middle Triassic of the Augusta Mountains (Nevada, USA) and their implications for mixosaur taxonomy. *Palaentographica A* **270**, 133–162 (2004).

40. J. C. Merriam, Preliminary note on a new marine reptile from the Middle Triassic of Nevada. *Univ. Calif. Publication Bull. Dept. Geol.* **5**, 5–79 (1906).

41. B. Gauzens, A. Barnes, D. P. Giling, J. Hines, M. Jochum, J. S. Lefcheck, B. Rosenbaum, S. Wang, U. Brose, Fluxweb: An R package to easily estimate energy fluxes in food webs. *Methods Ecol. Evol.* **10**, 270–279 (2018). doi:10.1111/2041-210X.13109

42. N. D. Martinez, Allometric trophic networks from individuals to socio-ecosystems: Consumer-resource theory of the ecological elephant in the room. *Front. Ecol. Evol.* **8**, 92 (2020). doi:10.3389/fevo.2020.00092

43. R. Motani, D.-Y. Jiang, A. Tintori, C. Ji, J.-D. Huang, Pre- versus post-mass extinction divergence of Mesozoic marine reptiles dictated by time-scale dependence of evolutionary rates. *Proc. Biol. Sci.* **284**, 20170241 (2017). doi:10.1098/rspb.2017.0241 Medline

44. J. H. Brown, J. F. Gillooly, A. P. Allen, V. M. Savage, G. B. West, Toward a metabolic theory of ecology. *Ecology* **85**, 1771–1789 (2004). doi:10.1890/03-9000

45. E. L. Nicholls, M. Manabe, Giant ichthyosaurs of the Triassic – A new species of *Shonisaurus* from the Pardonet Formation (Norian, Late Triassic) of British Columbia. *J. Vertebr. Paleontol.* **24**, 838–849 (2004). doi:10.1671/0272-4634(2004)024[0838:GIOTTN]2.0.CO;2

46. C. R. McClain, M. A. Balk, M. C. Benfield, T. A. Branch, C. Chen, J. Cosgrove, A. D. M. Dove, L. Gaskins, R. R. Helm, F. G. Hochberg, F. B. Lee, A. Marshall, S. E. McMurray, C. Schanche, S. N. Stone, A. D. Thaler, Sizing ocean giants: Patterns of intraspecific size variation in marine megafauna. *PeerJ* **3**, e715 (2015). doi:10.7717/peerj.715 Medline

47. A. Brayard, L. J. Krumenacker, J. P. Botting, J. F. Jenks, K. G. Bylund, E. Fara, E. Vennin, N. Olivier, N. Goudemand, T. Saucède, S. Charbonnier, C. Romano, L. Doguzhaeva, B. Thuy,

M. Hautmann, D. A. Stephen, C. Thomazo, G. Escarguel, Unexpected Early Triassic marine ecosystem and the rise of the Modern evolutionary fauna. *Sci. Adv.* **3**, e1602159 (2017). doi:10.1126/sciadv.1602159 Medline

48. H. Song, P. B. Wignall, A. M. Dunhill, Decoupled taxonomic and ecological recoveries from the Permo-Triassic extinction. *Sci. Adv.* **4**, eaat5091 (2018). doi:10.1126/sciadv.aat5091 Medline

49. P. M. Sander, A. Christian, M. Clauss, R. Fechner, C. T. Gee, E.-M. Griebeler, H.-C. Gunga, J. Hummel, H. Mallison, S. F. Perry, H. Preuschoft, O. W. M. Rauhut, K. Remes, T. Tütken, O. Wings, U. Witzel, Biology of the sauropod dinosaurs: The evolution of gigantism. *Biol. Rev. Camb. Philos. Soc.* **86**, 117–155 (2011). doi:10.1111/j.1469-185X.2010.00137.x Medline

50. M. J. Benton, Q. Zhang, S. Hu, Z.-Q. Chen, W. Wen, J. Liu, J. Huang, C. Zhou, T. Xie, J. Tong, B. Choo, Exceptional vertebrate biotas from the Triassic of China, and the expansion of marine ecosystems after the Permo-Triassic mass extinction. *Earth Sci. Rev.* **137**, 85–128 (2014). doi:10.1016/j.earscirev.2014.08.004

51. M. J. Orchard, Conodont diversity and evolution through the latest Permian and Early Triassic upheavals. *Palaeogeogr. Palaeoclimatol. Palaeoecol.* **252**, 93–117 (2007). doi:10.1016/j.palaeo.2006.11.037

52. R. Motani, B. M. Rothschild, W. J. Wahl Jr., Large eyeballs in diving ichthyosaurs. *Nature* **402**, 747 (1999). doi:10.1038/45435

53. D.-E. Nilsson, E. Warrant, S. Johnsen, Computational visual ecology in the pelagic realm. *Philos. Trans. R. Soc. London Ser. B* **369**, 20130038 (2014). doi:10.1098/rstb.2013.0038 Medline

54. J. M. Grady, B. S. Maitner, A. S. Winter, K. Kaschner, D. P. Tittensor, S. Record, F. A. Smith, A. M. Wilson, A. I. Dell, P. L. Zarnetske, H. J. Wearing, B. Alfaro, J. H. Brown, Metabolic asymmetry and the global diversity of marine predators. *Science* **363**, eaat4220 (2019). doi:10.1126/science.aat4220 Medline

55. C. Pimiento, J. L. Cantalapiedra, K. Shimada, D. J. Field, J. B. Smaers, Evolutionary pathways toward gigantism in sharks and rays. *Evolution* **73**, 588–599 (2019). doi:10.1111/evo.13680 Medline

56. A. T. Boersma, N. D. Pyenson, *Albicetus oxymycterus*, a new generic name and redescription of a basal physeteroid (Mammalia, Cetacea) from the Miocene of California, and the evolution of body size in sperm whales. *PLOS ONE* **10**, e0135551 (2015). doi:10.1371/journal.pone.0135551 Medline

57. R. W. Boessenecker, M. Churchill, E. A. Buchholtz, B. L. Beatty, J. H. Geisler, Convergent evolution of swimming adaptations in modern whales revealed by a large macrophagous dolphin from the Oligocene of South Carolina. *Curr. Biol.* **30**, 3267–3273.e2 (2020). doi:10.1016/j.cub.2020.06.012 Medline

58. J. H. Geisler, M. W. Colbert, J. L. Carew, A new fossil species supports an early origin for toothed whale echolocation. *Nature* **508**, 383–386 (2014). doi:10.1038/nature13086 Medline

59. J. A. Goldbogen, P. T. Madsen, The evolution of foraging capacity and gigantism in cetaceans. *J. Exp. Biol.* **221**, jeb166033 (2018). doi:10.1242/jeb.166033 Medline

60. E. E. Maxwell, D. Y. Cortés, P. Patarroyo, M. L. P. Ruge, A new specimen of *Platypterygius sachicarum* (Reptilia, Ichthyosauria) from the Early Cretaceous of Colombia and its

phylogenetic implications. *J. Vertebr. Paleontol.* **39**, e1577875 (2019). doi:10.1080/02724634.2019.1577875

61. W. P. Maddison, D. R. Maddison, Mesquite: A modular system for evolutionary analysis. Version 3.02 (2015); www.mesquiteproject.org.

62. P. A. Goloboff, J. S. Farris, K. C. Nixon, TNT, a free program for phylogenetic analysis. *Cladistics* **24**, 774–786 (2008). doi:10.1111/j.1096-0031.2008.00217.x

63. J.-D. Huang, R. Motani, D. Y. Jiang, A. Tintori, O. Rieppel, M. Zhou, X.-X. Ren, R. Zhang, The new ichthyosauriform *Chaohusaurus brevifemoralis* (Reptilia, Ichthyosauromorpha) from Majiashan, Chaohu, Anhui Province, China. *PeerJ* **7**, e7561 (2019). doi:10.7717/peerj.7561 Medline

64. D. Swofford, *PAUP*. Phylogenetic Analysis Using Parsimony (* and Other Methods). Version 4.0b10* (Sinauer Associates, 2002).

65. R Core Team, R software, version 3.5.2 (R Foundation for Statistical Computing, Vienna, Austria, 2020); www.R-project.org/.

66. J. H. Geisler, A. E. Sanders, Morphological evidence for the phylogeny of Cetacea. *J. Mamm. Evol.* **10**, 23–129 (2003). doi:10.1023/A:1025552007291

67. G. T. Lloyd, G. J. Slater, A total-group phylogenetic metatree for Cetacea and the importance of fossil data in diversification analyses. *Syst. Biol.* **70**, 922–939 (2021). doi:10.1093/sysbio/syab002 Medline

68. S. Bajpai, P. D. Gingerich, A new Eocene archaeocete (Mammalia, Cetacea) from India and the time of origin of whales. *Proc. Natl. Acad. Sci. U.S.A.* **95**, 15464–15468 (1998). doi:10.1073/pnas.95.26.15464 Medline

69. A. E. Hernández Cisneros, J. Velez-Juarbe, Paleobiogeography of the North Pacific toothed mysticetes (Cetacea: Aetiocetidae): A key on the Oligocene cetacean distributional patterns. *Palaeontology* **64**, 51–61 (2021). doi:10.1111/pala.12507

70. M. Viglino, M. R. Buono, R. E. Fordyce, J. I. Cuitiño, E. M. G. Fitzgerald, Anatomy and phylogeny of the large shark-toothed dolphin *Phoberodon arctirostris* Cabrera, 1926 (Cetacea: Odontoceti) from the early Miocene of Patagonia (Argentina). *Zool. J. Linn. Soc.* **185**, 511–542 (2019). doi:10.1093/zoolinnean/zly053

71. C. M. Peredo, M. D. Uhen, M. D. Nelson, A new kentriodontid (Cetacea: Odontoceti) from the early Miocene Astoria Formation and a revision of the stem delphinidan family Kentriodontidae. *J. Vertebr. Paleontol.* **38**, e1411357 (2018). doi:10.1080/02724634.2017.1411357

72. M. R. McGowen, G. Tsagkogeorga, S. Álvarez-Carretero, M. Dos Reis, M. Struebig, R. Deaville, P. D. Jepson, S. Jarman, A. Polanowski, P. A. Morin, S. J. Rossiter, Phylogenomic resolution of the cetacean tree of life using target sequence capture. *Syst. Biol.* **69**, 479–501 (2020). doi:10.1093/sysbio/syz068 Medline

73. N. D. Pyenson, S. N. Sponberg, Reconstructing body size in extinct crown Cetacea (Neoceti) using allometry, phylogenetic methods and tests from the fossil record. *J. Mamm. Evol.* **18**, 269–288 (2011). doi:10.1007/s10914-011-9170-1

74. N. Cooper, G. H. Thomas, C. Venditti, A. Meade, R. P. Freckleton, A cautionary note on the use of Ornstein Uhlenbeck models in macroevolutionary studies. *Biol. J. Linn. Soc. Lond.* **118**, 64–77 (2016). doi:10.1111/bij.12701 Medline

75. D. L. Pisor, *Registry of World Record Size Shells* (ConchBooks, ed. 5, 2008).

76. S. Montanari, "This amazing fossil rode to Los Angeles in a beer truck," *Forbes Magazine*, 12 May 2017.

77. D. Jiang, L. Schmitz, W.-C. Hao, Y.-L. Sun, A new mixosaurid ichthyosaur from the Middle Triassic of China. *J. Vertebr. Paleontol.* **26**, 60–69 (2006). doi:10.1671/0272-4634(2006)26[60:ANMIFT]2.0.CO;2

78. C. Dal Sasso, G. Pinna, *Besanosaurus leptorhynchus* n. gen. n. sp., a new shastasaurid ichthyosaur from the Middle Triassic of Besano (Lombardy, N. Italy). *Paleontol. Lomb. Nuov. Ser.* **4**, 1–23 (1996).

79. J.-D. Huang, R. Motani, D. Y. Jiang, X. X. Ren, A. Tintori, O. Rieppel, M. Zhou, Y. C. Hu, R. Zhang, Repeated evolution of durophagy during ichthyosaur radiation after mass extinction indicated by hidden dentition. *Sci. Rep.* **10**, 7798 (2020). doi:10.1038/s41598-020-64854-z Medline

80. M. W. Maisch, X.-R. Pan, Z.-Y. Sun, T. Cai, D.-P. Zhang, J.-L. Xie, Cranial osteology of *Guizhouichthyosaurus tangae* (Reptilia: Ichthyosauria) from the Upper Triassic of China. *J. Vertebr. Paleontol.* **26**, 588–597 (2006). doi:10.1671/0272-4634(2006)26[588:COOGTR]2.0.CO;2

81. E. L. Nicholls, D. B. Brinkman, in *Vertebrate Fossils and the Evolution of Scientific Concepts*, W. A. S. Sarjeant, Ed. (Gordon and Breach Publishers, 1996), pp. 521–535.

82. E. L. Nicholls, C. Wei, M. Manabe, New material of *Qianichthyosaurus* Li, 1999 (Reptilia, Ichtyosauria) from the Late Triassic of Southern China, and implications for the distribution of Triassic ichthyosaurs. *J. Vertebr. Paleontol.* **22**, 759–765 (2003). doi:10.1671/0272-4634(2002)022[0759:NMOQLR]2.0.CO;2

83. T. Shikama, T. Kamei, M. Murata, Early Triassic ichthyosaurus, Utatsusaurus hataii gen. et sp. nov. from the Kitakami Massif, Northeast Japan. *Sci. Rep. Tohoku Univ. Sendai Sec. Ser. Geol.* **48**, 77–97 (1978).

84. R. Motani, Redescription of the dental features of an Early Triassic Ichthyosaur, *Utatsusaurus hataii*. *J. Vertebr. Paleontol.* **16**, 396–402 (1996). doi:10.1080/02724634.1996.10011329

85. D.-Y. Jiang, R. Motani, W. Hao, L. Schmitz, O. Rieppel, Y. Sun, Z. Sun, New primitive ichthyosaurian (Reptilia, Diapsida) from the Middle Triassic of Panxian (Guizhou, southwestern China) and its position in the Triassic Biotic Recovery. *Prog. Nat. Sci.* **18**, 1315–1319 (2008). doi:10.1016/j.pnsc.2008.01.039

86. V. S. Engelschiøn, L. L. Delsett, A. J. Roberts, J. H. Hurum, Large-sized ichthyosaurs from the Lower Saurian Niveau of the Vikinghøgda Formation (Early Triassic), Marmierfjellet, Spitsbergen. *Nor. J. Geol.* **98**, 239–265 (2018).

87. R. Motani, Phylogeny of the Ichthyopterygia. *J. Vertebr. Paleontol.* **19**, 473–496 (1999). doi:10.1080/02724634.1999.10011160

88. D.-Y. Jiang, R. Motani, J.-D. Huang, A. Tintori, Y.-C. Hu, O. Rieppel, N. C. Fraser, C. Ji, N. P. Kelley, W.-L. Fu, R. Zhang, A large aberrant stem ichthyosauriform indicating early rise and demise of ichthyosauromorphs in the wake of the end-Permian extinction. *Sci. Rep.* **6**, 26232 (2016). doi:10.1038/srep26232 Medline

89. R. Motani, D. Y. Jiang, A. Tintori, O. Rieppel, G. B. Chen, Terrestrial origin of viviparity in mesozoic marine reptiles indicated by early triassic embryonic fossils. *PLOS ONE* **9**, e88640 (2014). doi:10.1371/journal.pone.0088640 Medline

90. X. Chen, P. M. Sander, L. Cheng, X. Wang, A new Triassic primitive ichthyosaur from Yuanan, South China. *Acta Geol. Sin.* **87**, 672–677 (2013). doi:10.1111/1755-6724.12078

91. R. Motani, N. Minoura, T. Ando, Ichthyosaurian relationships illuminated by new primitive skeletons from Japan. *Nature* **393**, 255–257 (1998). doi:10.1038/30473

92. E. Repossi, Il mixosauro degli strati triassici di Besano in Lombardia. *Atti Soc. Ital. Sci. Nat.* **41**, 361–372 (1902).

93. L. Cheng, A new species of *Mixosaurus* (Reptilia: Ichthyosauria) from the Middle Triassic of Pu'an, Guizhou, China. *Acta Palaeontologica Sin.* **49**, 251–260 (2010).

94. B. F. Kosch, A revision of the skeletal reconstruction of *Shonisaurus popularis* (Reptilia: Ichthyosauria). *J. Vertebr. Paleontol.* **10**, 512–514 (1990). doi:10.1080/02724634.1990.10011833

95. X. Chen, L. Cheng, A new species of large-sized and long-body ichthyosaur from the Late Triassic Guanling biota, Guizhou, China. *Geol. Bull. China* **22**, 228–235 (2003).

96. Q.-H. Shang, C. Li, On the occurrence of the ichthyosaur *Shastasaurus* in the Guanling biota (Late Triassic), Guizhou, China. *Vertebr. Palasiat.* **47**, 178–193 (2009).

97. J. H. Geisler, M. R. McGowen, G. Yang, J. Gatesy, A supermatrix analysis of genomic, morphological, and paleontological data from crown Cetacea. *BMC Evol. Biol.* **11**, 112 (2011). doi:10.1186/1471-2148-11-112 Medline

98. F. G. Marx, R. E. Fordyce, Baleen boom and bust: A synthesis of mysticete phylogeny, diversity and disparity. *R. Soc. Open Sci.* **2**, 140434 (2015). doi:10.1098/rsos.140434 Medline

99. O. Lambert, G. Bianucci, M. Urbina, J. H. Geisler, A new inioid (Cetacea, Odontoceti, Delphinida) from the Miocene of Peru and the origin of modern dolphin and porpoise families. *Zool. J. Linn. Soc.* **179**, 919–946 (2017).

100. Y. Tanaka, R. E. Fordyce, A new Oligo-Miocene dolphin from New Zealand: Otekaikea huata expands diversity of the early Platanistoidea. *Palaeontol. Electron.* **18.2.23A**, 1–71 (2015).

101. L. B. Albright III, A. E. Sanders, J. H. Geisler, An unexpectedly derived odontocete from the Ahsley Formation (Upper Rupelian) of South Carolina, U.S.A. *J. Vertebr. Paleontol.* **38**, e1482555 (2018). doi:10.1080/02724634.2018.1482555

102. M. Martínez-Cáceres, O. Lambert, C. Muizon, The anatomy and phylogenetic affinities of *Cynthiacetus peruvianus*, a large *Dorudon*-like basilosaurid (Cetacea, Mammalia) from the late Eocene of Peru. *Geodiversitas* **39**, 7–163 (2017). doi:10.5252/g2017n1a1

103. M. L. Gibson, J. Mnieckowski, J. H. Geisler, *Tupelocetus palmeri*, a new species of protocetid whale (Mammalia, Cetacea) from the middle Eocene of South Carolina. *J. Vertebr. Paleontol.* **38**, e1555165 (2019). doi:10.1080/02724634.2018.1555165

104. O. Lambert, G. Bianucci, R. Salas-Gismondi, C. Di Celma, E. Steurbaut, M. Urbina, C. de Muizon, An amphibious whale from the middle Eocene of Peru reveals early South Pacific dispersal of quadrupedal cetaceans. *Curr. Biol.* **29**, 1352–1359.e3 (2019). doi:10.1016/j.cub.2019.02.050 Medline

105. F. G. Marx, N. Kohno, A new Miocene baleen whale from the Peruvian desert. *R. Soc. Open Sci.* **3**, 160542 (2016). doi:10.1098/rsos.160542 Medline

106. M. Bisconti, O. Lambert, M. Bosselaers, Revision of "*Balaena*" *belgica* reveals a new right whale species, the possible ancestry of the northern right whale, *Eubalaena glacialis*, and the ages of divergence for the living right whale species. *PeerJ* **5**, e3464 (2017). doi:10.7717/peerj.3464 Medline

107. M. Bisconti, D. K. Munsterman, K. Post, A new balaenopterid whale from the late Miocene of the Southern North Sea Basin and the evolution of balaenopterid diversity (Cetacea, Mysticeti). *PeerJ* **7**, e6915 (2019). doi:10.7717/peerj.6915 Medline

108. M. R. Buono, M. S. Fernández, M. A. Cozzuol, J. I. Cuitiño, E. M. G. Fitzgerald, The early Miocene balaenid *Morenocetus parvus* from Patagonia (Argentina) and the evolution of right whales. *PeerJ* **5**, e4148 (2017). doi:10.7717/peerj.4148 Medline

109. R. E. Fordyce, F. G. Marx, Gigantism precedes filter feeding in baleen whale evolution. *Curr. Biol.* **28**, 1670–1676.e2 (2018). doi:10.1016/j.cub.2018.04.027 Medline

110. C. de Muizon, G. Bianucci, M. Martínez-Cáceres, O. Lambert, *Mystacodon selenensis*, the earliest known toothed mysticete (Cetacea, Mammalia) from the late Eocene of Peru: Anatomy, phylogeny, and feeding adaptation. *Geodiversitas* **41**, 401–499 (2019). doi:10.5252/geodiversitas2019v41a11

111. G. Aguirre Fernández, L. G. Barnes, F. J. Aranda-Manteca, J. R. Fernández-Rivera, *Protoglobicephala mexicana*, a new genus and species of Pliocene fossil dolphin (Cetacea; Odontoceti; Delphinidae) from the Gulf of California. *Mexico. Bol. Soc. Geol. Mex.* **61**, 245–265 (2009). doi:10.18268/BSGM2009v61n2a13

112. M. Murakami, C. Shimada, Y. Hikida, Y. Soeda, H. Hirano, *Eodelphis kabatensis*, a new name for the oldest true dolphin *Stenella kabatensis* Horikawa, 1977 (Cetacea, Odontoceti, Delphinidae), from the upper Miocene of Japan, and the phylogeny and paleobiogeography of Delphinoidea. *J. Vertebr. Paleontol.* **34**, 491–511 (2014). doi:10.1080/02724634.2013.816720

113. B. Ramassamy, Description of a new long-snouted beaked whale from the Late Miocene of Denmark: evolution of suction feeding and sexual dimorphism in the Ziphiidae (Cetacea: Odontoceti. *Zool. J. Linn. Soc.* **178**, 381–409 (2016). doi:10.1111/zoj.12418

114. Y. Tanaka, H. Ishichima, A new skull of the fossil porpoise Numataphocoena yamashitai (Cetacea: Phocoenidae) from the upper part of the Horokaoshirarika Formation (lower Pliocene), Numata Town, Hokkaido, Japan, and its phylogenetic position. *Palaeontol. Electron.* **19.3.49A**, 1–28 (2016).

115. G. Bianucci, C. Di Celma, M. Urbina, O. Lambert, New beaked whales from the late Miocene of Peru and evidence for convergent evolution in stem and crown Ziphiidae (Cetacea, Odontoceti). *PeerJ* **4**, e2479 (2016). doi:10.7717/peerj.2479 Medline

116. G. Bianucci, F. Pesci, A. Collareta, C. Tinelli, A new Monodontidae (Cetacea, Delphinoidea) from the lower Pliocene of Italy supports a warm-water origin for narwhals and white whales. *J. Vertebr. Paleontol.* **39**, e1645148 (2019). doi:10.1080/02724634.2019.1645148

117. G. Bianucci, C. de Muizon, M. Urbina, O. Lambert, Extensive diversity and disparity of the Early Miocene Platanistoids (Cetacea, Odontoceti) in the Southeastern Pacific (Chilcatay Formation, Peru). *Life (Basel)* **10**, 27 (2020). doi:10.3390/life10030027 Medline

118. Y. Tanaka, J. Abella, G. Aguirre-Fernández, M. Gregori, R. E. Fordyce, A new tropical Oligocene dolphin from Montañita/Olón, Santa Elena, Ecuador. *PLOS ONE* **12**, e0188380 (2017). doi:10.1371/journal.pone.0188380 Medline

119. J. Vélez-Juarbe, A new stem odontocete from the late Oligocene Pysht Formation in Washington State, U.S.A. *J. Vertebr. Paleontol.* **37**, e1366916 (2017). doi:10.1080/02724634.2017.1366916

120. A. Benites-Palomino, J. Vélez-Juarbe, R. Salas-Gismondi, M. Urbina, *Scaphokogia totajpe*, sp. nov., a new bulky-faced pygmy sperm whale (Kogiidae) from the late Miocene of Peru. *J. Vertebr. Paleontol.* **39**, e1728538 (2020). doi:10.1080/02724634.2019.1728538

121. J. G. M. Thewissen, S. T. Hussain, Systematic review of the Pakicetidae, early and middle Eocene Cetacea (Mammalia) from Pakistan and India. *Bull. Carnegie Mus.* **34**, 220–238 (1998).

122. J. G. M. Thewissen, E. M. Williams, L. J. Roe, S. T. Hussain, Skeletons of terrestrial cetaceans and the relationship of whales to artiodactyls. *Nature* **413**, 277–281 (2001). doi:10.1038/35095005 Medline

123. P. Gingerich, Land-to-sea transition of early whales: Evolution of Eocene Archae-oceti (Cetacea) in relation to skeletal proportions and locomotion of living semiaquatic mammals. *Paleobiology* **29**, 429–454 (2003). doi:10.1666/0094-8373(2003)029<0429:LTIEWE>2.0.CO;2

124. M. D. Uhen, The origin(s) of whales. *Annu. Rev. Earth Planet. Sci.* **38**, 189–219 (2010). doi:10.1146/annurev-earth-040809-152453

125. M. T. Clementz, A. Goswami, P. D. Gingerich, P. L. Koch, Isotopic records from early whales and sea cows: Contrasting patterns of ecological transition. *J. Vertebr. Paleontol.* **26**, 355–370 (2006). doi:10.1671/0272-4634(2006)26[355:IRFEWA]2.0.CO;2

126. A. Houssaye, P. Tafforeau, C. de Muizon, P. D. Gingerich, Transition of Eocene whales from land to sea: Evidence from bone microstructure. *PLOS ONE* **10**, e0118409 (2015). doi:10.1371/journal.pone.0118409 Medline

127. F. G. Marx, O. O. Lambert, M. D. Uhen, *Cetacean Paleobiology* (Wiley, 2016).

128. A. Berta, J. L. Sumich, C. Buell, *Return to the Sea: The Life and Evolutionary Times of Marine Mammals* (Univ. California Press, 2012).

129. L. J. Harmon, J. T. Weir, C. D. Brock, R. E. Glor, W. Challenger, GEIGER: Investigating evolutionary radiations. *Bioinformatics* **24**, 129–131 (2008). doi:10.1093/bioinformatics/btm538 Medline

130. M. W. Pennell, J. M. Eastman, G. J. Slater, J. W. Brown, J. C. Uyeda, R. G. FitzJohn, M. E. Alfaro, L. J. Harmon, geiger v2.0: An expanded suite of methods for fitting macroevolutionary models to phylogenetic trees. *Bioinformatics* **30**, 2216–2218 (2014). doi:10.1093/bioinformatics/btu181 Medline

131. J. Felsenstein, Maximum-likelihood estimation of evolutionary trees from continuous characters. *Am. J. Hum. Genet.* **25**, 471–492 (1973). Medline

132. M. A. Butler, A. A. King, Phylogenetic comparative analysis: A modeling approach for adaptive evolution. *Am. Nat.* **164**, 683–695 (2004). doi:10.1086/426002 Medline

133. L. J. Harmon, J. B. Losos, T. Jonathan Davies, R. G. Gillespie, J. L. Gittleman, W. Bryan Jennings, K. H. Kozak, M. A. McPeek, F. Moreno-Roark, T. J. Near, A. Purvis, R. E. Ricklefs, D. Schluter, J. A. Schulte Ii, O. Seehausen, B. L. Sidlauskas, O. Torres-Carvajal, J. T. Weir, A. Ø. Mooers, Early bursts of body size and shape evolution are rare in comparative data. *Evolution* **64**, 2385–2396 (2010). doi:10.1111/j.1558-5646.2010.01025.x Medline

134. S. P. Blomberg, T. Garland Jr., A. R. Ives, Testing for phylogenetic signal in comparative data: Behavioral traits are more labile. *Evolution* **57**, 717–745 (2003). doi:10.1111/j.0014-3820.2003.tb00285.x Medline

135. C. Boettiger, G. Coop, P. Ralph, Is your phylogeny informative? Measuring the power of comparative methods. *Evolution* **66**, 2240–2251 (2012). doi:10.1111/j.1558-5646.2011.01574.x Medline

136. M. Friedman, Parallel evolutionary trajectories underlie the origin of giant suspension-feeding whales and bony fishes. *Proc. Biol. Sci.* **279**, 944–951 (2012). doi:10.1098/rspb.2011.1381 Medline

137. J. Potvin, J. A. Goldbogen, R. E. Shadwick, Metabolic expenditures of lunge feeding rorquals across scale: Implications for the evolution of filter feeding and the limits to maximum body size. *PLOS ONE* **7**, e44854 (2012). doi:10.1371/journal.pone.0044854 Medline

138. D. R. Lomax, P. De la Salle, J. A. Massare, R. Gallois, A giant Late Triassic ichthyosaur from the UK and a reinterpretation of the Aust Cliff 'dinosaurian' bones. *PLOS ONE* **13**, e0194742 (2018). doi:10.1371/journal.pone.0194742 Medline

139. E. Paradis, K. Schliep, ape 5.0: An environment for modern phylogenetics and evolutionary analyses in R. *Bioinformatics* **35**, 526–528 (2019). doi:10.1093/bioinformatics/bty633 Medline

140. H. Wickham, R. François, L. Henry, K. Müller, Dplyr: a grammar of data manipulation. R package version 0.8.5 (2020); https://CRAN.R-project.org/package=dplyr.

141. J. Bryan, googlesheets4: Access Google Sheets using the Sheets API V4. R package version 0.2.0 (2020); https://CRAN.R-project.org/package=googlesheets4.

142. H. Wickham, *Ggplot2: Elegant Graphics for Data Analysis* (Springer, 2016).

143. J. Clavel, G. Escarguel, G. Merceron, mvMORPH: An R package for fitting multivariate evolutionary models to morphometric data. *Methods Ecol. Evol.* **6**, 311–1319 (2015). doi:10.1111/2041-210X.12420

144. D. W. Bapst, Paleotree: An R package for paleontological and phylogenetic analyses of evolution. *Methods Ecol. Evol.* **3**, 803–807 (2012). doi:10.1111/j.2041-210X.2012.00223.x

145. S. W. Kembel, P. D. Cowan, M. R. Helmus, W. K. Cornwell, H. Morlon, D. D. Ackerly, S. P. Blomberg, C. O. Webb, Picante: R tools for integrating phylogenies and ecology. *Bioinformatics* **26**, 1463–1464 (2010). doi:10.1093/bioinformatics/btq166 Medline

146. H. Wickham, Reshaping data with the reshape package. *J. Stat. Softw.* **21**, 1–20 (2007). doi:10.18637/jss.v021.i12

147. M. A. Bell, G. T. Loyd, strap: Stratigraphic Tree Analysis for Palaeontology. R package version 1.4 (2014); https://CRAN.R-project.org/package=strap.

148. H. Bucher, A new middle Anisian (Middle Triassic) ammonoid zone from northwestern Nevada USA. *Eclogae Geol. Helv.* **81**, 723–762 (1988).

149. P. M. Sander, H. Bucher, On the presence of *Mixosaurus* (Ichthyopterygia: Reptilia) in the Middle Triassic of Nevada. *J. Paleontol.* **64**, 161–164 (1990). doi:10.1017/S0022336000042396

150. P. M. Sander, O. C. Rieppel, H. Bucher, A new pistosaurid (Reptilia: Sauropterygia) from the Middle Triassic of Nevada and its implications for the origin of plesiosaurs. *J. Vertebr. Paleontol.* **17**, 526–533 (1997). doi:10.1080/02724634.1997.10010999

151. P. M. Sander, O. C. Rieppel, H. Bucher, New marine vertebrate fauna from the Middle Triassic of Nevada. *J. Paleontol.* **68**, 676–680 (1994). doi:10.1017/S0022336000026020

152. O. Rieppel, P. M. Sander, G. W. Storrs, The skull of the pistosaur *Augustasaurus* from the Middle Triassic of northwestern Nevada. *J. Vertebr. Paleontol.* **22**, 577–592 (2002). doi:10.1671/0272-4634(2002)022[0577:TSOTPA]2.0.CO;2

153. E. M. Wemple, New cestraciont teeth from the West-American Triassic. *Univ. Calif. Publ. Bull. Dept. Geol.* **5**, 71–73 (1906).

154. J. C. Merriam, The skull and dentition of a primitive ichthyosaurian from the Middle Triassic. *Univ. Calif. Publication Bull. Dept. Geol.* **5**, 381–390 (1910).

155. L. Schmitz, The taxonomic status of *Mixosaurus nordenskioeldii* (Ichthyosauria). *J. Vertebr. Paleontol.* **25**, 983–985 (2005). doi:10.1671/0272-4634(2005)025[0983:TTSOMN]2.0.CO;2

156. C. Carbone, D. Codron, C. Scofield, M. Clauss, J. Bielby, Geometric factors influencing the diet of vertebrate predators in marine and terrestrial environments. *Ecol. Lett.* **17**, 1553–1559 (2014). doi:10.1111/ele.12375 Medline

157. D.-Y. Jiang, R. Motani, A. Tintori, O. Rieppel, C. Ji, M. Zhou, X. Wang, H. Lu, Z.-G. Li, Evidence supporting predation of 4-m marine reptile by Triassic megapredator. *iScience* **23**, 101347 (2020). doi:10.1016/j.isci.2020.101347 Medline

158. D. P. Hocking, F. G. Marx, T. Park, E. M. Fitzgerald, A. R. Evans, A behavioural framework for the evolution of feeding in predatory aquatic mammals. *Proc. Biol. Sci.* **284**, 20162750 (2017). doi:10.1098/rspb.2016.2750 Medline

159. T. Wintrich, R. Jonas, H.-J. Wilke, L. Schmitz, P. M. Sander, Neck mobility in the Jurassic plesiosaur *Cryptoclidus eurymerus*: Finite element analysis as a new approach to understanding the cervical skeleton in fossil vertebrates. *PeerJ* **7**, e7658 (2019). doi:10.7717/peerj.7658 Medline

160. P. M. Sander, C. Faber, The Triassic marine reptile *Omphalosaurus*: Osteology, jaw anatomy, and evidence for ichthyosaurian affinities. *J. Vertebr. Paleontol.* **23**, 799–816 (2003). doi:10.1671/6

161. D. Pauly, V. Christensen, C. Walters, Ecopath, ecosim, and ecospace as tools for evaluating ecosystem impact of fisheries. *ICES J. Mar. Sci.* **57**, 697–706 (2000). doi:10.1006/jmsc.2000.0726

162. O. Maury, B. Faugeras, Y.-J. Shin, J.-C. Poggiale, T. B. Ari, F. Marsac, Modeling environmental effects on the size-structured energy flow through marine ecosystems. Part 1: The model. *Prog. Oceanogr.* **74**, 479–499 (2007). doi:10.1016/j.pocean.2007.05.002

163. J. Steele, Assessment of some linear food web methods. *J. Mar. Syst.* **76**, 186–194 (2009). doi:10.1016/j.jmarsys.2008.05.012

164. J. C. Moore, P. C. De Ruiter, *An Analysis of Real and Model Ecosystems* (Oxford Univ. Press, 2012).

165. I. Valiela, *Marine Ecological Processes* (Springer, 2015).

166. Y. Nakajima, A. Houssaye, H. Endo, Osteohistology of *Utatsusaurus hataii* (Reptilia: Ichthyopterygia): Implications for early ichthyosaur biology. *Acta Palaeontol. Pol.* **59**, 343–352 (2014).

167. K. L. Anderson, P. S. Druckenmiller, G. M. Erickson, E. E. Maxwell, Skeletal microstructure of *Stenopterygius quadriscissus* (Reptilia, Ichthyosauria) from the Posidonienschiefer (Posidonia Shale, Lower Jurassic) of Germany. *Palaeontology* **62**, 433–449 (2019). doi:10.1111/pala.12408

168. P. M. Sander, in *Vertebrate Skeletal Histology and Paleohistology*, V. de Buffrénil, A. de Ricqlès, L. Zylberberg, K. Padian, Eds. (CRC Press, 2021), pp. 458–466.

169. J. A. Massare, Swimming capabilities of Mesozoic marine reptiles: Implications for method of predation. *Paleobiology* **14**, 187–205 (1988). doi:10.1017/S009483730001191X

170. J. A. Massare, in *Mechanics and Physiology of Animal Swimming*, L. Maddock, Q. Bone, J. M. V. Rayner, Eds. (Cambridge Univ. Press, 1994), pp. 133–149.

171. R. Motani, Swimming speed estimation of the extinct marine reptiles: Energetic approach revisited. *Paleobiology* **28**, 251–262 (2002). doi:10.1666/0094-8373(2002)028<0251:SSEOEM>2.0.CO;2

172. J. Lindgren, P. Sjövall, V. Thiel, W. Zheng, S. Ito, K. Wakamatsu, R. Hauff, B. P. Kear, A. Engdahl, C. Alwmark, M. E. Eriksson, M. Jarenmark, S. Sachs, P. E. Ahlberg, F. Marone, T. Kuriyama, O. Gustafsson, P. Malmberg, A. Thomen, I. Rodríguez-Meizoso, P. Uvdal, M. Ojika, M. H. Schweitzer, Soft-tissue evidence for homeothermy and crypsis in a Jurassic ichthyosaur. *Nature* **564**, 359–365 (2018). doi:10.1038/s41586-018-0775-x Medline

173. A. Bernard, C. Lécuyer, P. Vincent, R. Amiot, N. Bardet, E. Buffetaut, G. Cuny, F. Fourel, F. Martineau, J.-M. Mazin, A. Prieur, Regulation of body temperature by some Mesozoic marine reptiles. *Science* **328**, 1379–1382 (2010). doi:10.1126/science.1187443 Medline

174. J. J. Head, J. I. Bloch, A. K. Hastings, J. R. Bourque, E. A. Cadena, F. A. Herrera, P. D. Polly, C. A. Jaramillo, Giant boid snake from the Palaeocene neotropics reveals hotter past equatorial temperatures. *Nature* **457**, 715–717 (2009). doi:10.1038/nature07671 Medline

175. P. M. Sander, An evolutionary cascade model for sauropod dinosaur gigantism—Overview, update and tests. *PLOS ONE* **8**, e78573 (2013). doi:10.1371/journal.pone.0078573 Medline

176. W. F. Humphreys, Production and respiration in animal populations. *J. Anim. Ecol.* **48**, 427–453 (1979). doi:10.2307/4171

177. M. Cusson, E. Bourget, Global patterns of macroinvertebrate production in marine benthic habitats. *Mar. Ecol. Prog. Ser.* **297**, 1–14 (2005). doi:10.3354/meps297001

178. S. Gaichas, G. Skaret, J. Falk-Petersen, J. S. Link, W. Overholtz, B. A. Megrey, H. Gjøsæter, W. T. Stockhausen, A. Dommasnes, K. D. Friedland, K. Aydin, A comparison of community and trophic structure in five marine ecosystems based on energy budgets and system metrics. *Prog. Oceanogr.* **81**, 47–62 (2009). doi:10.1016/j.pocean.2009.04.005